INVESTIGATION OF THERMAL PERFORMANCE OF TWO PHASE NATURAL CIRCULATION LOOP FILLED WITH NANOFLUID

Submitted in partial fulfillment of the requirements
For the award of the degree of

DOCTOR OF PHILOSOPHY

In

MECHANICAL ENGINEERING

By

MR. S VENKATA SAI SUDHEER
(Roll No. 715026)

Supervisor:

Dr. K. KIRAN KUMAR
Associate Professor
Dr. KARTHIK BALASUBRAMANIAN
Assistant Professor

DEPARTMENT OF MECHANICAL ENGINEERING
NATIONAL INSTITUTE OF TECHNOLOGY
WARANGAL-506 004, TELANGANA
INDIA

May 2020

Dedicated

to

- **My beloved Parents & Family**
- **All my Teachers and Professors who taught and encouraged me with positive thoughts.**
- **All my beloved Friends who supported me in every situation.**

NATIONAL INSTITUTE OF TECHNOLOGY
WARANGAL (T.S) INDIA 506 004

CERTIFICATE

This is to certify that the thesis entitled **"Investigation of thermal performance of two phase natural circulation loop filled with nanofluid"**, that is being submitted by **Mr. S Venkata Sai Sudheer (715026)** in partial fulfillment for the award of Doctor of Philosophy (**Ph.D.)** in the Department of Mechanical Engineering, National Institute of Technology Warangal, is a record of bonafide work carried out by him under our guidance and supervision. The results embodied in this thesis have not been submitted to any other Universities or Institutes for the award of any degree or diploma.

Dr. K. Kiran Kumar
Associate Professor
Thesis Supervisor
Department of Mechanical Engineering,
National Institute of Technology, Warangal.

Dr. Karthik Balasubramanian
Assistant Professor
Thesis Supervisor
Department of Mechanical Engineering,
National Institute of Technology, Warangal.

NATIONAL INSTITUTE OF TECHNOLOGY
WARANGAL (T.S) INDIA 506 004

DECLARATION

This is to certify that the work presented in the thesis entitled **"Investigation of thermal performance of two phase natural circulation loop filled with nanofluid"**, is a bonafide work done by me under the supervision of Dr. K Kiran Kumar and Dr. Karthik Balasubramanian and was not submitted elsewhere for the award of any degree.

I declare that this written submission represents my idea in my own words and where other's ideas or words have not been included. I have adequately cited and referenced the original sources. I also declare that I have adhered to all principles of academic honesty and integrity and have not misrepresented or fabricated or falsified any idea/data/fact/source in my submission. I understand that any violation of the above will be a cause for disciplinary action by the Institute and can evoke penal action from the sources which have thus not been properly cited or from whom proper permission has not taken when needed.

Date:

Place: Warangal

(S Venkata Sai Sudheer)

Research Scholar,

Roll No.715026.

ACKNOWLEDGEMENTS

I would like to express my sincere gratitude and it gives me immense pleasure to acknowledge the people who were the part of this research work in plenty of ways. It would not have been possible without a close association with many people. I take this opportunity to extend my sincere gratitude and appreciation to all those who made this research work possible. First and foremost, I would like to express my sincere gratitude to my research supervisor **Assoc. Prof. K Kiran Kumar** for introducing me to this exciting field of natural circulation systems and for his dedicated help, advice, inspiration, encouragement and continuous support, throughout my research work. His enthusiasm, integral view on research and mission for providing high-quality work, has made a deep impression on me. I indebted to him for his persistence in moulding me as a researcher with his methodical supervision that enabled me to complete the research work in the present form. I will never forget his association and encouragement and whole hearted support during my entire tenure of research. During my course of interaction, I have learned many things, especially the idea of purchasing new equipment, writing research proposals, explore new possibilities and how to approach a problem by systematic thinking. I owe him lots of gratitude for showing me this way of research.

I would like to express special words of thanks to my research co-supervisor **Asst. Prof. Karthik Balasubramanian** for his continuous support, guidance, cooperation, encouragement and for facilitating all the requirements, going out of his way. He supported me a lot, especially in the two phase flow and how to write good journals for my research work. He taught me another aspect of life, that, “goodness can never be defied and good human beings can never be denied”. His constant motivation and support have always kept me going ahead. I owe a lot of gratitude to him for always being there for me in spite of his busy schedule and I feel privileged to be associated with him.

I wish to sincerely thank university authorities, **Prof. N. V. Ramana Rao**, Director, National Institute of Technology, Warangal and other top officials who gave me an opportunity to carry out research work.

I would like to acknowledge with gratitude to **Prof. Narasimha Rao R**, Head, and Department of Mechanical Engineering for providing the necessary facilities to carry out the research.

I wish to express my sincere and whole hearted thanks and gratitude to my doctoral scrutiny committee (DSC) members **Prof. K Madhu Murthy**, Professor, Mechanical Engineering Department, **Dr. G Naga Srinivasulu,** Associate Professor, Mechanical Engineering Department, **Dr. P V Suresh,** Associate Professor, Chemical Engineering Department, National Institute of Technology, Warangal for their kind help, encouragement and valuable suggestions for successful completion of research work.

I am always grateful to my institute NITW, where I learn many things along with the research. I express my heart-felt gratitude to some of the faculty members of the institute during the stay. They are very kind enough to extend their help at various phases of this research, whenever I approached them, and I do hereby acknowledge all of them. Prof. R.V Chalam, Prof. K Madhu Murthy, Prof. L Krishnanand, Prof. C.S.P Rao, Prof. A. Neelakanteswara Rao, Prof. C. Guru Raja Rao, Prof. A Venu Gopal, Prof. N Selvaraj, Prof. K V Sai Srinadh, Prof. Ravi Kumar Puli, Prof. G. Amba Prasada Rao, Prof. V. Suresh Babu, Dr. V. Hari Kumar, Dr. V. Vasu, Dr. V. R. K. Raju, Dr. Chandramohan V.P, Dr. Jaya Krishna. D, Dr. P.Vamsi Krishna Dr. Syed Ismail, and other faculty members of the department for their timely suggestions and cooperation during the entire period of research. I would like to express heartful thanks to Dr. M. R. Vishwanathan faculty member of the H&SS department for his timely suggestions during my thesis preparation.

My heartfelt thanks to fellow-scholars for their consistent help, moral support and encouragement. My special thanks to Dr. J. A. Ranga Babu, Dr. B Ramesh Babu, Dr. V Venkateswarlu, Dr. D Ravi Chandra, Brindavan Patro, V Ranjith Kumar, P Mahesh, D Nandan Hegde, N Nitin Kumar, N Reetu Mukherjee, P Raj Kumar and many others for always standing by my side and sharing a great relationship as compassionate friends. I will always cherish the warmth shown by them.

In this auspicious moment, I owe my deepest regards to my family members for their eternal support and understanding of my goals and aspirations. My heartfelt regards go to my parents, Sri S Balaiah, and Smt. S Sarala Devi, my brother S V Anil Kumar and sister in law Smt. S Vasantha, share a perpetual role with their infallible affection, love and support, it has always been my strength. Their patience and sacrifice will remain my inspiration throughout my life. Without their support, I would not have been able to complete what I have done and become who I am. My brother kid S Dhruva Karthekeya miss many cherishable moments in his life due to busy in research. I also must thank all my hostel mates and neighbours near my hostel room for making my stay at NIT Warangal become more memorable.

As always it is impossible to mention everybody who had an impact to this work, however, there are those whose spiritual support is even more important. I feel a deep sense of gratitude to each and every one who directly or indirectly extended their support to fulfill my research.

Finally, I am thankful to library staff and administrative staff of NITW for their cooperation.

NIT Warangal (**S Venkata Sai Sudheer**)

May 2020

Abstract

Natural circulation loops arose as an innovative solution in the diverse engineering heat transfer problems. Among the available heat transfer systems Natural Circulation Loops (NCL) are specially promising in nature due to their non-dependence on external power. Hence, these are considered to be viable option due to simplicity in design and reliabile during the operation. Many researchers focused their research on NCL due to its versatile application in different engineering fields such as nuclear reactor cooling, gas turbine cooling, solar water heater and waste heat recovery boilers.

A simple NCL consists of a heater and condenser and are connected by two vertical adiabatic limbs (riser and downcomer). The loop fluid becomes low density fluid by absorbing the heat at the heater. The low density fluid rises in the riser and enters into condenser. At condenser, the low density loop fluid becomes high density fluid by the rejecting heat. The high density loop fluid enters the heater through the downcomer due to gravity. The distinct density difference in the loop fluid at the heater outlet and condenser outlet causes the fluid to circulate inside the loop. According to state of the loop fluid at the heater exit, NCLs are classified as single-phase NCL and two-phase NCL. In two-phase NCL the loop consists of vapour liquid mixture in the riser section and liquid phase in the downcomer section during the steady state operation.

In general, conventional fluids such as water and refrigerants are commonly used as heat transfer fluids. But, the conventional fluids are not capable of transferring more heat form the systems due to poor thermo-physical properties. The suspension of nano sized solid particles in to the conventional fluids is a key technique to enhance the thermal conductivity and other favourable thermo-physical properties. Then a new class of fluids called nanofluids was introduced to the scientific community. Though most of the earlier studies was focused on single phase nanofluids, two phase nanofluid is the latest topic of interest for heat transfer applications.

The main objective of this research is to carry out numerical and experimental studies on nanofluid based two phase NCL. For this research work Al_2O_3-water nanofluid at different particle concentrations were used. Initially a one-dimensional (1-D) numerical model was developed to analyse rectangular NCL filled with water and nanofluid operating at steady-state condition. This study predicts the balanced mass flow rates of NCL. From the results, it was

concluded that for a given input conditions at heater inlet, there exist a peak mass flow rate. By using this numerical model the effect of geometrical parameters (heater and condenser orientation, aspect ratio and loop diameter) and operating parameters (pressure) on the loop performance was analysed. The noteworthy conclusions drawn from this study are, the heater orientation has insignificant effect on the mass flow rate in the loop whereas the orientation of condenser is significant. The increase of aspect ratio increases the mass flow rate. Similarly, increase of riser diameter increases the mass flow rate.However increase of downcomer diameter does not have much effect on mass flow rate. Further it was found that by decreasing the system pressure i.e. from 1 atm to 0.8 atm, the sub atmospheric loop exhibits peak mass flow rate at lower heat flux.

Then after, an experimental study was carried out to understand the flow boiling behaviour of nanofluid by varying its particle concentration, heat flux and mass flux. The results obtained were compared with deionised water. It was observed that the flow boiling curve for nanofluid follows same trend as that of water but with low wall superheat. The reduction of wall superheat increases with particle concentration of nanofluid. The heat transfer coefficient of nanofluid was high as compared with water and it increases with heat flux, mass flux and particle concentration. Deposition of nanoparticles on the heater surface influences the bubble growth phenomena. The amendment of boiling mechanism in nanofluids eliminates the churn flow pattern, the same was observed in the present study. A new empirical correlation has been proposed to predict the flow boiling heat transfer coefficient of nanofluids.

Based on the numerical studies, a rectangular NCL perfectly instrumented was fabricated with heater as heat source. Experiments were conducted on single phase and two phase operating condition with nanofluids as loop fluid and results were compared with water. The experimental results were validated with the numerical results. A good agreement was obtained. The experimental results show that NCL operated with nanofluid quickly reaches boiling as compared with that of water. Within the range of study, oscillation flow is found inside the loop at 136.61kW/m^2 heat input. These oscillations were high for water as compared with nanofluid. Influence of heat sink condition (cold fluid flow rate and temperature) on loop mass flow rate is analysed. Finally based on the theoretical and experimental work, several conclusions were drawn and recommendations were made for future studies.

Contents

List of figures

List of tables

Nomenclature

A	Area, m^2	Bo	Boiling number
C	Condenser/Friction factor	Co	Courant number
D	Diameter, m	Fr	Froude number
G	Mass flux kg/s-m^2	g	Acceleration due to gravity, m/s^2
Gr	Grashof number	H	Heater/Length of horizontal arm, m
I	Current, A	J_f	Superficial liquid velocity, m/s
J_g	Superficial vapour velocity, m/s	k	Thermal conductivity, Wm/ ^OC
L or z	Length, m	l_{sh}	Sub cooled length in evaporator, m
l_{sc}	Sub cooled length in condenser, m	l_h	Heater length, m
l_c	Cooler length, m	m	Mass ,kg
$\dot{m}$	Mass flow rate, kg/s	P	Perimeter, m
p	Pressure, bar/atm	Pr	Prandtl number
Q	Heat, kW	$\dot{q}$	Heat flux, kW/m^2
$\dot{q}_H$	Heat flux at heater, kW/m^2	$\dot{q}_C$	Heat flux at condenser, kW/m^2
R	Riser/Resistance, ohms	Re	Reynolds number
s	Space coordinate, m	T	Temperature, ^OC
u	Velocity, m/s	V	Voltage, Volts
v	Specific volume, m^3/kg	v_{bar}	Two phase mixture specific volume,m^3/kg
x	Dryness fraction, dimensionless	$I.D$	Inner diameter, m
$O.D$	Outer diameter, m	ψ	Ratio of two phase heat transfer coefficient to single phase heat transfer coefficient
ρ	Density, kg/m^3	σ	Stefan Boltzmann constant
μ	Dynamic viscosity, kg/m-s	dp/ds	Pressure gradient, N/m^3

h	Specific enthalpy (kJ/kg) / heat transfer coefficient (kW/m^2 ^{O}C)	∅	Volume concentration
ξ	Diameter ratio	$\bar{h}$	Average heat transfer coefficient, kW/m^2 ^{O}C
$\bar{T}$	Average Temperature, ^{O}C	AR	Aspect ratio
θ	Angle		

Subscripts

a	Acceleration	amb	Ambient
avg	Average	bf	Base fluid
bs	Bubble suppression region	cbd	Convection boiling region
conv	Convection	cs	Cross sectional
f	Saturated liquid/frictional	fd	Fully developed flow
fg	Difference between gas(vapour) and liquid properties at saturated state	fi	Main heater inlet
g	Saturated gas(vapour)/gravitational	gp	Gravitational pressure
i	inlet	in	Inlet/inner
loss	Losses	nbd	Nucleate boiling region
net	Net value	np	Nanoparticles
rad	Radiation	sat	Saturation
sc	Subcooled	surf	Surface
tp	Two phase	Wall	Wall surface

Abbreviations

Al_2O_3	Aluminium oxide (alumina)	BWR	Boiling water reactor
cc	Cubic centimeter	CHF	Critical heat flux
HTC	Heat transfer coefficent	NCL	Natural circulation loop
nm	Nano meters	PWR	Pressurised water reactor

Chapter 1

Introduction

Chapter 1

Introduction

1.1 Background

Natural circulation is a simple phenomenon, in which the fluid in a system circulates continuously. This principle can be seen in tornadoes, ocean currents and household ventilation. The driving force for the circulation is solely by the thermal imbalance of the fluid, which creates a density gradient at different parts of the medium (fluid) and it is the cause for the circulation. Owing to this concept, heat transfer loops such as natural circulation loops (NCLs) and heat pipes are developed. This type of system consists of a heat source and heat sink and former should be placed below the latter. The basic difference between NCL and heat pipe is as follows: in heat pipe, the liquid is returned from the condenser to the evaporator by surface tension acting in a wick, but NCL rely on gravity for the liquid to return to the evaporator. In NCL systems, a portion of the fluid is in contact with both heat source and heat sink. At the heat source the loop fluid absorbs the heat, becomes lighter and rises, while at the heat sink, loop fluid rejects the heat, becomes denser and is flows down by gravity. This combined effect establishes circulation. Furthermore, the greater feasibility of these systems is the absence of active components like pumps and therefore requires no regular maintenance. Moreover, the process is self-controlled either by varying the imposed heat flux interactions or temperature difference at heat source and heat sink [1][2]. Due to these specific features, natural circulation systems are more reliable, safer and requires less maintenance. Hence they are considered as lucrative choice in distinctive cooling applications such as Geothermal systems [3], Nuclear reactor cooling systems [4], [5], Solar evaporators [6], Thermosyphon re-boilers[7], [8]and Gas turbine blade cooling[9].

1.2 Natural circulation loop

1.2.1 Working principle

NCL is a passive device and transfers heat from source to the sink over a distance without aid of any active components like pump, fan etc. Sometimes NCLs can also be called as

thermosyphons. Japikse [10] presented the difference between NCL and thermosyphon[10][10][10][10][10][10][10][10][10][10][. In NCL, fluid circulates in one direction along the loop. Whereas in thermosyphon, fluid rises along the heated wall and returns through the cooler wall or down the core (Fig. 1.1(b)). NCL consists of heat source/heater and heat sink/condenser. Two vertical limbs connect the heater and condenser called riser and downcomer, as shown in Fig. 1.1(a). In NCL, loop fluid (fluid flowing through the loop) circulation arises due to the buoyancy forces. The loop fluid involves in heat interactions at heater and condenser and is subjected to distinct density gradients. These density gradients develop the buoyancy force that drives the loop fluid. This mechanism is explained in a simple manner by considering a small pocket of fluid or control volume in NCL. Let us consider a fluid pocket at either side of heater or condenser exits. This fluid pocket experiences two forces. The first force is an upward force by the result of the hydrostatic pressure difference (buoyancy force). The second force is a downward force due to gravity. Now the fluid pocket moves either upwards or downwards depending on the net resultant force. As a result, the fluid in the simple vertically orientated loop (Fig.1.1 (a)), flows with a mass flow rate in a clockwise or anti-clockwise direction provided that one vertical section is heated (riser) and the other vertical section is cooled (downcomer).

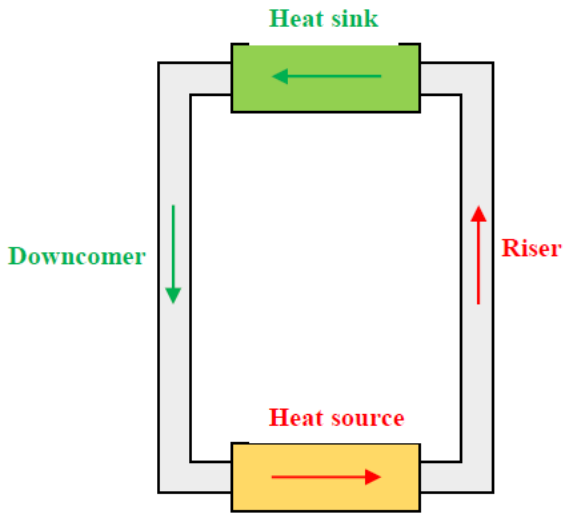

Fig.1.1(a) Schematic diagram of simple NCL

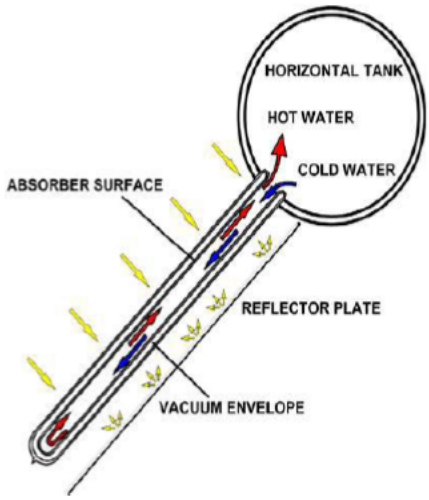

Fig. 1.1 (b) An Example of Thermosyphon is evacuated tube solar water heater

The loop fluid absorbs the heat at the heater and density decreases. This low density fluid rises in the vertical section (riser) and reaches to the condenser. In the condenser loop fluid rejects the heat and density increases. This high density fluid flows down from the condenser due to gravity through the other vertical section (downcomer) and reaches to the heater, and this makes a complete cycle. Once the heat source and heat sink attains constant temperature it is implied that NCL has reached steady state. At the steady state, the fluid circulates in one direction unless external input parameters are changed. Thus, the fluid circulation is dependent on the boundary conditions of the heater and condenser. So, it is well known that the loop flow rate is enhanced by varying the density difference between the riser and downcomer.

1.2.2 NCL configuration and classifications

The natural circulation flow can be achieved by various body forces such as electromagnetic, centrifugal or gravitational forces. So, depending upon the application**,** various configurations are possible in NCls. Some of the applications are shown in Fig.1.2. In the open literature, Vijayan [11] made a classification in NCL based on the body force field, interaction with surroundings, state of the working fluid, inventory and number of channels. A clear classification tree is shown in Fig.1.3.

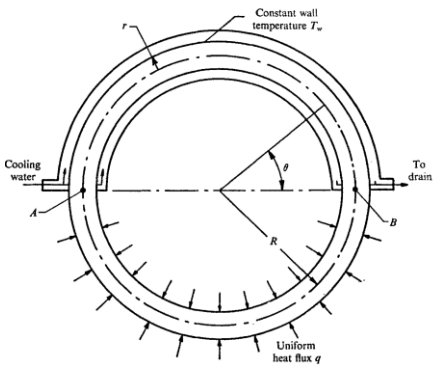

Toroidal NCL [12]

Rectangular NCL with point heat source & sink [13]

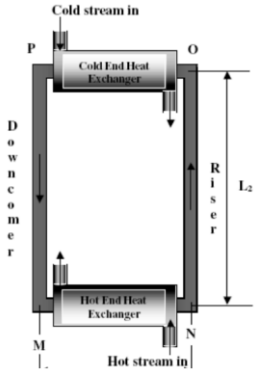

Rectangular NCL with end heat exchangers [14]

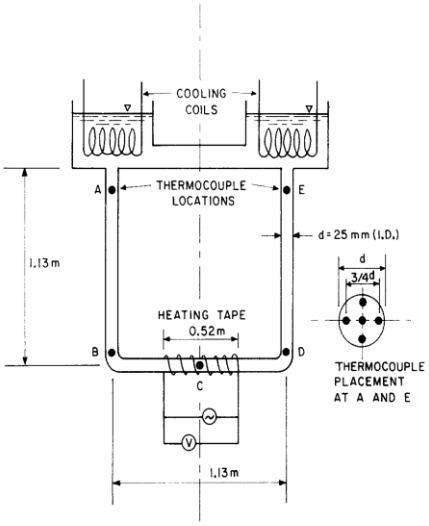

Open-type rectangular NCL [15]

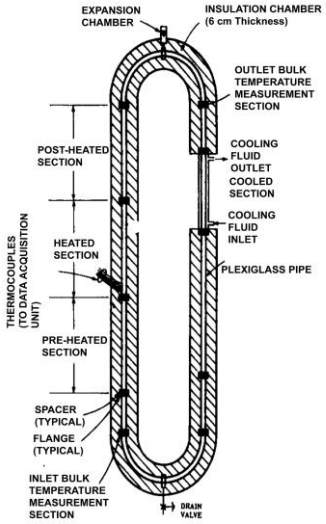

Semi-rectangular NCL with vertical heat transfer sections [16]

Fig.1.2 Various Geometric Configurations of Natural Circulation Loop

1.2.3 Advantages and disadvantages of NCL

It is common in nature that every system has its own advantages and disadvantages. Likewise, NCL also has its typical advantages like simple configuration, easy to construct, less maintenance because of the absence of the pump. However, NCLs are mainly susceptible to unstable operation and high sensitivity to operating conditions due to the completely coupled nature of flow and temperature fields. They have a specific start up procedure. Due to the absence of pump, the driving head is very less. The major advantages and disadvantages are tabulated in table 1.1.

Table 1.1: Advantages and disadvantages of NCL

Advantages	Disadvantages
Simplicity and low cost	Specific start-up procedures required
More thermal inertia	Maximum power per passage is less
Uniform flow distribution	Potential instabilities
No pumps required	Driving head is less
Better two phase characteristics	Low critical heat flux

1.2.4 Applications

The conventional NCL with loop-type design has the main advantage of the distinctive location of source and sink. Hence NCLs have been employed very successfully in a wide variety of engineering and industrial applications mention a few of them are:

- Solar heaters (Close [17]; Mertol et al. [6]; Ong [18]; Shitzer et al. [19]; Zvirin et al. [20]; Koca et al. [21])
- Geothermal energy extraction (Kreitlow et al. [22])
- Nuclear power generation (Heisler [5])
- Turbine blade cooling (Cohen and Bayley [9])
- Thermosyphon reboilers (McKee [7]; Sarma et al. [8])
- Electronic chip cooling (Tuma et al. [23])
- Chemical process industries (Joshi, [24])
- Refrigeration (Kiran et al. [25])
- Recently in the field of liquid fuels, Gumus et al. [26] proposed a model to improve combustion performance as well.

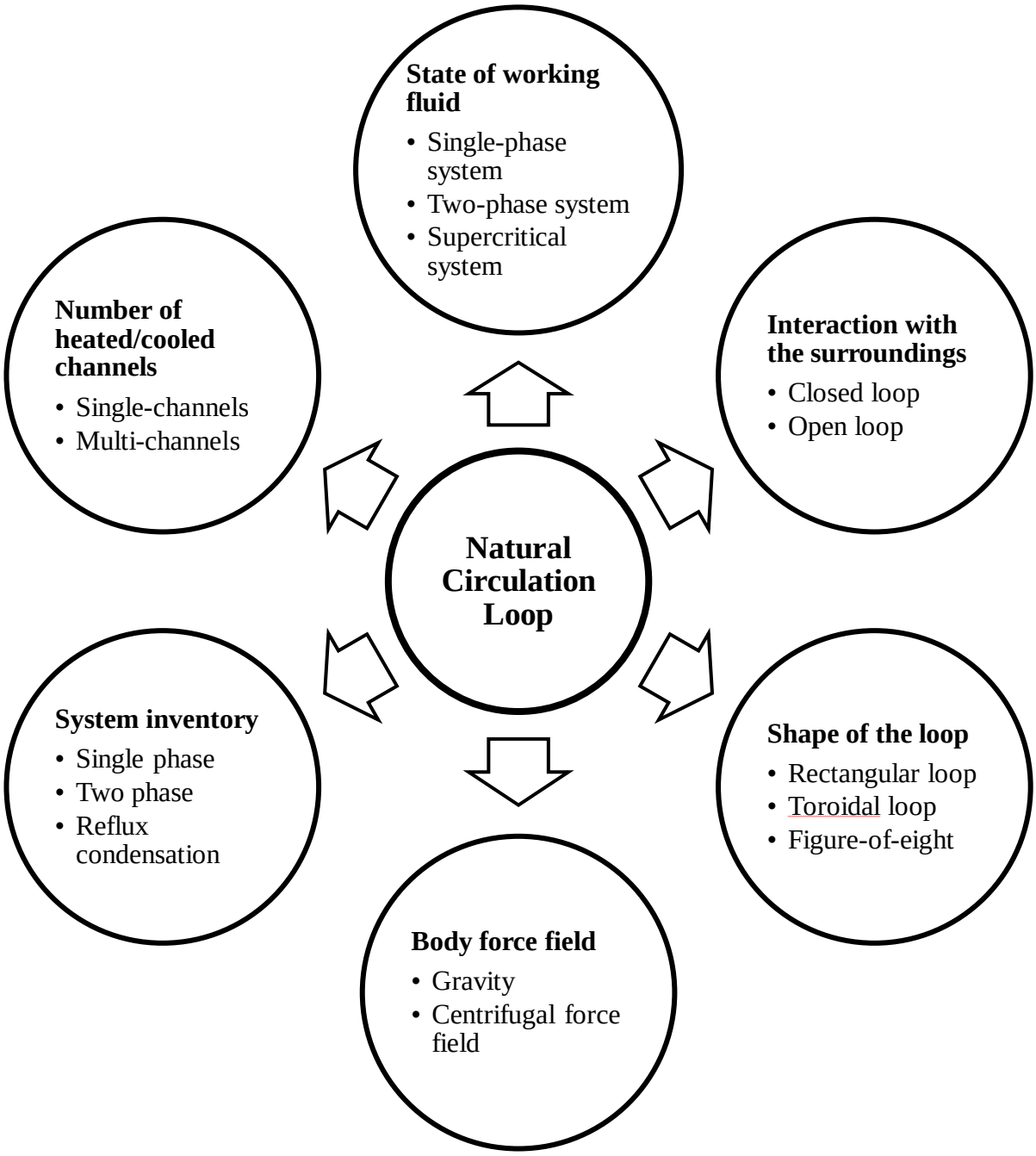

Fig. 1.3. Classification of NCL

1.3 Two phase NCL

Two phase NCL is one type NCL comes under the state of the working fluid classification. In the NCL, loop fluid may or may not undergo a phase change process. If the fluid in the loop doesn't undergo phase change, then it called as single phase NCls. It is to be noted that supercritical NCLs also comes under the category of single phase NCL. The single phase liquid

NCLs has it's own constrain w.r.t loop fluid saturation point. If the heat capacity at the source is increased or modifying the geometrical parameters in the loop leads to the phase change process, i.e. either boiling or flashing in the system. When loop fluid local temperature reaches to the saturation temperature corresponding to the pressure in the heater, boiling starts otherwise loop fluid is in the subcooled state at heater exit. Further, when the loop fluid local pressure reaches the saturation pressure corresponding to the local temperature flashing will take place. This flashing phenomenon occurs in the riser section due to pressure drop. As the circulating fluid undergoes phase change in one of the section and condensation or phase separation at other section, the loop is seem to be filled with high density single phase fluid at the heat sink and low density two phase mixture at the heat source. This substantial density differences in the loop improve the buoyancy effect resulting more heat transfer. Fig. 1.4 shows the schematic diagram of a two phase NCL. It is same as single phase NCL (Fig. 1.1 (a)) where the fluid state differs in heater or riser sections. The loop fluid in the evaporator extracts heat from the source and increases the temperature. Depending upon the imposed heat input, loop fluid undergoes phase change in either the heater or riser section and density reduces. Due to low density, the two phase mixture moves upwards up to the condenser through the riser. In the condenser, loop fluid rejects the heat and the resultant high density condensate flows through downcomer and reaches the evaporator due to gravitational force, the cycle repeats. This always situates riser is filled with low density two phase mixture and downcomer with high density single phase liquid in the loop.

Single-phase NCLs are always limited by the saturation-point criterion of the working fluid. This limitation can be overcome by using two phase NCL. Due to the higher latent heat of vapourisation values, for the same mass of working fluid, more amount of heat can be extracted from the source. In two phase NCL, the phase change of loop fluid depends on the quantity of heat extracted, thermos-physical properties of the fluid and loop configuration.

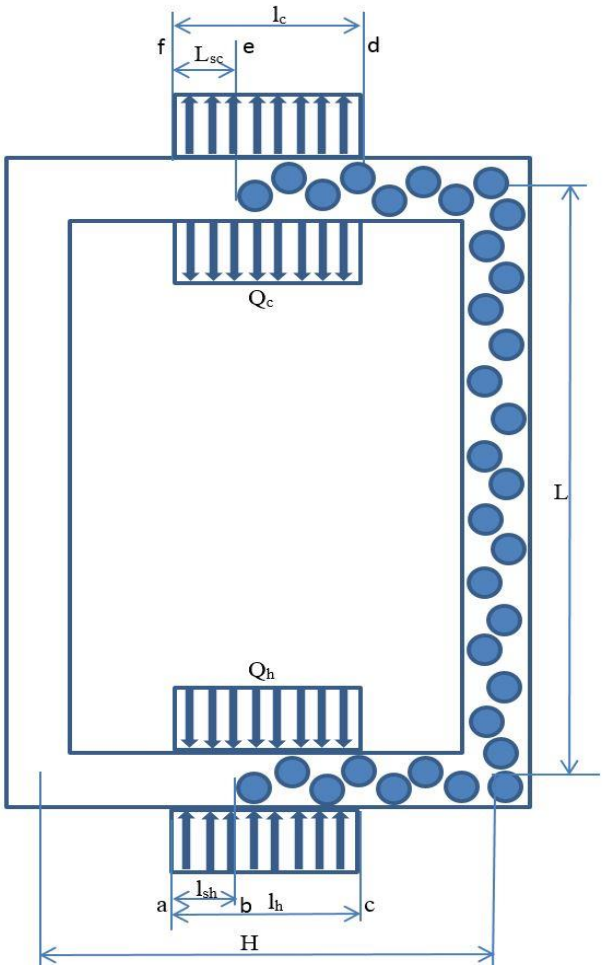

Fig. 1.4 Schematic diagram of two phase NCL

1.4 Boiling of nanofluids

It is noteworthy to know some basics of flow boiling phenomena in water and nanofluid for a clear understanding of the thesis work/report.

1.4.1 Boiling

Boiling is a process where the fluid undergoes phase change at its saturation temperature from liquid to vapour by absorbing heat. While the same phase change process occurs if the pressure applied to a hot liquid is reduced and the phenomena is called flashing. Boiling can be categorised into two types; pool boiling where the fluid is in stagnation state, flow boiling where the fluid flows inside or over a hot surface. There is a distinct difference in the heat transfer mechanism in the pool and flow boiling. In pool boiling only the fluid and heated surface characteristics influences the heater transfer mechanism, whereas in flow boiling,

together with fluid and heated surface characteristics, flow characteristics also influence the heat transfer mechanism.

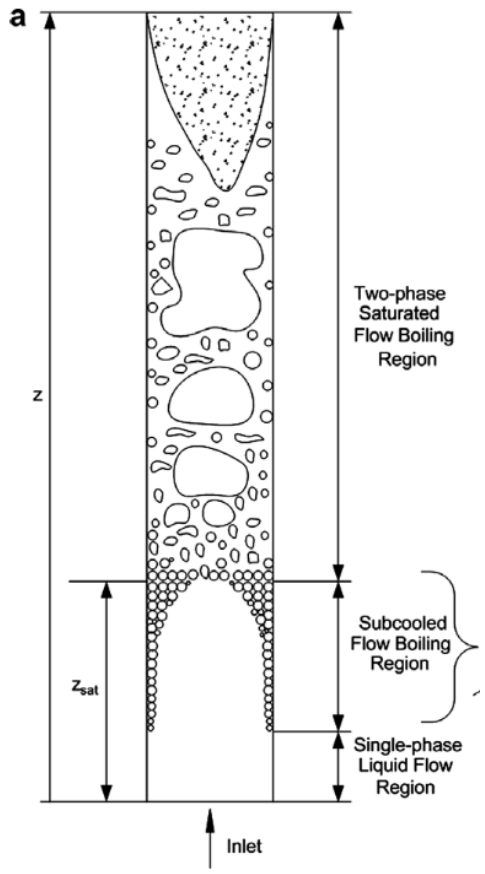

Fig.1.5 Heat transfer regions during the vertical flow boiling [27]

1.4.2 The flow boiling heat transfer regions

Fig. 1.5 shows a diagrammatic form of forced flow boiling process for a vertical tube and corresponding heat transfer regions. In the beginning, the liquid is in subcooled state at heater inlet, heat transfer take place by single phase forced convection in this region. The subcooled liquid is being heated up while the corresponding wall temperature remains below that necessary for nucleation. Along the heated wall at some point, the wall temperature reaches required superheat to generate bubbles. The primary formation of bubbles is known as the onset of nucleate boiling (ONB). The bubble formation takes place in the subcooled liquid (bulk fluid temperature is below the saturation temperature), but the heater surface is hot enough to form bubbles. The formed bubble condense as they move out of the developing saturation boundary layer. In the subcooled boiling region, once the wall achieves required superheat,

active nuclei bubble generates at preferred cavities only. The increase in the temperatures of the wall and bulk fluid across the heater section increases the active nuclei sites, so the heat transfer by nucleate boiling increases and the single-phase convective heat transfer decreases. Further downstream of the heater, bulk fluid reaches to saturation temperature, and the saturated boiling region starts. In this region heat transfer takes place by nucleate boiling. The continuous generation of vapour in the saturated boiling region transits the flow pattern from the bubble or slug to annular flow. This implies that there is a fundamental transition of heat transfer mechanism from boiling to evaporation.

1.4.3 Flow patterns

The liquid and vapour spatial distribution is called as flow pattern. The respective distribution of gas (vapour) and liquid two phase flow inside a tube for a co current up flow possess wide range flow patterns as shown in Fig. 1.6.

Bubble flow

The gas phase is distributed in the form of detached bubbles in the continuous liquid phase and appears as bubble flow.

Slug flow

The vapour (gas) void fraction increases by means of more detachment of bubbles. These bubbles continue to grow and coalesce with other bubbles to form a bullet shaped bubble (Taylor bubble/vapour slug). This slug is surrounded by a thin liquid film between them and the tube wall and is separated from one another by plugs of liquid.

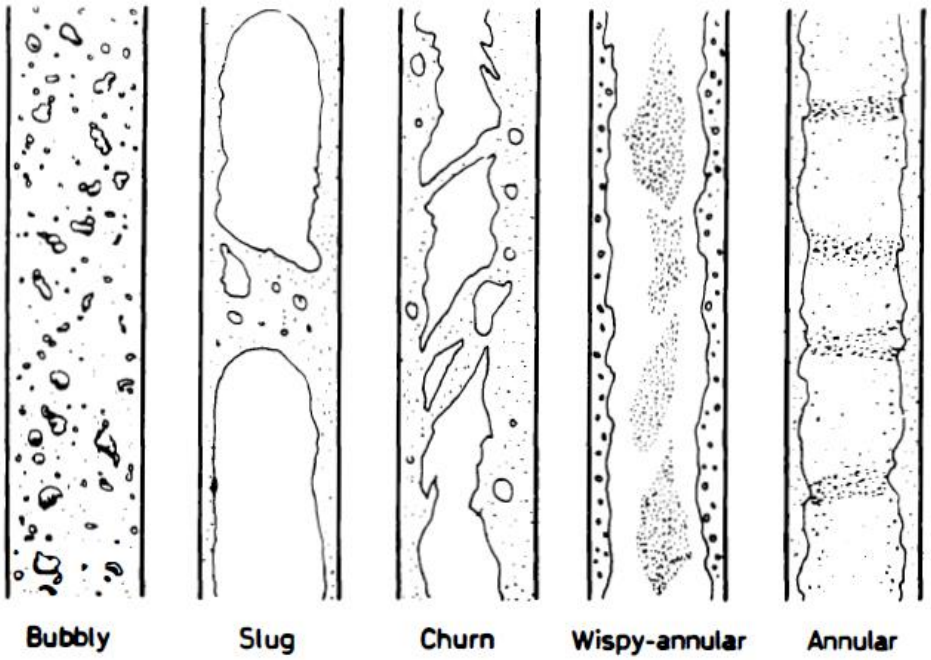

Fig.1.6 Flow patterns in vertical flow [28]

Churn flow

Further increasing the velocity of a slug flow causes the structure of the flow to become unstable. The relative parity between the gravitational and frictional forces act in opposite direction on liquid Taylor bubble and so Taylor bubbles are unstable, fragile, and reform to small bubbles, cap shaped bubbles with liquid coexisting In churn flow, the vapour and liquid interface is chaotic in nature, and net flow moves upwards.

Annular flow

Once the interfacial shear of the high velocity gas on the liquid film becomes dominant over gravity, then liquid film flows on the channel wall (forming an annular ring of liquid) while the gas flows as a continuous phase up in the center of the tube. The flow core is disturbed by high frequency waves and ripples and liquid may be entrained in the gas core as small droplets. This flow regime is particularly stable, and it is the desired flow regime for high-velocity, high-quality two-phase fluid flow.

Wispy annular flow

The small gas bubbles aerate a further increase in flow rate. The liquid in the film and the entrained liquid phase appears as large droplets which have agglomerated into long, irregular filaments or wisps.

1.4.4 Nanofluid boiling

In boiling, heat transfer occurs by the fluid that undergoes a phase change from liquid to vapour and vice versa. It is known that more heat transfer is possible in such cases due to the latent heat of vapourisation. Hence the boiling heat transfer concept is used in various cooling applications. But the rapid change in science and technology increases the heat dissipation rate in devices. So, there is a need for the cooling system which provides high heat transfer coefficient (HTC) and high critical heat flux (CHF). The increase of HTC makes the boiling systems more energy efficient, which results in a reduction in the size of the devices. In addition, high CHF is also required in order to dissipate very high heat flux from the heater before reaching the dry out point.

One of the novel techniques to increase HTC and CHF is to use of nanofluids in the boiling process [29], [30]. Nanofluids offers exciting new possibilities to enhance heat transfer performance compared to pure liquids. So, the nanofluids are treated to be next-generation promising heat transfer fluids. Nanofluids are this kind of fluid where nano sized (<100 nm) solid particles are suspended in base fluid, and it was first reported by Choi in 1955 [31]. The basic concept is to introduce highly conductive nanoparticles into the inherently poor conductive conventional working fluid to enhance the superior characteristics such as high specific surface energy, higher thermal conductive capabilities and enhanced thermos-physical properties. Which are favourable characteristics to use nanofluids in NCLs [21], [32], [33]. The base fluids used in nanofluids are water, refrigerants, and refrigerant/oil mixtures, while solid nanoparticle materials used are metals (Al, Cu, Ag) and metal oxides (Cuo, Zno, Al_2O_3, CeO_2, TiO_2 & SiO_2).

Since then, several studies have been conducted; most of the available studies mainly focused on their thermo-physical properties such as conductivity, viscosity, specific heat, etc. In recent times, research on nanofluids boiling has grabbed attention. Researchers are

addressing the boiling behaviour of the nanofluid [34], [35], and it is very much different from water. It is also observed that there is a paucity of experimental studies on nanofluid flow boiling. Based on the available literature, a group of researchers concluded that nanofluids deteriorate the heat transfer [36]–[39]. But many other researchers [40]–[46] have reported that nanofluids enhance the heat transfer. The common reason mentioned for enhancement and deterioration was the same, i.e. deposition of nanoparticles on the heater surface. The modified heater surface characteristics (surface roughness and wettability) along with the presence of nanoparticles in the boiling fluid, significantly influence the heat transfer. So use of nanofluid in two phase NCL system should be an important research topic, and it potentially improves heat transfer and performance of the system.

1.5 Structure of thesis

- Chapter 1 presents a brief introduction to natural circulation loops, flow boiling phenomena and state of the art on nanofluid boiling.
- A comprehensive review of important literature related to present research work is presented in chapter 2. This is accompanied by the research gaps identified, and conclusions drawn from the literature review are furnished. All the major objectives and the scope of the research work are also included.
- A one-dimensional (1-D) mathematical model developed for two phase natural circulation loop filled with water and nanofluid. By using this model, the effect of geometrical and operating parameters on the natural circulation loop behaviours is presented in chapter 3.
- In chapter 4, the influence of particle concentration, mass flux and heat flux on flow boiling phenomena of Al_2O_3/water nanofluid is experimentally analysed/studied.
- The test rigs have been designed based on the numerical results. Experiments conducted by filling the natural circulation loop with water and nanofluid. The loop performance is analysed by varying the operating parameters (heat input and heat sink condition) is presented in chapter 5.
- Chapter 6 presents the general conclusions and scope for future work

1.6 Closure

The present chapter elaborates the background and motivation governing the research problem taken up for investigation in the present thesis. It also documents various relevant features of all the chapters of the thesis to provide a clear idea to the reader.

Chapter 2

Literature survey

Chapter 2

Literature survey

The present chapter briefly discusses the state of art work done on natural circulation loops (NCLs) with major focus on two phase NCLs. This chapter covers the major contribution of researchers in experimental and numerical studies and various methods to simulate two phase NCLs. In addition to this, detailed studies on boiling behaviour of nanofluid are presented.

2.1 State of art on natural circulation loop

In NCL, energy is transported from a high temperature source to the low temperature sink in the absence of a mechanical device like a pump. The absence of mechanical elements in NCLs exhibits highly reliable performance at an economical cost. Hence NCLs are used in a wide range of engineering applications such as solar heaters [17] [6], cooling of turbine blades [3], nuclear reactors [4], [5] etc. Zvirin [47] and Greif [48] have given the various possible applications by using NCLs. The NCLs can be classified as per the fluid state such as single phase NCL, two phase NCL and supercritical NCL. From the past few decades, there is sufficient amount of work cited in the open literature for single phase NCLs. Some of the review articles provided complete information to understand the phenomena [47][48][49][50] and the progress of single phase NCL [51]. However, the single-phase NCLs are always limited by the saturation-point criterion of the working fluid. This limitation can be overcome by using two phase NCLs. Due to the higher latent heat of vapourisation values, for the same mass of working fluid, more amount of heat can be extracted from the source. In two phase NCL, the phase change of loop fluid depends on the quantity of heat extracted, thermo-physical properties of the fluid and loop configuration.

In two phase NCLs the circulating loop fluid undergoes a phase change, i.e. either boiling or flashing at one section and condensation or phase separation at some other section in the loop. This keeps loop fluid filled with low density two phase mixture in the riser section and high density single phase liquid in the downcomer section. The large density difference between the single phase liquid and two phase mixture of the fluid creates stronger buoyancy forces. This results in large circulation and enhancement in the loop performance. However, the complexity in boiling, condensation process and two phase flow phenomena makes the

design difficult, especially in NCL, due to absence of pumps. So, in this aspect, investigation of the two phase NCL provides greater challenges to frontiers. It was observed from the literature that past two decades had witnessed a considerable amount of research in two phase NCL. The researchers numerically and experimentally analyse the NCL modelling and performance by varying the operating and geometrical parameters. It is truly an arduous job to have an elaborate discussion on each of the available studies in a few pages. Hence, in the present section, efforts have been made mention some of the most significant contributions from the literature and to generate some idea about the recent developments in two phase NCLs.

2.1.1 Experimental and theoretical/numerical studies on two phase NCL

Some applications like nuclear reactor core cooling [4], [5] and electronic chip cooling [23] requires a critical zero tolerance while they are in use. So, the designing of two phase NCLs is a challenging task due to the enormous promise and intricate thermal-hydraulic phenomena of two phase flows. In the open literature, various experimental and numerical models are presented. Below are some of the important studies discussed in recent times.

Earlier the researchers Piret and Isbin [52], Johnson [53], Smith [54], Shah [55], Johnson and Yukawa [56] are/have experimentally determined circulation rate in the thermosyphons. Kamil et al. [52] proposed a correlation by including the Lockhart–Martinelli parameter (X_{tt}). This correlation successfully estimates the experimental data of the nine different working fluids within an error margin of ±20%. Later Gartia et al. [57] proposed a generalised correlation in non-dimensional form for two phase NCLs.

Lee and Mital [58] experimentally investigate the heat transfer performance of a two-phase NCL. Experiments conducted using R-11 and water, which show similar results. Since the boiling point of R-11 is relatively very low as compared with water, it is a suitable fluid for low-temperature applications. For their analysis system parameters such as the quantity of the working fluid, heat flux, mean operating pressure and heated length to cooled length ratio are varied. From the results, they concluded that the heat transfer coefficient (HTC) strongly depends on the loop pressure and temperatures and is less dependent on the mass flow rate. The decrement in the evaporator to condenser length ratio enhances the H. They proposed a theoretical analysis to predict the maximum heat transfer rate.

Chen et al. [59] performed experiments on a two phase square NCL with water and steam as working fluid. In their experiments, heat input and working fluid charging level are varied. Results showed that pressure and temperature increases with the increase of heat input for a fixed working fluid charge level. It is also observed that, at the low percentage of working fluid charge levels, higher working fluid temperatures are obtained in the loop. This advocates two phase NCLs early undergoes dry out as the working fluid charge level decreases.

Chowdhury and Kaminaga [60] conducted experiments by using Freon R-113 in a vertically small diameter tube having inner diameter 1.45 mm and length 100 mm at a pressure range of 19-269 kPa under natural circulation condition. The flow path is almost annular except at entrance due to the operating conditions. Results show that there is no significant effect in increasing heat transfer for a pressure range of 19-269 kPa.

Ali and Alam [61] experimentally studied the influence of heat flux, submergence level, inlet subcooling and circulation rate on boiling heat transfer in a thermosyphon reboiler. They used water, acetone, and ethylene glycol as working fluids. They developed a correlation for steady-state Reynolds number relating to Peclet number, subcooling number, and liquid level. Their correlation predicted the experimental data with a maximum reported deviation of ±40%.

The pioneering work on CO_2 based NCLs is done by Kiran kumar et al. [62], [63]. The authors developed a numerical model to investigate the performance of CO_2 based NCLs. Authors considered heat exchangers for the heat source and heat sink. They also studied the influence of system pressure, i.e. CO_2 inventory on the loop performance. By fixing the parameters such as external fluid temperatures and external fluid flow rates and varying the CO_2 inventory, the loop is either in single phase state or two phase state. For two phase NCL homogeneous model is used. Influence of different two phase viscous models on loop performance is also studied. From the results, it concluded that the heat carrying capacity of the loop increases with the decrease of loop pressure and reaches a peak value. Then after starts decreasing with a further decrease in loop pressure. The same authors [64] conducted experiments on a CO_2 based NCL by varying the CO_2 inventory. Depending on CO_2 inventory, the loop fluid (CO_2) is in the vapour state, liquid state and vapour- liquid state. From the experiments, they concluded that the two phase NCL had taken more time to reach steady state as compared with single phase NCLs. The experimental results also reveal that the system has

an optimum CO_2 inventory where the maximum heat transfer rate obtained. Similar to this, Rao et al. [65] developed a numerical model for two phase natural circulation loop with end heat exchanger.

Chang et al. [66] conducted experiments on two phase loop thermosyphon (TPLT) at sub atmospheric pressure. The thermal performance of TPLT is examined by using the overall thermal resistance, boiling heat transfer and instabilities. From the results, it is observed that the total thermal resistance decreases with the increase of heat flux. This happened because of a decrease in evaporator thermal resistance and boiling instability thermal resistance. It is better to suppress the boiling instability thermal resistance for product advancement. The extension to this work done by Chang and Lin [67] by providing scale imprints on the boiling surface to enhance TPLT performance. It is observed that the scaled boiling surface follows the smooth boiling surface flow boiling transition pattern. In the scaled surfaces nucleation site increases, so the bubble departure rate also increases, which leads to the increase of heat transfer rate. It is also observed that the segmentation of Taylor bubbles significantly reduces the constituent thermal resistance triggered by boiling instabilities and enhance the thermal performance of scaled boiling surface TPLT.

Wang et al. [68] analyse the performance of two phase NCL with Thermo Electric Generator (TEG). The electricity produced by the TEG supplied to a pump and a group of agitators and improves fluid circulation and heat transfer. Their results indicate that circulation flow and heat transfer are markedly enhanced. Liu et al [69] experimentally studied the influence of filling ratio and inclination angle on heat transfer performance and instability characteristics of a NCL. Under the high filling ratios, the advantage is avoiding the possible evaporator dryout in the loop. This happened because of the heat transfer capacity is limited due to the phase-change suppression and pressure soaring. Whereas at moderate filling ratio heat transfer capacity increases, but the geyser boiling instability occurs at a large range of input heat flux. Under the low filling ratios, the heat transfer capacity is the highest, while the transient local “Near-dryout” is easier to occur.

Cao et al. [70] numerically and experimentally studied the role of refrigerant column height in the downcomer in a TPLT system. It is found that flow resistance, working pressure and the amount of liquid refrigerant driven by the rising vapour influences the refrigerant

column height in the downcomer. The intensity of impact of these factors may change when a TPLT system's geometric parameters and the filling ratio are different. Zhu and Yu [71] experimentally studied the start-up performance of two thermosyphon loops. The experiments conducted on two-phase loop thermosyphon with separator assisted (STLTP) and the reservoir two-phase loop thermosyphon (RTLTP). From the results, it is observed that the stabilized time for RTLTP is 420s shorter than the STLTP. The oscillations during start-up for RTLTP is less as compared with STLTP, due to lower two phase pressure drop.

Zahang et al. [72] experimentally analysed the transient behaviour dual evaporator thermosyphon loop. The experiments conducted at uniform and non-uniform heating conditions. From the results, they concluded oscillation and periodical bypass flow occurs under high power uniform heating condition.

Some other researchers [73]–[76] tried to develop models, design methods and computer programs for estimating the circulation rate in the thermosyphons. On those Homogeneous equilibrium model (HEM) and drift flux model (DFM) are the most popular and produces reasonably satisfactory results. Knaani and Zvirin [77] developed a theoretical model to study the steady-state flow and heat transfer in two-phase thermosyphons. Their model predicts the multiple steady state solutions for a given range of the parameters. Duffey and Sursock [78] derived a model to predict the flow phenomena and circulation rate in PWR and BWR. The model is compared with available data, and for the PWR case, a good agreement is obtained. For the BWR a new semi theoretical correlation is derived. From the study, it concluded that the circulation rate in PWR is strongly dependent on liquid inventory and weakly dependent on power levels. Whereas in BWRs circulation rate is a strong function of liquid inventory and power levels.

Similar to the above studies the pioneering studies came from Ramos et al. [79], Chen and Chang [59], Rao et al. [80] and Nayak et al. [81] to develop models, design methods and computer programs for estimating the circulation rate in the thermosyphons/NCLs. On those Homogeneous equilibrium model (HEM) and drift flux model (DFM) are the most popular and produces reasonably satisfactory results. In this context, Ramos et al. [79] analysed single phase and two phase NCLs with variable cross section area. In their analysis, both the loops exist multiple solutions, but the reasons are different. Buoyancy and viscosity effects lead to

the two solutions in single phase NCLs. Whereas in the two-phase NCLs, non-linearity of the inertia forces permits the existence of two possible solutions. Similarly, 1D approach is used by Lin and Faghri [82] in two-phase thermosyphon with tube separator, which resembles an NCL. From the study, it concluded that the diameter of the tube separator has a strong influence in mass flux.

Rao et al. [80] numerically investigated the performance of two-phase NCL by using homogeneous equilibrium model (HEM) and thermodynamic equilibrium drift flux model (TEDFM). In their analysis, a rectangular two-phase NCL with vertical heater and condenser orientation considered with an assumption of thermodynamic equilibrium between two phases. They also studied the effect of different parameters such as loop height, heater inlet subcooling and heat flux on the loop performance. As an extension of this, Basu et al. [83] proposed a new model by considering the non-thermal equilibrium condition between the phases to predict the performance of two-phase NCLs. The reported results showed a satisfactory level of conformity with experimental data.

Goudarzi, and Talebi [84] developed a model to analyse the stability of the double channel two phase NCLs. From the analysis, the authors concluded that single phase NCL has two instability regions. It is also observed that the stability of double channel two phase NCL is sensitive to the inlet temperature and power. NCL is more stable at lower power region and vice versa, and increasing inlet subcooling leads to unstable NCL.

The steady and transient behaviour of two phase thermosyphon is numerically studied by Bodjona et al. [85]. In their numerical model one-dimensional space discretization of the loop is considered and methanol used as loop fluid. The governing equations are solved by using HLLC Riemann solver. Simulations are carried out by varying the heat load at the evaporator. The numerical results show that the model successfully predicts the behavior of the loop and reveals the different mechanisms of energy storage in its different forms when thermal load is applied. Similarly Braz Filho et al. [86] used RELAP5 solver to study the two phase NCL.

Vijayan et al. [87] analysed various void fraction and two phase pressure drop correlations in two phase NCLs. 33 void faction correlations and 14 pressure drop correlations are considered in this study. Among the all void fraction correlations, 14 correlations are found to be satisfactory, among those 14 correlations Chexal et al. [88] correlation is a better one. Later assessment of pressure drop correlations done by considering the Chexal et al. [88] void fraction correlation and Saha and zuber [89] onset of subcooled boiling model. It was observed that most of the correlations were predicting the pressure drop close to each other.

In the NCLs at a low pressure start-up condition, heat addition in the core is not sufficient to boil the loop fluid. But the loop fluid gets heated up to some level that can cause adiabatic flashing in the riser section, downstream of the heating zone. In those NCLs the driving force for circulation is created mainly by flashing. This phenomena is getting importance in the operation of two-phase natural circulation loop and is recognized by many researchers Chatoorgoon [90], Avdeev [91], Inada and Ohkawa [92], Van Bragt et al. [93]. Use of HEM with different modification and DFM models successfully applied to the flash induced flows. Recently Dewangan et al. [94] and Sudheer et al. [95] considered flashing phenomena in two phase NCLs. The flash induced vapour quality has a significant influence on loop performance.

Tanimoto et al. [96] conducted experiments on two NCL to study the flashing characteristics. The flashing characteristics observed are the period and duration of flashing, peak flow rate, amount of flow carryover per flashing, lowest-peak liquid level within the condenser, and the peak void distribution in the riser section. Experiments conducted by varying the parameters such as heater power input, valve friction at the heater inlet, condenser cooling, degree of subcooling at the heater inlet, and the heat loss to the surroundings. From the results, it is observed that the heater power input, valve friction, and the rate of heat removal by the condenser showed a significant effect on flashing. The remaining parameters seemed to be relatively marginal.

Dewangan et al. [94] numerically studied the influence of flashing in two phase NCLs. HEM and DFM models used in their study. By considering flashing phenomena, the loop fluid circulation rate substantially reduced. But at the same time, the loop is more stable against

ledinegg instability. It is also observed that the flashing phenomena is predominant at low pressure and low heat flux conditions.

Sudheer et al. [95] developed a numerical model to study the thermo-hydraulic behaviour of two phase NCL by considering the flashing phenomena at atmospheric and sub-atmospheric conditions. From their results, it is observed that, as the system pressure decreases from atmospheric to sub-atmospheric, the loop fluid experiences early flashing or boiling, hence at lower heat fluxes the loop exhibits higher density gradients. So sub-atmospheric NCLs have high mass flow rates at lower heat fluxes as compared to atmospheric loop.

2.2 State of art on boiling of nanofluids

The increase of heat dissipation rate in the devices needs a cooling system that provides a high heat transfer coefficient (HTC) and high critical heat flux (CHF). The increase of HTC makes the boiling systems more energy efficient, which results in a reduction in the size of the devices. One of the novel techniques to increase HTC and CHF is the use of nanofluids in place of base fluid (water) in the boiling process. Nanofluids are a kind of fluid where nano sized (<100 nm) solid particles are suspended in the base fluid. It is observed from the literature that the past two decades have witnessed a considerable amount of research on nanofluids. However, research on nanofluids was mainly focused on their thermo-physical properties such as conductivity, viscosity, specific heat etc. Some of the review articles address the complete information of the thermo-physical properties of nanofluids [97]–[100]. In recent times, research on nanofluids boiling has grabbed attention. Studies available in open literature reveals that nanofluids are successfully used in the boiling process [37], [38], [101], [102]. From the literature, it is also observed that most of the research has been focused only on pool boiling heat transfer [102]–[105] as compared with flow boiling. In this context, some of the most significant contributions from the literature are discussed here.

Sarafraz et al. [103] showed that there was a considerable enhancement in pool boiling HTC by using CNT and functionalized CNT nanofluids. Liu et al. [104] reported 50% enhancement in pool boiling HTC by using CuO/water nanofluids. Shi et al. [106] conducted experiments using Al_2O_3/water nanofluid and noticed that pool boiling HTC is increased by up to 64%. Similar kind of enhancement of pool boiling HTC was observed by Sarafraz et al. [40],

[41] various studies reported that nanofluids could deteriorate the boiling performance. Researchers such as Coursey and Kim, [107] Bang and Heung Chang [108] and Sajith et al. [105] conducted experiments by using Al_2O_3/water nanofluids and the common observation was deterioration in pool boiling HTC. This was due to scale formation by the deposition of nanoparticles on the heater surface. Similarly, Kim et al. [102] also observed a reduction of pool boiling HTC for CuO, ZrO_2, SiO_2 and Al_2O_3 water-based nanofluids.

Similar to pool boiling, research results reported by various researchers on flow boiling of nanofluids are contradictory [37], [39], [109], [110]. For instance, Peng et al.[110] conducted experiments on refrigerant based nanofluid (CuO/R113). In their experiments, nanoparticle concentration varied from 0 to 0.5 by wt. %, heat flux varied from 3.08 to 6.16 kW/m^2 while inlet vapour quality varied from 0.2 to 0.7. Their experimental results revealed that the addition of nanoparticles to the base fluid enhances HTC by an average of 29.7%. The credible reason for HTC enhancement as reported by the authors was due to the reduction of the boundary layer. The presence of nanoparticles in base fluid disturbs the boundary layer formation, and also nanoparticles form a molecular adsorption layer on the surface of the heating section. The combined effect of these two factors reduces the boundary layer thickness. In another experimental study, Rana et al. [34], [111] experimentally investigated the flow boiling behaviour of ZnO/water nanofluid with different volume concentrations. HTC was seen to increases with increasing nanofluid concentration. They visualised the heater surface characteristics by using Scanning Electron Microscope (SEM) and observed that the boiling surface is changing in each experimental run. They reported that the enhanced boiling heat transfer might be due to the heater surface modification and an increase in thermal conductivity of nanofluid.

In other studies, Kim et al. [42] experimentally investigated flow boiling heat transfer characteristics of ZnO/water, diamond/water and Al_2O_3/water nanofluids with particle concentrations of 0.001, 0.01 and 0.1 vol%, respectively. They conducted experiments at atmospheric condition while the fluid was flowing in a vertical direction in 5.33 mm of stainless steel with a length of 100 mm. The mass flux was varied from 1500 to 2500 kg/m^2-s and heat flux from 100 to 7500 kW/m^2. It was observed that the HTC of the nanofluids was not more than 20% compared to the water. Sun and Yang [43] experimentally studied the horizontal flow boiling heat transfer characteristics of nano-refrigerants. In their experimental

analysis, Al, Al_2O_3, Cu and CuO nanoparticles were used by varying wt. concentration 0.1, 0.2 & 0.3 % with R141b as base fluid. From the results, it was noticed that HTC for nano refrigerants is enhanced with the increases of velocity, concentration and quality. The highest enhancement was observed for Cu-R141b nano-refrigerant compared to other fluids considered in this study. Seung et al. [44] experimentally observed the critical heat flux enhancement in nanofluids. In their experimental study Al_2O_3/water and SiC/water nanofluids at 0.01 vol. % were used. From their results, they found that SiC nanofluid exhibits more CHF enhancement followed by Al_2O_3/water nanofluid and water. They also reported that the contact angle of the inner surface reduced due to deposition of nanoparticles on the heater surface.

Similar studies were reported in the open literature. In this context, Prajapati and Rohatgi [45] conducted experiments in the annular test section by using ZnO/water nanofluids for different concentrations. From their results, they concluded that heat transfer increases with heat flux, mass flux and concentrations of the nanofluid. The reasons attributed to heat transfer enhancement are higher thermal conductivity, the surface roughness of the heater rod and Brownian motion of the nanoparticles. Sarafraz et al. [46] experimentally identified that MgO/therminol-66 nanofluids offer more heat transfer during the flow boiling compared to the base fluid. In their experiments, they varied the wt. concentration of nanofluids between 0.1%-0.3% and found that the maximum heat transfer enhancement of MgO/therminol-66 nanofluids for the concentrations of 0.1%, 0.2% and 0.3% was 23.7%, 16.2% and 13.3% respectively. However, there were other contradictory results by the same authors [39]. The authors experimentally investigated the influence of operating parameters such as heat flux, mass flux and volume concentration of nanofluid. Experiments were conducted in a closed test loop with Al_2O_3/water nanofluid by varying volumetric concentrations of 0.5%, 1% and 1.5%. For experimental operating conditions, they observed two heat transfer regimes (forced convection and nucleate boiling). The heat transfer increased with a volume concentration of nanofluid in the forced convection region and deteriorated in the nucleate boiling region. The credible reason for heat transfer deterioration is given by the nanoparticle deposition on the heater surface, which contradicts earlier studies.

Based on the available literature, a group of researchers concluded that nanofluids deteriorate the heat transfer [36]–[39]. But many other researchers [40]–[46] have reported that nanofluids enhance the heat transfer. The common reason mentioned for enhancement and

deterioration was the same, i.e. deposition of nanoparticles on the heater surface. The modified heater surface characteristics (surface roughness and wettability) along with the presence of nanoparticles in the boiling fluid, significantly influences the heat transfer.

2.3 Gaps identified from the literature review

- Though numerical and experimental studies on water based NCLs were carried out by many researchers, studies on two phase NCLs with special emphasis on flow regimes are very few.
- Recently, nanofluids are successfully used in NCLs, but most of the studies on nanofluid based NCL are limited to single phase (liquid) only.
- From the open literature, it is concluded that the boiling heat transfer phenomenon of nanofluid is significantly different from that of water. However, studies on effect of boiling phenomenon difference on heat transfer (especially in nanofluid based NCLs) are almost scarce.

2.4 Objective and scope of the present research work

The objective of the present work is:

1. To develop a mathematical model for two phase NCL filled with water and nanofluid, in order to study the effects of geometric and operating parameters on its performance.
2. To study the nanofluid flow boiling behaviour under different operating conditions.
3. To study the flow behaviour of water filled NCL under flow boiling conditions.
4. To study the flow behaviour of nanofluid filled NCL under flow boiling conditions.

2.5 Research approach

In the current research, numerical and experimental investigations have been carried out to evaluate the thermal performance of the two phase natural circulation loop filled with Al_2O_3/water nanofluid by varying the particle concentration. A comparative study has been conducted on NCL with water and nanofluids.

1. (a) A mathematical model is developed and systems of equations are solved by the developed in-house code (in MATLAB).

   (b) Using the developed mathematical model, the influence of geometrical and operating parameters are analysed.

2. Flow boiling experimental set up is designed and fabricated to study the nanofluid flow boiling behaviour.

3. Based on the numerical result, an NCL test rig is designed and fabricated. Experiments are conducted to study the effect of operating parameters such as heat input, particle concentration, external fluid temperature and mass flow rate, etc.

4. Flow visualisation studies are carried out using the camera, and images are analysed to study the transition of flow boiling regimes for water and nanofluid.

2.6 Conclusion

A comprehensive review of the literature concerning two phase natural circulation loops and nanofluid boiling phenomena has been provided. From an exhaustive exploration of literature, the various parameters that influence thermal performance of NCL are known to be (i) geometrical and operating parameters and (ii) the properties of the working fluid. In conclusion, the factors that are useful and provide the appropriate background information for consideration to the present research problems have been provided. The different principal objectives of current research work are provided, which provide a detailed view of the thesis. The ensuing chapters one devoted to presenting the numerical analysis on two phase NCL behaviour. In this study, a numerical model developed and validated with P K Vijayans experimental data.

Chapter 3

Numerical studies on two phase natural circulation loop

Chapter 3

Numerical studies on two phase natural circulation loop

This chapter describes steady state performance of two phase natural circulation loop (NCL). A numerical model is developed to analyse the thermo-hydraulic behaviour of a two phase NCL. One dimensional approach is used in this study i.e., fluid is assumed to be perfectly mixed (uniform velocity) at any cross-section. To maintain the saturation state locally, additional vaporization (flash evaporation or flashing) takes place and the void fraction of the mixture increases continuously. So the influence of flashing phenomena in the loop is accounted in the proposed model. Then after the influence of various geometrical parameters such as heater and condenser orientation and position, diameter of the NCL and its individual parts and height of the loop are analysed. Similar to the geometrical parameters, influence of operating parameters are also analysed. The operating parameters considered in this study are heat flux, inlet subcooling at heater section, sub-atmospheric pressure at heater inlet and addition of nanoparticles to working fluid.

3.1 Numerical modelling of two phase NCL

Fig. 3.1 shows the schematic diagram of rectangular NCL. The loop contains four distinct parts namely heater (a-b), riser (b-c), condenser(c-d) and downcomer (d-a). The heater and condenser are horizontally positioned. Circulation of the fluid takes place due to the density differences in the loop. Hence, it is always preferable to place the condenser section at an elevation than the heater to get a favourable gravity head. On the basis following assumptions two phase NCL mathematical model is developed.

1. Uniform heat flux condition is imposed on heater and condenser sections.
2. Riser and downcomer sections are perfectly insulated i.e. no heat leakage to the surrounding.
3. Minor losses due to bends and fittings are neglected and the loop is assumed to have smooth wall.
4. Axial conduction effect is negligible.

5. The spatial variation of thermo-physical properties of the working fluid is considered. The variations of pressure, temperature, velocity and quality along the axial direction are estimated as per the local working fluid state.
6. Vaporization of the liquid starts after the bulk of liquid reaches the saturation temperature. In practice, there could be substantial temperature difference across the flow area and boiling may start at the wall even when the bulk of the liquid is subcooled.
7. Thermodynamic non-equilibrium is neglected: there is no sub- cooled boiling or local superheating of the vapour phase.

3.1.1 Governing equations for different sections in the loop

One dimensional steady state continuity equation at any section in the loop is given by

$$\frac{d(\rho u A)}{ds} = 0 \qquad (3.1)$$

For uniform cross section of the loop the above equation rewritten in terms of mass flux

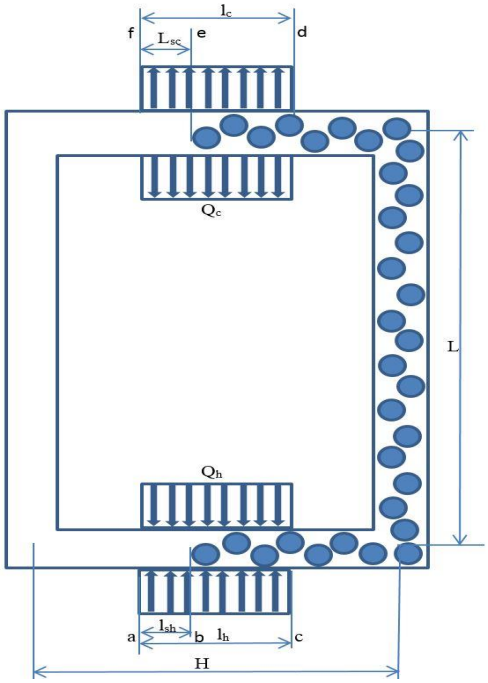

Fig.3. 1 Schematic diagram of NCL

$G = constant$, where, $G = \rho u$ (3.2)

Heater section

Either two phase mixture or sub cooled loop fluid is the initial fluid state condition for the heater. So, corresponding equations are derived according to the state of the loop fluid. Let us consider sub cooled liquid enter into the heater and absorb heat, fluid's temperature rises. If the loop fluid reaches saturation state then bulk boiling starts in the remaining part of the heater. So, either single phase liquid or two phase mixture exists at the heater exit. Hence the governing equation is derived for both single phase as well as two phase mixture.

Let $\dot{q}_H$ amount of heat flux is absorbed by the loop fluid. The governing equation for energy in the single-phase liquid heat region is given by

$$\frac{d(\rho_f h_f)}{dt} + \frac{d(\rho_f u_f h_f)}{ds} = \frac{\dot{q}_H P}{A_{cs}} \tag{3.3}$$

Under steady state condition, the above equation can be rewritten as

$$\frac{d(\rho_f u_f h_f)}{ds} = \frac{\dot{q}_H P}{A_{cs}} \tag{3.4}$$

Substituting continuity equation eq. (3.2) in the above equation and simplifying it in the form of

$$\frac{d(h)}{ds} = \frac{\dot{q}_H P}{G A_{cs}} = \left(\frac{4}{D}\right)\left(\frac{\dot{q}_H}{G}\right) \tag{3.5}$$

By balancing the forces acting on the fluid element the conservation momentum equation expressed in terms of pressure gradient is as follows

$$\rho u \frac{du}{ds} = \frac{dp}{ds} - \frac{2}{D} C_f G^2 v_f \tag{3.6}$$

By neglecting the acceleration pressure drop in single phase flow the above eq.(3.6) can be rewritten as

$$\frac{dp}{ds} = -\frac{2}{D} C_f \frac{G^2}{\rho} \tag{3.7}$$

Where C_f is the single phase friction factor and it is estimated as

$C_f = \frac{16}{Re}$ for laminar flow $\quad C_f = \frac{0.079}{Re^{0.25}}$ for turbulent flow

The single phase Reynolds number is estimated as

$$Re = \frac{GD}{\mu} \tag{3.8}$$

If loop fluid reaches saturation state, further heat interactions results shows variation of quality in the heater. Under constant heat flux condition linear variation of quality assumption the generalized energy equation of two phase mixture in the heater is given by

$$\frac{\partial(x)}{\partial s} = \left(\frac{4}{D}\right)\left(\frac{\dot{q}_H}{Gh_{fg}}\right) \tag{3.9}$$

Similar to single-phase fluid, for the two phase mixture, the momentum equation expressed in terms of pressure gradients given by in eq.(3.10)

$$\frac{\partial p}{\partial s} = \frac{\frac{2}{D}C_{tp}G^2 v_f\left(1+x\left(\frac{v_{fg}}{v_f}\right)\right)+G^2 v_f\left(\frac{v_{fg}}{v_f}\right)\frac{dx}{ds}+\frac{gsin(\theta)}{v_f\left(1+x\left(\frac{v_{fg}}{v_f}\right)\right)}}{1+G^2\left[x\frac{\partial v_g}{\partial p}\right]} \tag{3.10}$$

The compressibility of gaseous phase neglected for the water, this assumption is valid from the literature[112], so the above equation rewritten as

$$\frac{\partial p}{\partial s} = \frac{2}{D}C_{tp}G^2 v_f\left(1+x\left(\frac{v_{fg}}{v_f}\right)\right)+G^2 v_f\left(\frac{v_{fg}}{v_f}\right)\frac{dx}{ds}+\frac{gsin(\theta)}{v_f\left(1+x\left(\frac{v_{fg}}{v_f}\right)\right)} \tag{3.11}$$

Where C_{tp} is the two phase friction factor and it is estimated as

$C_{tp} = \frac{16}{Re_{tp}}$ for laminar flow $\quad C_f = \frac{0.079}{Re_{tp}^{0.25}}$ for turbulent flow

The two phase Reynolds number is estimated as follows

$$Re_{tp} = \frac{GD}{\mu_m} \tag{3.12}$$

Where μ_m is mean two phase viscousity [112] and is estimated as follows

$$\frac{1}{\mu_m} = \frac{x}{\mu_g} + \frac{1-x}{\mu_f} \tag{3.13}$$

Riser section

Similar to the above section governing equations are derived as per the loop fluid state. If single phase loop fluid is enter in to the riser section, then the momentum equation by considering the gravitational head is

$$\frac{dp}{ds} = -\frac{2}{D} C_f \frac{G^2}{\rho} - g\rho \tag{3.14}$$

As riser section is fully adiabatic section, so no heat transfer taken place then the energy equation is written by using steady flow energy equation is

$$\frac{dh}{ds} + \frac{d}{ds}\left(\frac{u^2}{2}\right) + g = 0 \tag{3.15}$$

Otherwise two phase mixture is enter in to the riser, and corresponding governing equation for momentum is

$$\frac{\partial p}{\partial s} = \frac{2}{D} C_{tp} G^2 v_f \left(1 + x\left(\frac{v_{fg}}{v_f}\right)\right) + G^2 v_f \left(\frac{v_{fg}}{v_f}\right)\frac{dx}{ds} + \frac{gsin(\theta)}{v_f\left(1+x\left(\frac{v_{fg}}{v_f}\right)\right)} \tag{3.16}$$

To find the $\frac{dx}{ds}$ term in the riser by considering a small control volume and applying energy balance is gives

$$dh + d\left(\frac{u^2}{2}\right) + gsin\theta ds = 0 \tag{3.17}$$

Where, $h = h_f + xh_{fg}$, and $u = \frac{G}{\rho_m} = G v_m = G\left(v_f + x v_{fg}\right)$

Differentiating the above equations w.r.t spatial co-ordinate gives

$$\frac{dx}{ds} = -\frac{g}{h_{fg} + \left(\frac{G}{\rho_f \rho_g}\right)(\rho_f - \rho_g)(\rho_f + x\rho_{fg})} \tag{3.18}$$

Condenser section

In condenser section if the loop fluid entering state is either two phase mixture or single phase depending on the riser exit. If single phase state exits, then the corresponding equations for energy and momentum similar to the single phase equations in heater section and they are given by

$$\frac{\partial(h)}{\partial s} = \frac{Q_c P}{G A_{cs}} = \left(\frac{4}{D}\right)\left(\frac{\dot{q}_C}{G}\right) \tag{3.19}$$

$$\frac{dp}{ds} = -\frac{2}{D} C_f \frac{G^2}{\rho} \tag{3.20}$$

Otherwise two phase mixture is entering into the condenser. If condensation takes place either completely or partially. The equations for two phase mixture in the condenser is

$$\frac{\partial(x)}{\partial s} = \left(\frac{4}{D}\right)\left(\frac{\dot{q}_C}{G h_{fg}}\right) \tag{3.21}$$

and the corresponding pressure gradient equation for two phase mixture is

$$\frac{\partial p}{\partial s} = \frac{2}{D} C_{tp} G^2 v_f \left(1 + x\left(\frac{v_{fg}}{v_f}\right)\right) + G^2 v_f \left(\frac{v_{fg}}{v_f}\right)\frac{dx}{ds} + \frac{g\sin(\theta)}{v_f\left(1+x\left(\frac{v_{fg}}{v_f}\right)\right)} \tag{3.22}$$

Suppose the two phase mixture loop fluid completely condensate within the condenser section and the equations of the single phase loop fluid for remaining section of the condenser as same as eq. (3.19) & (3.20).

Downcomer section

Similar to the riser section governing equations are derived as per the state of the loop fluid by considering the gravitational head. If the state of the loop fluid at condenser exit is single phase, the momentum and energy equations are as follows

$$\frac{dp}{ds} = -\frac{2}{D} C_f \frac{G^2}{\rho} + g\rho \tag{3.23}$$

$$\frac{dh}{ds} = -\frac{G^2}{\rho}\left(\frac{dv}{dp}\frac{dp}{ds}\right) + g \tag{3.24}$$

On the other hand, in condenser, partial condensation takes place, then two phase mixture enters in to the downcomer. The corresponding equations are

$$\frac{\partial p}{\partial s} = \frac{2}{D} C_{tp} G^2 v_f \left(1 + x\left(\frac{v_{fg}}{v_f}\right)\right) + G^2 v_f \left(\frac{v_{fg}}{v_f}\right)\frac{dx}{ds} + \frac{gsin(\theta)}{v_f\left(1+x\left(\frac{v_{fg}}{v_f}\right)\right)} \quad (3.25)$$

$$dh + d\left(\frac{u^2}{2}\right) - gsin\theta ds = 0 \quad (3.26)$$

$$\frac{dx}{ds} = \frac{g}{h_{fg}+\left(\frac{G}{\rho_f \rho_g}\right)(\rho_f - \rho_g)(\rho_f + x\rho_{fg})} \quad (3.27)$$

The exit state of the loop fluid in down comer is decide the suitable governing equations used in the evaporator section.

Heat transfer coefficient correlation

single phase flow

Nusselt number for laminar flow condition (Re < 2300) inside the smooth circular tubes given by Shah [113] which is used to calculate heat transfer coefficient of the loop fluid.

$$Nu = 1.61 \times \left(Re.Pr.\frac{d_i}{L}\right)^{1/3} \quad (3.28)$$

For turbulent flow (Re>2300) M. Al-Arabi [114] developed a correlation by considering the entrance length influence and is given by eq.3.29 (a)

$$Nu = Nu_{fd}\left[1 + S\left(\frac{D}{x}\right)\right] \quad (3.29a)$$

Where S is a factor and is estimated as follows

$$\frac{SPr^{1/6}}{(x/D)^{0.1}} = 0.68 + \frac{3000}{Re^{0.81}} \quad (3.29b)$$

The Nusselt number (Nu_{fd}) is estimated by using Dittus-Boelter equation and is given by

$$Nu_{fd} = 0.023 \times Re^{0.8} \times Pr^{0.4} \quad (3.29c)$$

In general, the entrance length influence is neglected for turbulent flows and the heat transfer is estimated by considering the fully developed flow i.e. by Dittus-Boelter equation. It is also observed that the average difference in Nu across the heater by neglecting the entrance length is 5.34%.

Two phase flow

Kandlikar correlation [115] used to estimate the two phase heat transfer coefficient and is given by

$$\frac{h_{tp}}{h_l} = C_1 Co^{C_2} (25 Fr_{lo})^{C_5} + C_3 Bo^{C_4} F_{fl} \tag{3.30}$$

Where Bo is boiling number, Co is convection number, and Fr_{lo} is Froude number, and these are given by

$$Bo = \frac{\dot{q}}{G h_{fg}} \tag{3.31a}$$

$$Co = \left(\frac{1-x}{x}\right)^{0.8} \left(\frac{\rho_g}{\rho_l}\right)^{0.5} \tag{3.31b}$$

$$Fr_{lo} = \frac{G^2}{\rho_l^2 g D} \tag{3.31c}$$

The constants in eq. (3.30) are given in below

Constant	**Convective region**	**Nucleate boiling region**
C_1	1.1360	0.6683
C_2	-0.9	-0.2
C_3	667.2	1058
C_4	0.7	0.7
C_5^*	0.3	0.3

C_5^* =0 for vertical tubes and horizontal tubes with $Fr_l > 0.04$

3.2. Solution procedure

Loop is discretized by finite difference method. The differential equations are applied at corresponding loop section based on state of loop fluid. Thermo-physical properties of the loop fluid (water) are evaluated by IAPWS-97 guidelines. An in-house MATLAB code developed to solve these governing equations and solution algorithm as shown in Fig. 3.2.

3.2.1 Validation

There is lack of test data in the literature for the same configuration to validate the present proposed model. However, an attempt has been made to validate the present model i.e. considering effect of local pressure on NCL performance. The steady state performance of a two phase rectangular NCL having horizontal heater and condenser at atmospheric and sub atmospheric pressure is numerically estimated by developing a In-house code and is validated with the Vijayan correlation [57] the same is written below.

$$Re_{ss} = 1.96\left(\frac{Gr_m}{N_G}\right)^{\frac{1}{2.75}} \qquad \text{For turbulent flow} \tag{3.32}$$

Where,

$$Gr_m = \left(\frac{D^3\rho^2 g\beta\dot{q}\Delta z}{A\mu^3 C_p}\right) \tag{3.33}$$

$$N_G = \frac{L_t}{d}\left[\left(l_{eff}\right)_{sp} + \overline{\emptyset}_{lo}^2\left(l_{eff}\right)_{sp}^{he} + \emptyset_{lo}^2\left(l_{eff}\right)_{sp}^{t}\right] \tag{3.34}$$

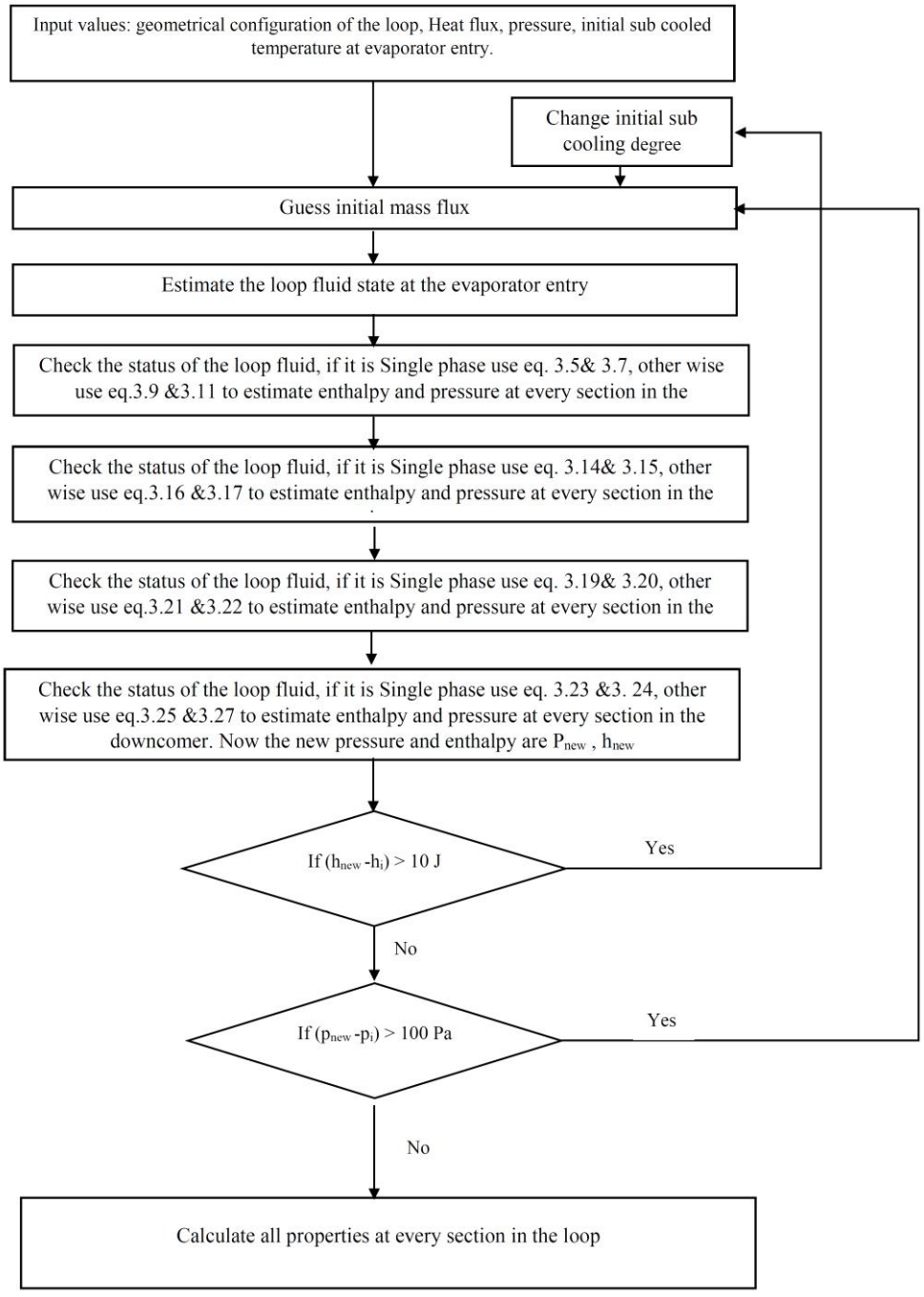

Fig.3.2 Algorithm for simulation of NCL

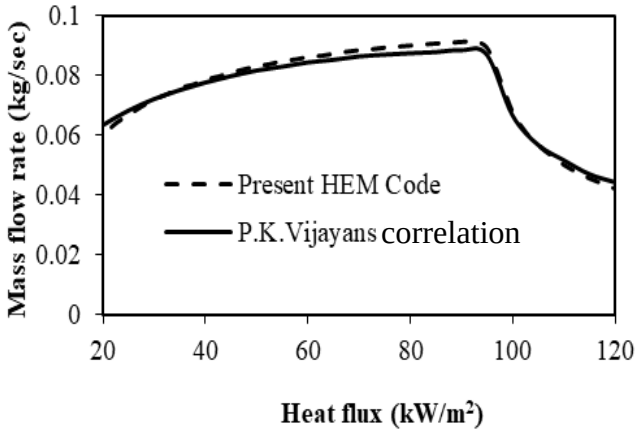

Fig.3. 3 Validation of the model

The computed results are compared with the analytical values of P.K.Vijayan correlation [57]. Fig. 3.3 depicts the effect of heat input on the mass flow rate. As discussed earlier, the mass flow rate increases with the heat input up to the peak value and then decreases. From Fig. 3.3, it is observed that a fare agreement is obtained between the proposed HEM and P.K.Vijayan data.

3.3 Thermo-hydraulic behaviour of the NCL at atmospheric condition

Mass flow rate

The variation of mass flow rate with the heat flux is described in Fig. 3.4. The developed gravitational force in the downcomer and developed buoyancy force in the riser are causes for the fluid circulation in the NCL. Thus, the mass flow rate is governed by these forces. For a given operating range of heat flux, Fig.3.4 shows the dominant zones in the loop. The presence of low density liquid-vapour mixture in the riser and high density liquid in the down comer lead to create high pressure gradient between the heat source and heat sink in the loop which causes mass flow rate increase. It is true in the gravitational dominant regions. Further increment in the heat input raises the vapour quality, and hence, more drag is developed in the riser section which result reduction in the mass flow rate. Therefore, the graph between the loop mass flow rate and the heat input is divided into two regions, namely, the gravitational dominant region and the friction dominant region which are separated at a specific heat input

and is treated as a critical heat input. The critical heat flux depends on the loop geometry and operating conditions.

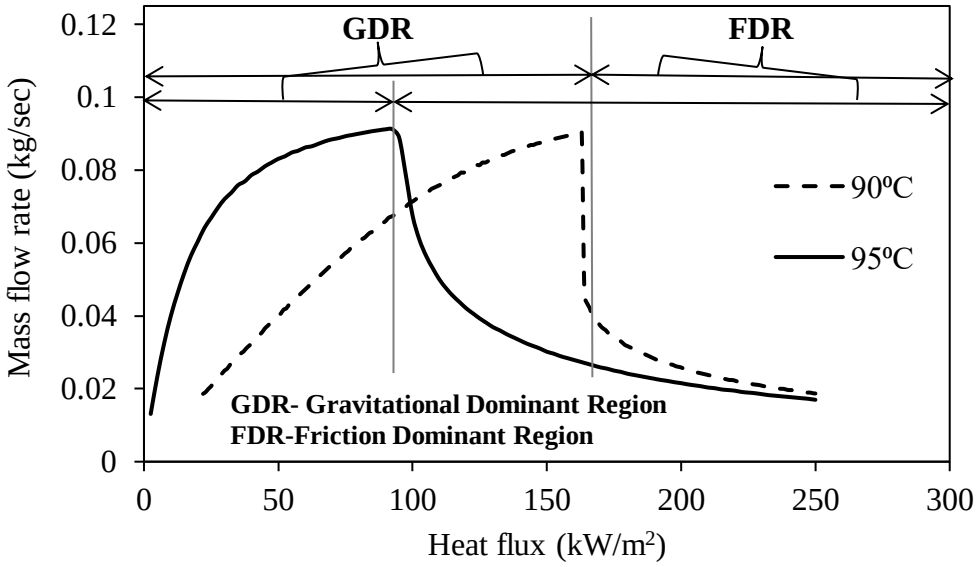

Fig.3. 4 Variation of mass flow rate with heat flux

Pressure

The parameters such as pressure, enthalpy, temperature and loop length are non-dimensionalized for analysing the loop behaviour. Fig. 3.5 shows the variation of the local pressure along the loop at different heat fluxes. Due to frictional and unfavourable gravitational forces, pressure decreases from the heater to the condenser exit. The pressure is raised in the downcomer because of favourable gravitational head in the downcomer. In the heater, the pressure drop is insignificant at the lower heat fluxes, whereas in the condenser the pressure drop is more. This happens due to lower heat fluxes, where the loop fluid does not reach saturation state. However, the reduced pressure in the riser induces flashing; hence, two phase mixture is available in the condenser results more pressure drop. At high heat fluxes, loop fluid exhibits two phase mixture in the heater, riser & condenser sections, and hence, pressure drop is more due to increased drag forces.

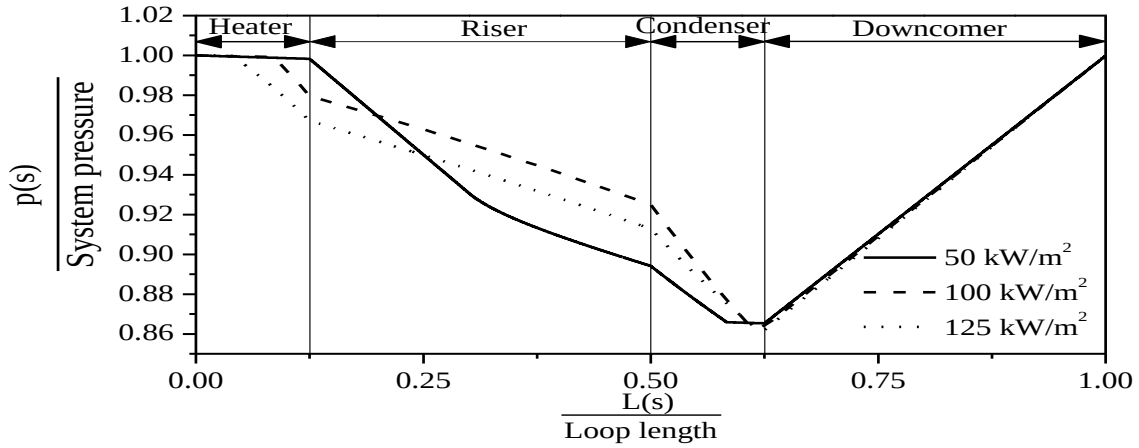

Fig.3. 5 Variation of local pressure along the loop

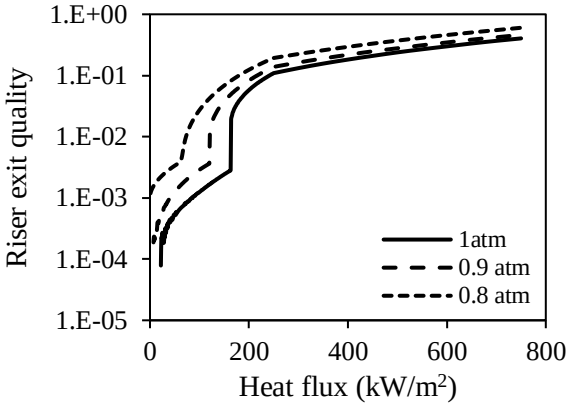

Fig.3.6 (a) Variation of quality with respect to heat flux at heater inlet temp. of 90ºC

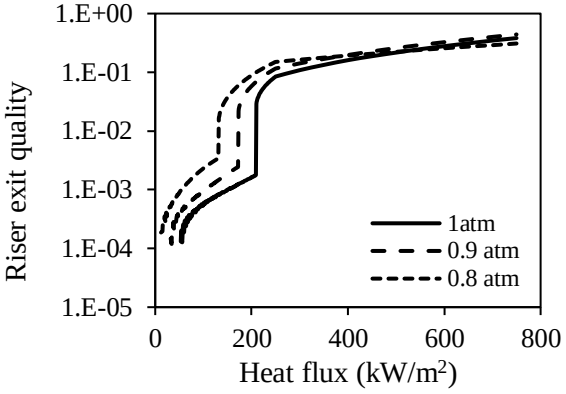

Fig.3.6 (b) Variation of quality with respect to heat flux at heater inlet temp. of 85ºC

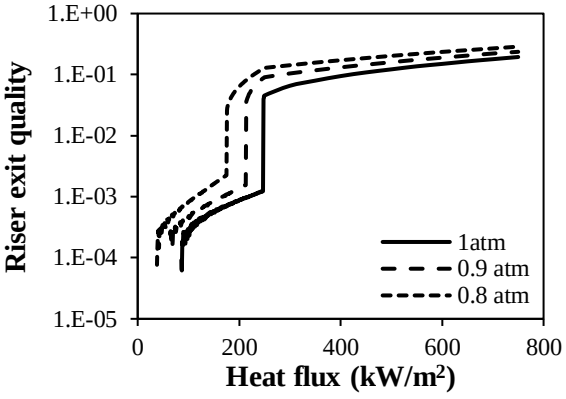

Fig.3.6 (c) Variation of quality with respect to heat flux at heater inlet temp. of 80ºC

At the lower heat flux of 50 kW/m^2, the loop fluid does not reach the saturation state in the heater, compared with the higher heat fluxes 100 and 125 kW/m^2. At the lower heat fluxes, the sub cooled loop fluid enters into the adiabatic riser section. The opposable frictional and

gravitational forces decrease the local pressure along the riser, and it is expected to reach the corresponding saturation state. The further decrement in the local pressure induces flashing in the riser section and the quality increases that can be observed from Fig. 3.6. The presence of low density two phase mixture in the riser increases the mass flow rate. As heat flux goes on increasing the fluid reaches the saturation state in the heater itself, and further addition of heat flux gives high quality of the steam at heater exit. Decrement of local pressure in the riser further increases the quality of the steam. The high quality loop fluid possesses more drag in the riser. Therefore, the driving head in riser decreases, results low mass flow rate that can be observed in Fig. 3.4.

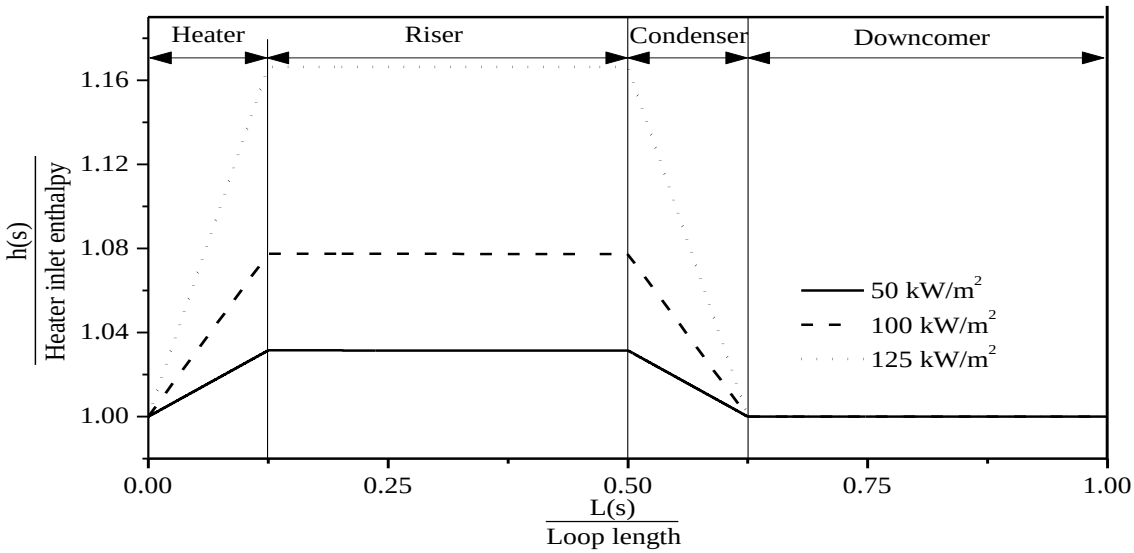

Fig. 3.7. Variation of local enthalpy along the loop

Enthalpy

The enthalpy variation along the loop at different heat fluxes under atmospheric condition is shown in Fig. 3.7. In the heater, the loop fluid absorbs heat and the enthalpy increases. Thereafter the loop fluid enters into the adiabatic riser, where the enthalpy remains constant. The enthalpy of loop fluid starts decreasing in the condenser due to heat rejected and enters into adiabatic downcomer. The heater exit enthalpy rapidly increases with heat flux as shown in Fig. 3.7. This happens because of the heat supplied to the heater is directly related to the mass flow rate and the subsequent change in the enthalpy. So, at higher heat fluxes, the loop mass flow rates decreases and enthalpy at heater exit increases.

Temperature

Fig. 3.8 shows the temperature profiles of loop fluid for different heat fluxes. Similar to the enthalpy, for the lower heat flux, temperature of loop fluid increases along the heater and remains constant in the adiabatic riser. However, for the higher heat fluxes, decrement trend in temperature is observed in both the heater as well as the riser. In the condenser, temperature decreases along the loop length, and thereafter loop fluid enters into the adiabatic downcomer section where temperature remains unchanged. At the lower heat flux, the loop fluid is in sub-cooled state at heater exit and hence, the temperature linearly increases in the heater section and remains constant in the riser section up to the local temperature reaches the corresponding saturation temperature i.e. flashing. Thereafter, loop fluid condition is in the two phase and the local pressure decreases along the loop length, and hence from the local saturation temperature decreases and subsequently the quality increases which can be observed from Fig. 3.6.

At the high heat fluxes the loop fluid attains two phases in the heater itself. After that, the local pressure decreases significantly along the length, as shown in Fig. 3.5. Therefore, the corresponding saturation temperature decreases and the quality of loop fluid increases. Then the two phase loop fluid enters into the adiabatic riser, where the pressure drop is more due to the frictional and gravitational forces along the riser. In the condenser, the loop fluid rejects heat and the temperature decreases. The loop fluid temperature profiles in the condenser section clearly differentiate the two phase and single phase zones as shown in Fig. 3.7. Then the single phase sub-cooled fluid enters into the adiabatic downcomer and the temperature remains constant.

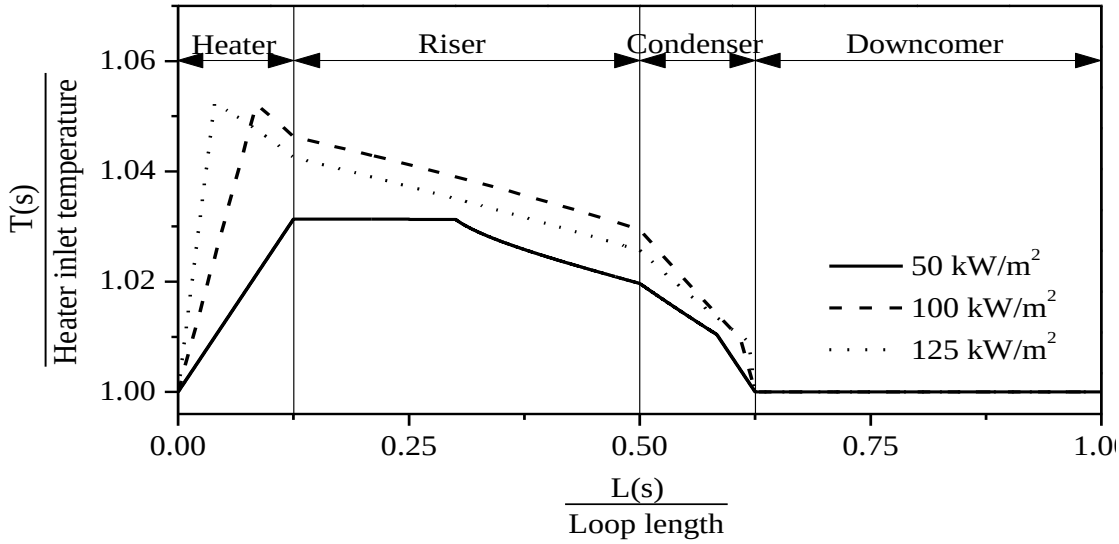

Fig. 3.8. Variation of local temperature along the loop

Heat transfer coefficient

The variation of average heat transfer coefficient (HTC) with the heat flux is described in. Fig. 3.9. The HTC is taken across the heater length as per the loop fluid state and the data is averaged. In the heater, either single phase or combination of single phase and two phase is present depending on the loop fluid state, so the average HTC is the combination of single phase and two phase. At initial heat fluxes the loop exhibits two phase by flashing in the riser section. That means loop fluid in heater section is in subcooled state. Which indicates heat transfer taking place in heater section is due to the single phase forced convection. So, the average HTC is low as indicated in the Fig. 3.9. As the mass flow rate of the loop increases with heat flux the HTC also increases that can be observed in Fig.3.9. The sudden increment in HTC is attributed to the initiation of saturated flow boiling in the heater section.

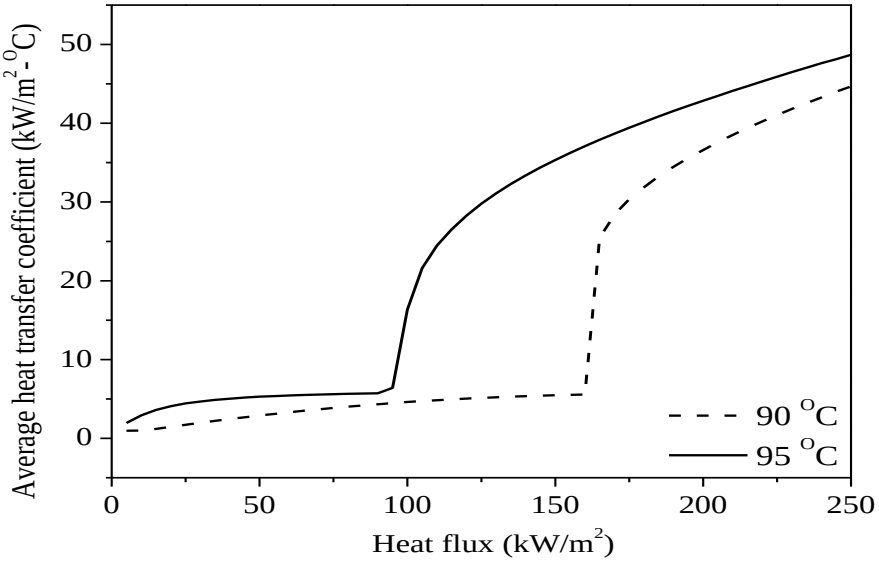

Fig.3.9: HTC variation with heat flux

3.4 Influence of geometrical parameters

3.4.1 Effect of heater and condenser orientation

In the loop, different combinations of heater and condenser section orientations creates various possibilities of density differences in the riser and downocmer, which strongly influences the system behaviour. Hence knowledge of loop behaviour by varying heater and condenser sections orientation is required. Several authors [116]–[118] investigated the steady state characteristics of loop for different orientations, but loop fluid is either single phase or supercritical. Investigation on the performance of NCL filled with two phase mixture in riser and single phase in downcomer sections in different orientations are rare or not found in open literature. And also in practical situations the geometrical constraints decide the orientation of the heater and condenser. In general it is preferable to operate natural circulation loop with maximum mass flow rate. Hence, in the present study, the effect of heater and condenser sections orientation on the two phase natural circulation loop performance is studied. Four possible orientations are proposed by varying the heater and condenser position namely Horizontal Heater and Horizontal Condenser (HHHC), Vertical Heater and Vertical Condenser (VHVC), Horizontal Heater and Vertical Condenser (HHVC) and Vertical Heater and Horizontal Condenser (VHHC).

Schematic representation of rectangular NCLs considered for the present study is shown in Fig. 3.10 (a-c). The HHHC model was already shown in Fig.3.1. All the four considered models are of same aspect ratio (loop height to width ratio). A uniform circular cross section throughout the loop is considered. In two-phase flow systems, the gravitational head plays an important role which in turn depends on the length of the vertical limbs (i.e. riser and downcomer). Depending on the position of heater and condenser, the length of single phase and two-phase fluid occupancy varies. Uniform and equal heat flux boundary condition is applied at both heater and condenser sections. The total loop is subdivided into six regions based on the state of the working fluid. The different zones in the loop are described in Table 3.1.

Table 3.1: Loop regions

S.No	**Regions**	**Zone description**
1	a-b	sub-cooled heating region
2	b-c	vaporization region
3	c-d	adiabatic two-phase region
4	d-e	condensation region
5	e-f	sub-cooled cooling region
6	f-a	adiabatic single phase region

Figure 3.11 depicts the variation of the mass flow rate with heat flux for different orientation of the NCLs. All geometric and operating parameters are same for all the orientations considered here. It is observed from the Fig. 3.11 that, though the trend is similar for all orientations but the heat flux values at peak mass flow rate are different. Every orientation has optimum heat flux value where the highest mass flow rate is observed. The buoyancy and gravitational forces at the riser and down-comer sections respectively produce different mass flow rates for the same heat input at heater. Higher mass flow rates reduce the loop friction because of reduced quality in riser. Consequently, it reduces the entropy generation and the concern of loop fluid dry out condition. Among all the orientations considered, HHHC& VHHC orientations have higher mass flow rates compared with any other orientations.

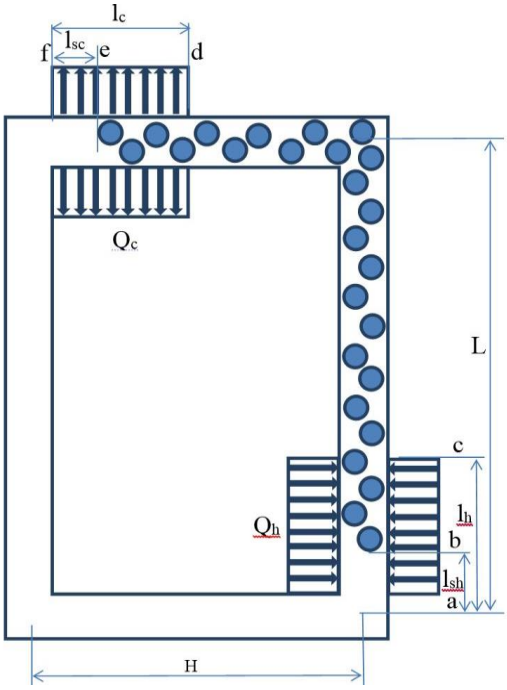

(a) VHHC

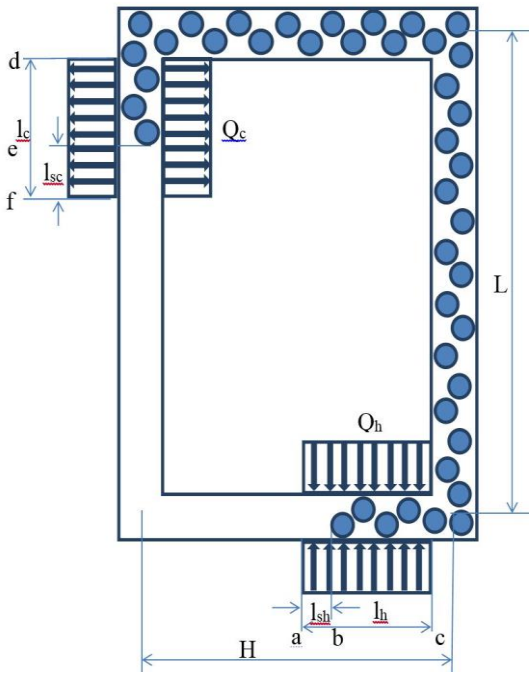

(b) HHVC

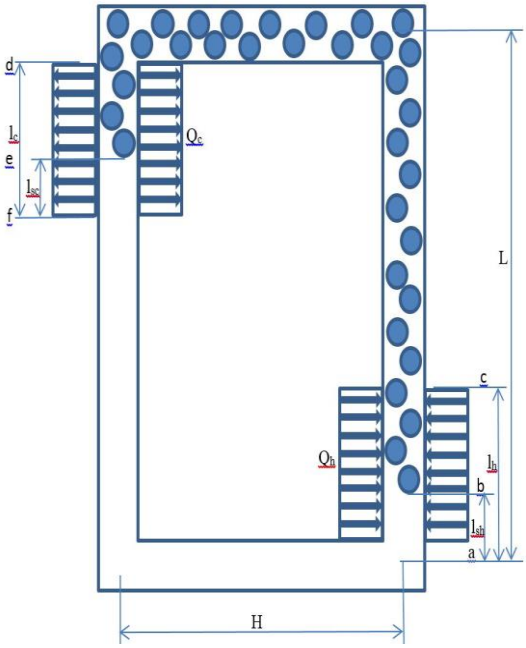

(c) VHVC

Figure 3.10 (a-c). Different two-phase NCL Models

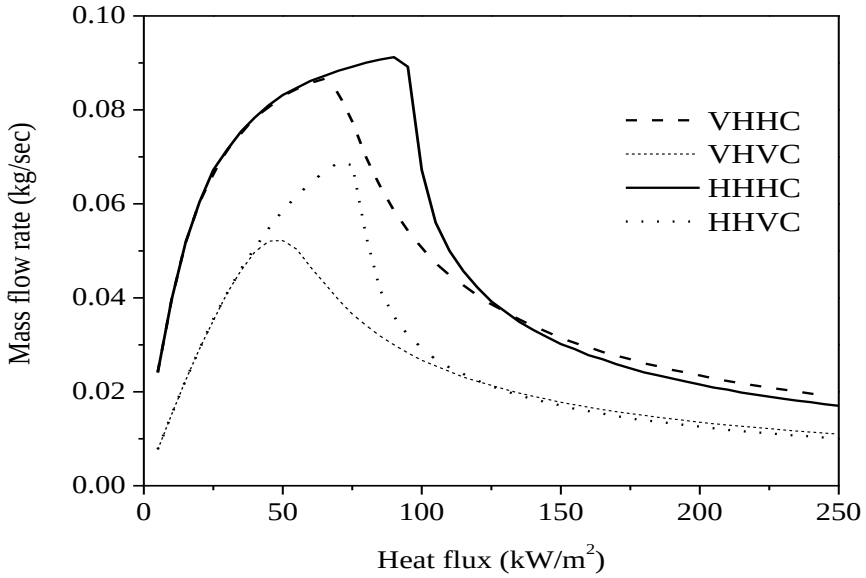

Fig. 3.11 Mass flow rate variation of all the loops with heat flux at 95 ^{O}C

Influence of heater orientation

It is expected that heater orientation strongly influences the mass flow rate of the loops. This is because, vertical heater loops have less riser length as compared with horizontal heater loops. But, from Fig. 3.11 it is observed that, for both HHHC and VHHC loops mass flow rate is almost same up to the heat flux of 65 kW/m^2. Similarly for HHVC and VHVC loops mass flow rate is same up to the heat flux of 40 kW/m^2. It is also observed that The HHHC and VHHC loops have high mass flow rate, at the same time HHVC and VHVC loops have minimum mass flow rate. This indicates that influence of heater orientation in NCL is insignificant.

The credible reason for mass flow rate variation in the loops is due to the pressure drop. In the loop the pressure drop depends upon the loop fluid state. In single phase, fluid frictional and gravitational pressure drops are accounted. While in the two phase mixture fluid frictional, gravitational and acceleration pressure drops are accounted. So the total pressure drop depends on the single phase and two phase pressure drops.

Figures 3.12, 3.13 and 3.14 plotted at 35kW/m^2, 100 kW/m^2 and 200 kW/m^2 heat fluxes respectively, represents the pressure and fluid quality profiles across the loops. At 35 kW/m^2 heat flux, the vapour available in the riser is due to flashing, as the fluid is still in sub-cooled state in the heater section. Whereas at 100 and 200 kW/m^2 boiling is initiated in the heater section. It is observed from Fig. 3.12 (a and c), Fig.3.13 (a and c) and Fig.3.14 (a and c) the

pressure at condenser exit is almost same. By fixing the condenser position and imposed boundary condition, the available gravitational head in downcomer is constant. The single phase frictional pressure drop in downcomer is less as compared to single phase gravitation head in downcomer. So, the pressure drop up to condenser exit is compensated by this gravitational pressure head. The pressure drop up to condenser exit depends on mass flux and loop fluid quality. At the 35 kW/m^2 heat flux both combination loops i.e. HHHC & VHHC, HHVC & VHVC have almost same pressure profiles (Fig.3.12 (a) and Fig.3.12 (c)). The vapour quality in the riser section is almost same and these loops have equal lengths of two phase regions that can be observed in Fig. 3.12 (b) and Fig.3.12 (d), which concludes that they do have same single phase length as the remaining portion of the loop. This results in same mass flow rate.

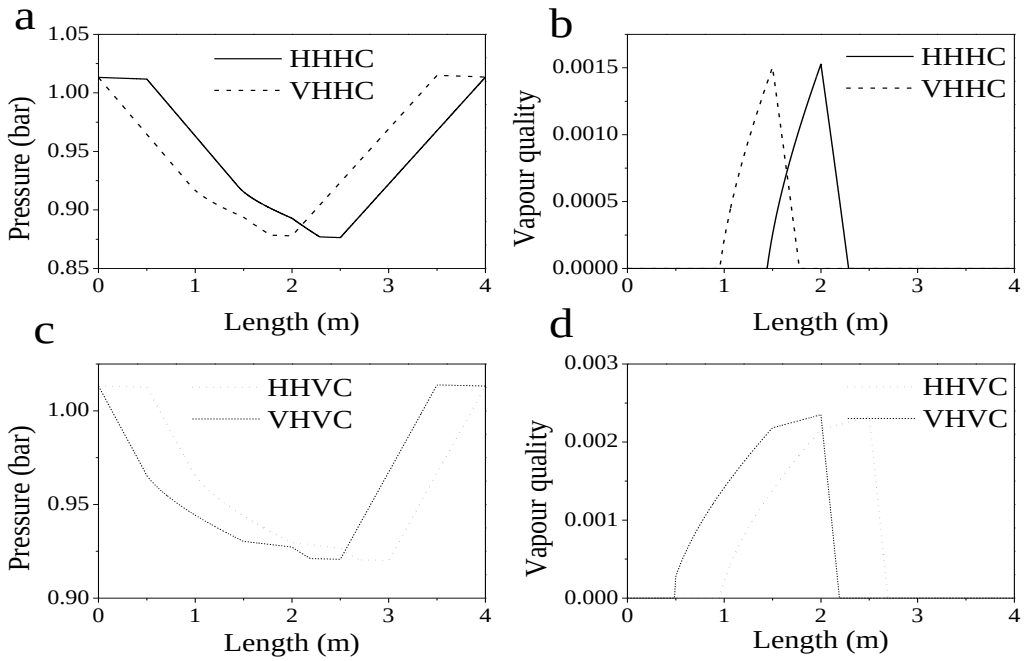

Fig. 3.12 local pressure and vapour quality profiles across the loop at 35 kW/m^2 heat flux

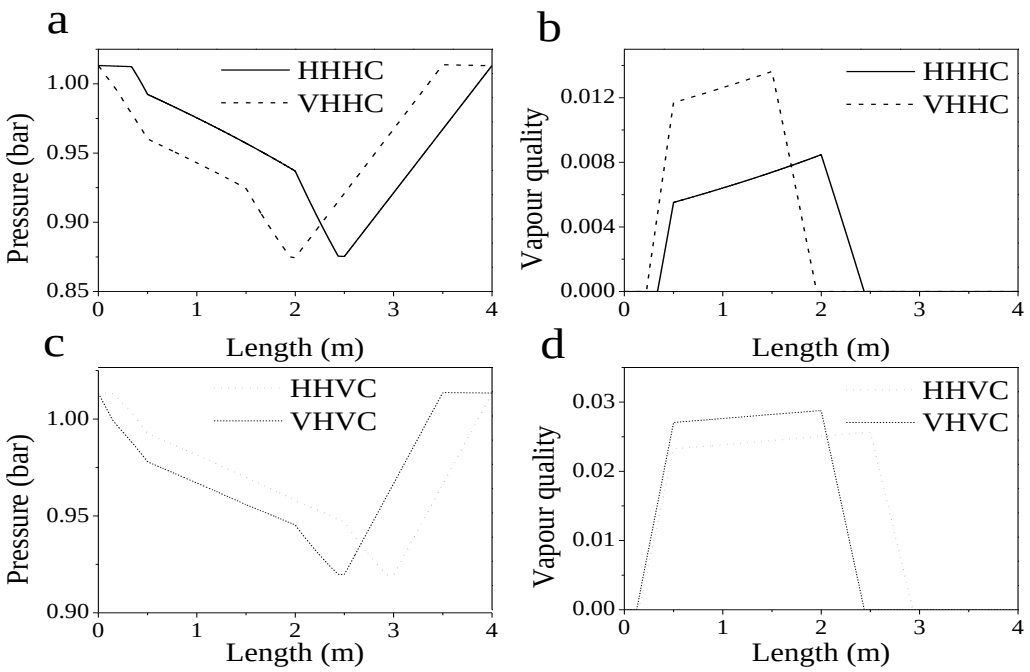

Fig. 3.13 local pressure and vapour quality profiles across the loop at 100 kW/m^2 heat flux

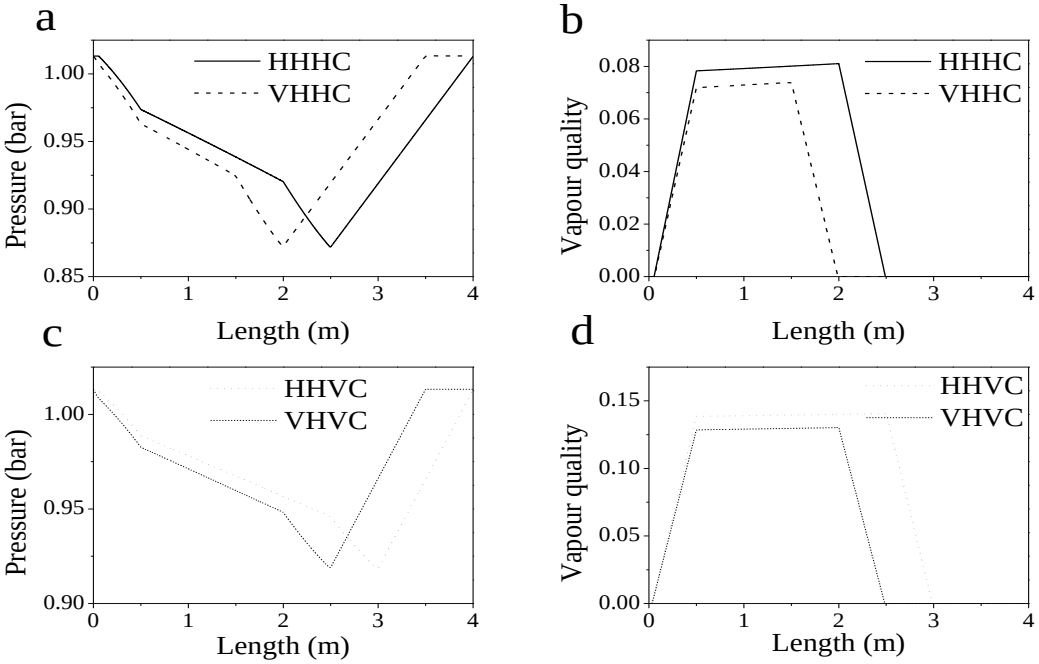

Fig. 3.14 local pressure and vapour quality profiles across the loop at 200 kW/m^2 heat flux

The mass flow rate at 100 and 200 kW/m^2 heat flux significantly varies for the loops. For a fixed condenser orientation, at 100 kW/m^2 heat flux the horizontal heater loops have high

mass flow rates. The two phase region length is more for horizontal heater loops as compared with vertical heater loops (Fig. 3.13 (a and c) and Fig. 3.14 (a and c)). These can create a difference in single phase and two phase pressure drop across the loop which causes variation in mass flow rate. From the loop fluid vapour quality profiles (Fig. 3.13 (b)) it is observed that VHHC loop has longer boiling region in the heater section and has more vapour quality in the riser section as compared with HHHC loop. This leads to higher vapour quality in riser and offers more drag so that mass flow rate decreases. However the pressure drop up to the condenser exit is same. This happens because the total pressure drop in every section comprises three parts - due to friction, gravitation, and acceleration. In the HHHC orientation impact of frictional pressure drop is more because of the length of 'a' to'd' is greater than VHHC orientation. However, in VHHC the contribution of gravitational pressure drop is more because of single-phase fluid in the riser up to the point of saturation, compensating for shorter length from 'a' to 'd'. Hence, the total pressure drop up to condenser exit remains same in both orientations. This phenomena happened up to the heat flux range of 65 kW/m^2 to 135 kW/m^2. For the HHVC and VHVC loops, the mass flow rate variation is small and HHVC loop has high mass flow rate. At 100 kW/m^2 both the loops already reache the peak mass flow rate. Hence, the pressure drop at condenser exit is same as explained earlier..

Further increase of heat flux from 130 kw/m^2 for HHHC & VHHC loops and from 120 kW/m^2 for HHVC & VHVC loops, causes the mass flow rate variation to reverse, i.e. vertical heater loops have high mass flow rate. For example at 200kW/m^2 the vapour quality profiles (Fig.3.14 (b and d)) depicts the deviation. The reason is at very high heat fluxes the horizontal heater loops have more two phase region i.e. total vertical length (riser) and it offers more drag, hence mass flow rate decreases. But the pressure up to condenser exit is same and the slopes of pressure profile changes which can be observed from Fig. 3.14 (a and c).

Influence of condenser orientation

Condenser orientation has significant effect on the mass flow rate of the system. Among the orientations considered here for the comparison, HHHC & VHHC have horizontal condensers and VHVC & HHVC have vertical condensers. Horizontal orientation condensers (HHHC & VHHC) show maximum mass flow rate than the vertical orientation condensers (VHVC & HHVC) as shown in Fig. 3.11. In general mass flow rate of NCL mainly depends on pressure

difference between two vertical limbs i.e. in riser and down comer. The loop riser and down comer sections either contains single-phase flow region and/or two-phase flow regions based on heater and condenser orientation and position.

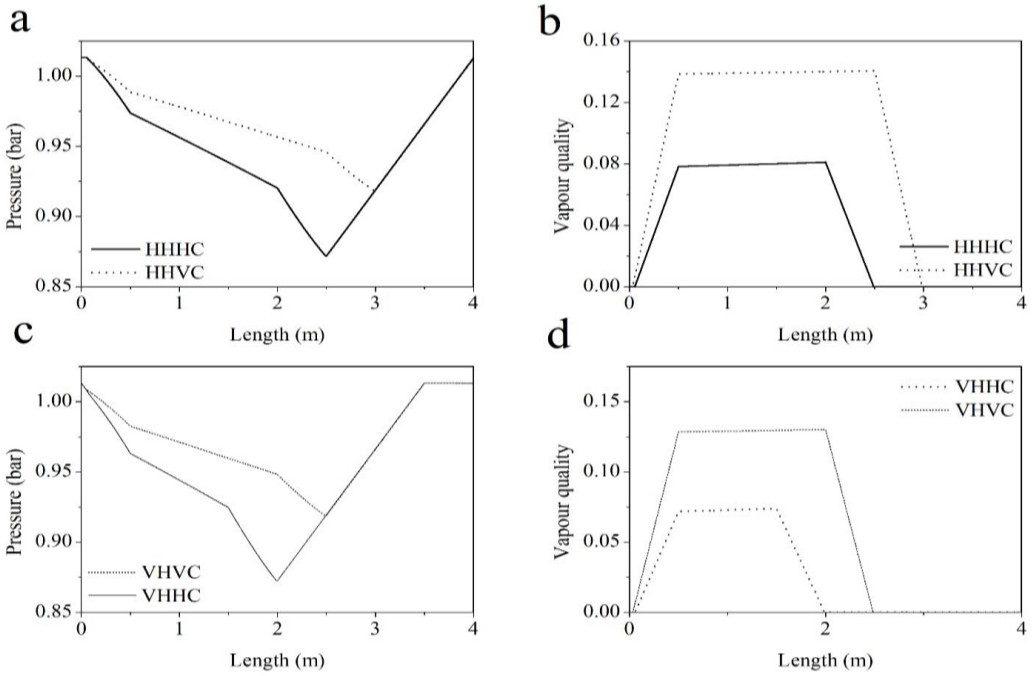

Fig. 3.15 local pressure and vapour quality profiles across the loop at 100 kW/m^2 heat flux

Fig. 3.15 shows the pressure and vapour quality profiles of the loops at 100 kW/m^2 heat flux. From the considered assumption to analyse the loop performance, the state of fluid at condenser outlet is completely single-phase. Hence, in down comer single-phase gravitational pressure drop has major influence on mass flow rate of the system. In horizontal condenser position loops (i.e. HHHC & VHHC), working fluid in down comer is completely in single phase liquid (high density) whereas in vertical condenser position NCLs, working fluid in down comer is in two-phase liquid (low density) for a certain length. Hence, the horizontal condenser loops have higher gravitational pressure gain in the down comer region compared with vertical condenser loops that can be observed in Fig.3.15 (a and c). The same behaviour is observed for all the considered heat flux range. The increase in gravitational pressure gain increases the mass flow rate. The increased mass flow rate decreases the vapour quality in the loop.

Heat transfer coefficient

Fig. 3.16 shows the variation of average HTC at heater section for for different orientation of the NCLs. The variation of average HTC with heat flux was already discussed earlier (section 3.3, Fig. 3.9). The HTC depends upon the mass flow rate. Therefore, the HTC variation is significant with condenser orientation but it is insignificant with heater orientation it is same as mass flow rate variation w.r.t heater and condenser orientation. The sudden increment in HTC is differ for different heater and condenser orientation, the attributed reason is the initiation of saturated flow boiling in the heater section is varies with heat flux.

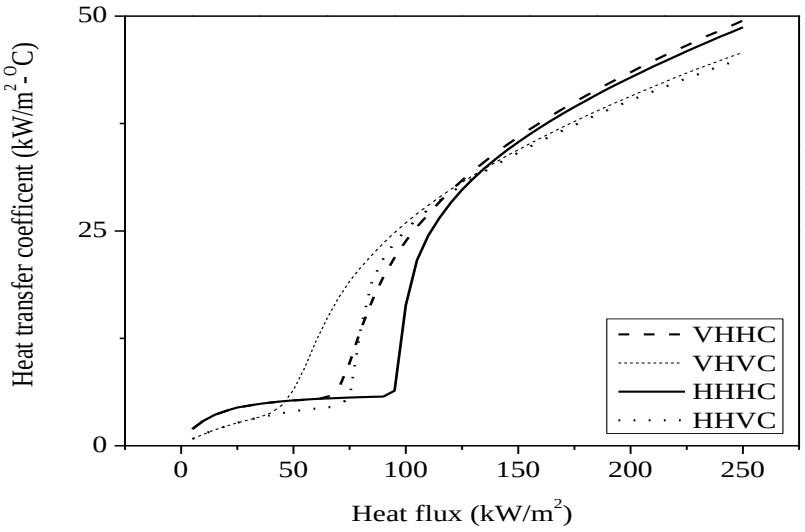

Fig.3.16 Average HTC variation of all the loops with heat flux at 95 ^{O}C

3.4.2 Influence of aspect ratio

From the previous study, it is concluded that HHHC and VHHC loops have maximum mass flow rate. Higher mass flow rates are preferred in the loop because of reduced quality in riser. Consequently it reduces the entropy generation and concern of loop fluid dry out condition. Hence, for further analysis HHHC orientation loop is considered. In general, for all NCLs, based on its applications for nuclear reactors, solar evaporators etc., the constraints like the fluid volume of the system and space availability for the installation is directly related to the initial investment cost and maintenance cost. So that the optimum loop configuration is to be

found in terms of maximum mass flow rate under the given constraints. So, in the present analysis, the effect of aspect ratio on two phase NCL is investigated. Water is used as the loop fluid. NCLs configuration (Fig.3.1) is obtained with aspect ratios of 1, 1.5, 2.33 and 4 by keeping the diameter and total volume of the loop constant (551.26 cc). The detailed NCL geometrical parameters and operating conditions considered for the analysis are given in table 3.2. In order to simplify the analysis, heater length is taken as the same as horizontal length for respective aspect ratios of the loop.

Table 3.2 Geometrical parameters and operating conditions of the loop

Parameters	**Value/Range**
Aspect ratio (L/H)	1, 1.5, 2.33 and 4
Diameter of the pipe	0.01325 mm
Loop horizontal length	1, 0.8, 0.6 and 0.4
Heater inlet temperature and pressure	95 ^{O}C and 1 atm
Heat input at the heater	0.2- 5.2 kW

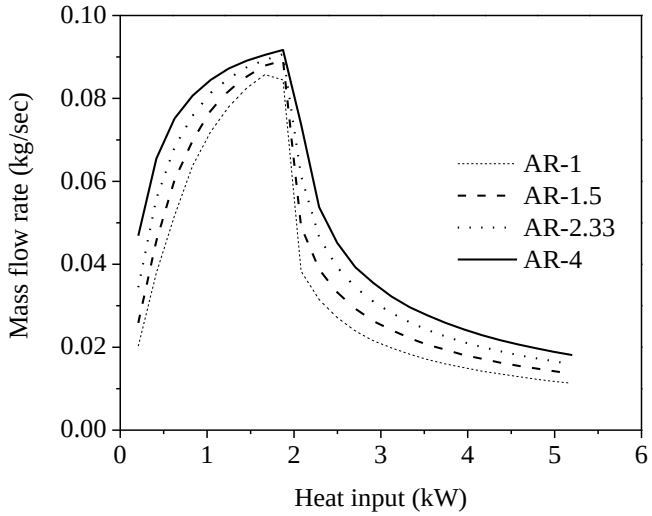

Fig. 3.17 Variation of mass flow rate with heat input

Fig.3.17 shows the effect of heat flux, aspect ratio and heater inlet temperature on the loop mass flow rates. The mass flow rate of the NCL increases linearly with the heat input. For a fixed configuration, as the heat input increases the vapour quality in the loop (heater and riser sections) increases which is shown in Fig. 3.18 (a) and Fig. 3.18 (b). This is due to the fact

that, the density difference between the heater outlet and condenser outlet increases with increasing heat input, resulting in more driving force. However, it can also be observed from Fig. 3.17 that further increase of heat input results in decrease in flow rates. This is due to increase in heat input which increases the vapour quality in riser section and it offers more frictional drag, which results in lower mass flow rate. So it can be concluded that there is a limiting heat input value for each configuration of the loop. It is evident from Fig. 3.17 that, mass flow rate is a strong function of aspect ratio. With increase in aspect ratio, loop fluid circulation rate increases. The maximum loop fluid circulation rate is observed for the aspect ratio 4. The average enhancement in mass flow rate at 95 ^{o}C heater inlet temperature is 56% as compared with the loop having aspect ratio 1. Heat flux values at peak mass flow rates are shifting towards the left and the optimum mass flow rate is obtained at higher heat inputs. This is because of the developed pressure gradients in the loop.

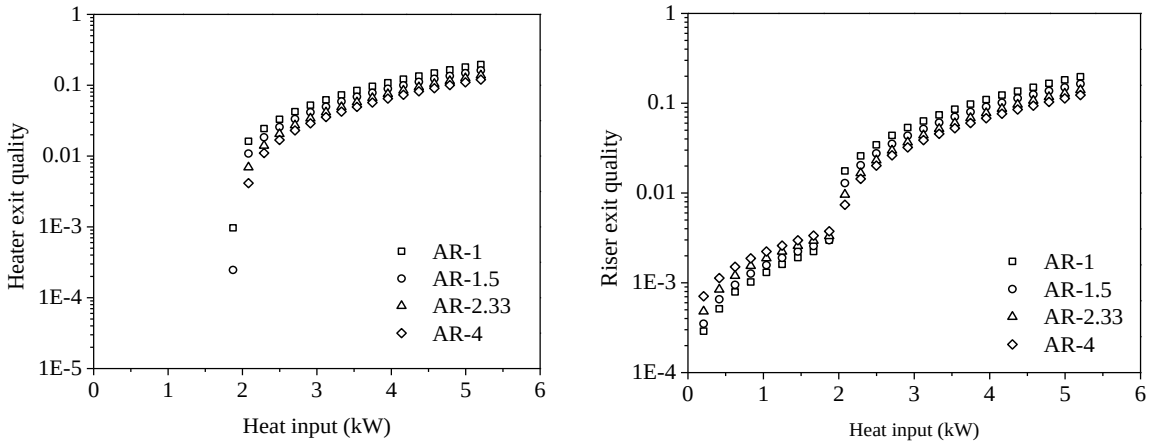

(a) Loop fluid vapour quality at heater exit (b) Loop fluid vapour quality at riser exit

Fig. 3.18 Variation of loop fluid quality at different locations with heat input

Fig.3.19 depicts the pressure profile across the loop at a heat input of 2.08 kW for loop aspect ratios of 1, 1.5, 2.33 and 4. As the aspect ratio increases loop height increases and heater length decreases. This results in high density gradient across riser and downcomer sections which can be observed in terms of local pressure profile along the loop. The loop fluid absorbs the heat at the heater and undergoes phase change and then enters into the riser. In riser, low density vapour liquid mixture is available. The low density vapour liquid mixture rises in the riser and the corresponding local pressure drops. The local pressure drop across the riser develops the pressure gradient in the riser section which increases with increase of aspect ratio that is observed in Fig.3.19. The developed pressure gradient in the riser is compensated by the

pressure gain in the downcomer and it also increases with aspect ratio. Therefore the pressure gradient across the riser and downcomer increases with increase in aspect ratio resulting in enhanced mass flow rate.

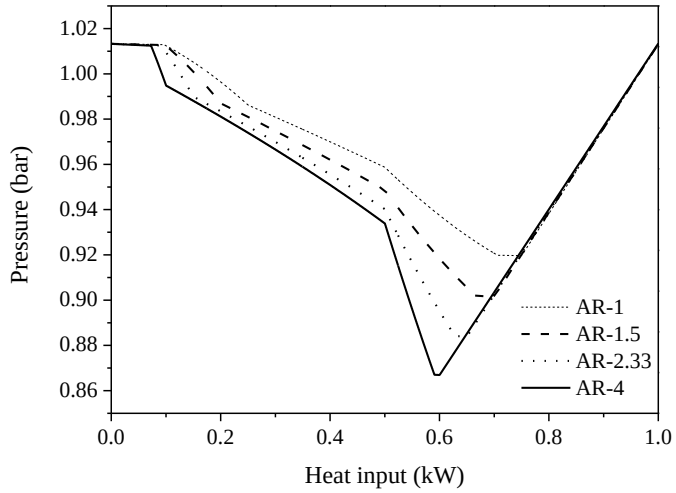

Fig.3.19 Variation of local pressure along the loop

Fig. 3.18 (a and b) shows the variation of heater exit quality and riser exit quality in the loop. As aspect ratio increases, vapour quality at heater exit and riser exit decreases that is observed in Fig. 3.18. This happens because of increase in mass flow rate, which is inversely proportional to the heater exit enthalpy. Thus for the same amount of heat input, decrease in heater exit enthalpy results in less vapour quality. It is also observed that there is a difference in heater exit vapour quality to the riser exit vapour quality as a result of flashing phenomena [5].

3.4.3 Effect of diameter

The effect of various tube diameters on the loop performance is studied in detail. Two different cases are considered here, first case heater and condenser diameter kept same and diameters of the riser and downcomer are varied simultaneously. Results obtained are shown in Fig. 3.20.

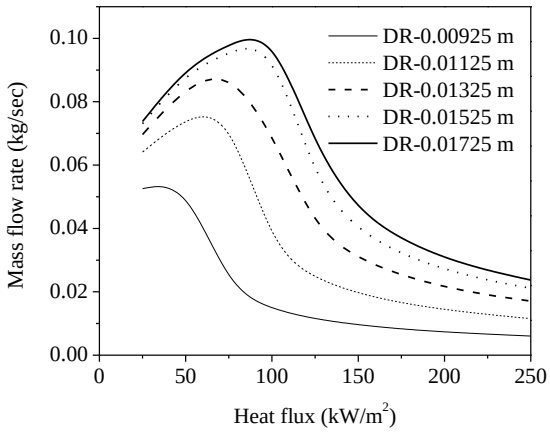

Fig.3.20 Variation of mass flow rate for different riser diameters

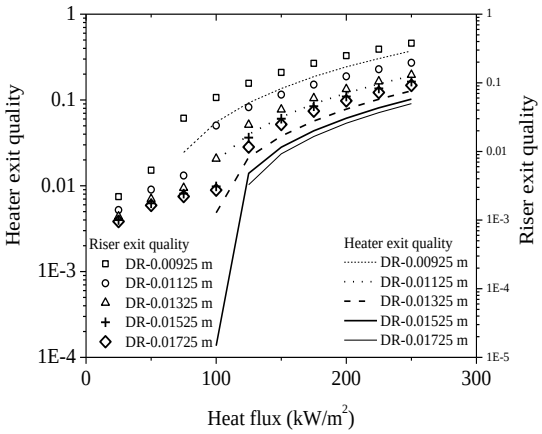

Fig.3.21 Variation of loop fluid quality for different riser diameters

The effect of riser diameter on the loop mass flow rate, heater exit vapour quality and riser exit vapour quality are shown in Fig.3.20, and Fig.3.21. By keeping the downcomer diameter same and decreasing the riser diameter, mass flow rate decreases. As riser diameter decreases it offers higher frictional resistance leading to lower mass flow rate. Due to decrement in mass flow rate the single phase subcooled length in heater section decreases and the vapour quality in the loop increases i.e. observed in Fig.3.21. Whereas, the effect of downcomer diameter on the loop mass flow rate has no significant effect (Fig.3.22.) This may be because the two-phase drop has a higher influence than that of single-phase pressure drop.

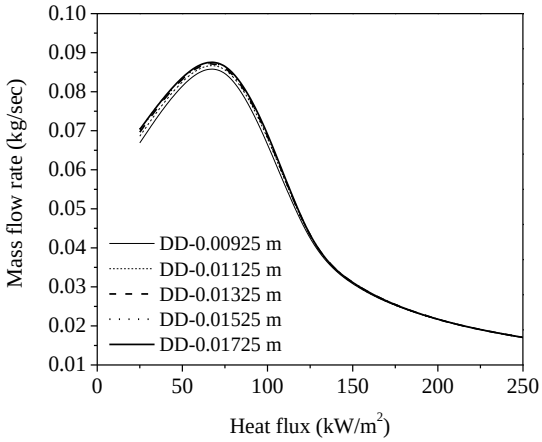

Fig.3.22 Variation of mass flow rate for different downcomer diameters

In the second case, the diameters of riser, downcomer, heater and condenser are assumed to be same, and they are varied simultaneously. These loops are uniform diameter loops (UDL). Fig. 3.23 shows the effect of diameter on loop mass flow rate for different heat fluxes. As the heat flux increases mass flow rate increases up to certain limit and then after

decreases. As diameter increases mass flow rate increases and the peak value is shifted to right. This happens because of the quality and pressure drop in the riser section. Fig. 3.24 shows the variation of quality in the loop. In homogeneous 1D modelling, quality is estimated as the area averaged value. As diameter increases the heater volume increases, hence the fluid quantity in the heater section increases. Thus, for the same amount of heat flux supplied at heater, exit quality of loop fluid decreases and higher quality can be obtained at higher heat fluxes. And as already discussed in the above section, the loop diameter increases the friction loss reduces. The decrease in quality provokes gravitational head in the riser. Hence the overall two phase pressure drop increases.

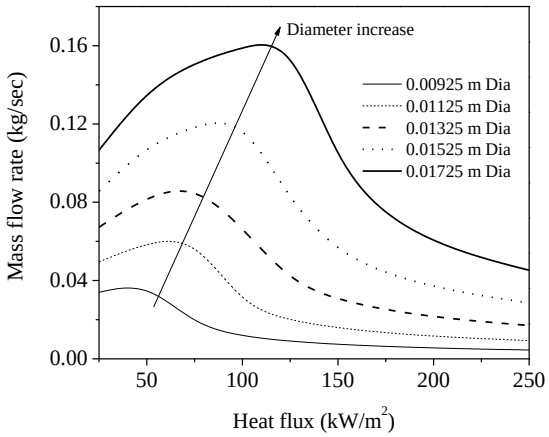

Fig.3.23 Variation of mass flow rate for different loop diameters

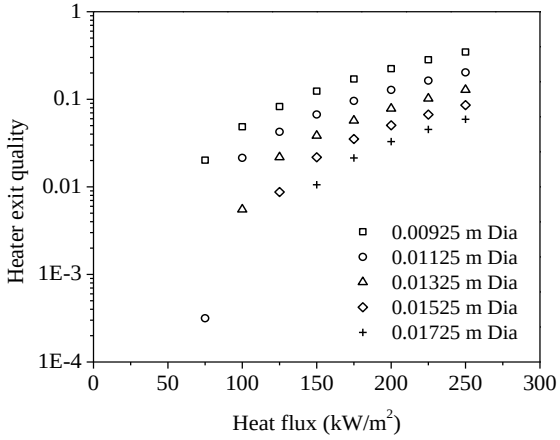

Fig.3.24 (a) Loop fluid vapour quality at heater exit

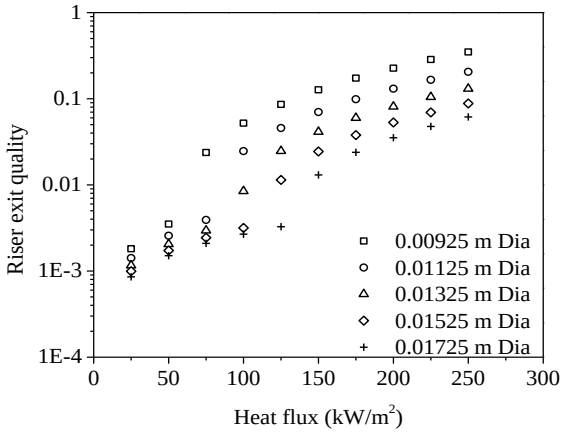

Fig.3.24 (b) Loop fluid vapour quality at riser exit

3.5 Influence of operating parameters

3.5.1 Influence of sub atmospheric pressure

Mass flow rate

The mass flow rate of the loop fluid is expressed as a function of the heat flux, inlet pressure and temperature as shown in Fig. 3.25. As the inlet temperature decrease the peak mass flow rates shift towards the right for all system pressures. The decrement in inlet temperature increases the sensible heat region in the heater, hence, the quality of loop fluid decreases. At the high heat fluxes, the quality of the loop fluid is more and possesses high drag forces in the riser. Fig 3.25 (a) shows the loop mass flow rate variation with the heat flux at the heater inlet temperature of 90^{o}C. At 0.8 atm system pressure, the loop has higher mass flow rate at low heat fluxes and sudden reaches the critical heat flux. The similar trend is followed for all pressures of atmospheric and sub-atmospheric conditions. The latent heat of sub atmospheric pressure is high, so, it is expected to sub atmospheric NCLs have lower quality. However, the saturation temperature decreases with decrease of pressure, hence the sensible heat region in the heater section decreases. So, the loop fluid early experiences the boiling or flashing. Therefore the quality in the riser is high for low system pressures, and hence, the corresponding mass flow rate is also improved. Further increasing the heat flux, the quality increases, and it offers frictional resistance, which causes to reduce the mass flow rate. Similar results are obtained for different inlet temperatures, as system pressure decreases.

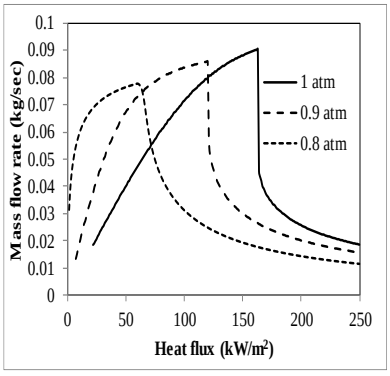

Fig.3.25 (a) variation of mass flow rate with respect to heat flux at heater inlet temp. of 90^{o}C

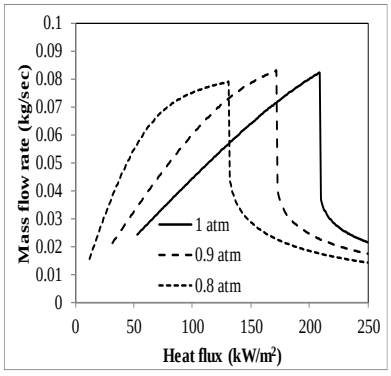

Fig.3.25 (b) variation of mass flow rate with respect to heat flux at heater inlet temp. of 85^{o}C

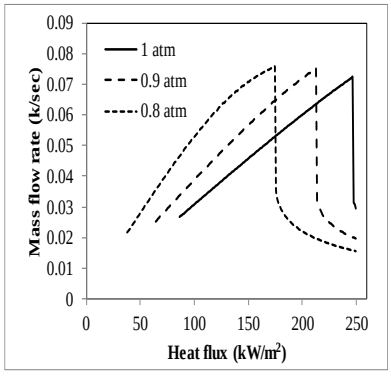

Fig.3.25 (c) variation of mass flow rate with respect to heat flux at heater inlet temp. of 80^{o}C

Pressure

The variation of local pressure along the loop length is plotted as a function of heat flux and system pressure at specific heater inlet temperature of 90 ^{O}C as shown in Fig. 3.26. The variation of local pressure follows the similar trend for both atmospheric and sub-atmospheric regions. Fig. 3.26 (a) to (c) individually shows the local pressure variation along the loop for a particular inlet temperature, at the system pressures of 0.8–1 atm. The pressure drop up to condenser is significantly varying with the system pressure. It is clear from Fig. 3.26 (a) that for a heat flux of 40kW/m^2 in the heater section the fluid is present in the sub-cooled state for all the system pressures considered. However in the riser section, the fluid in the loop with system pressure of 0.8 atm undergoes flashing earlier as compared to the other two loops. As the heat flux is increased to 60 and 120kW/m^2, as shown in Fig. 3.26 (b) and (c), respectively, the phase change happens in earlier locations within the heater and riser sections.

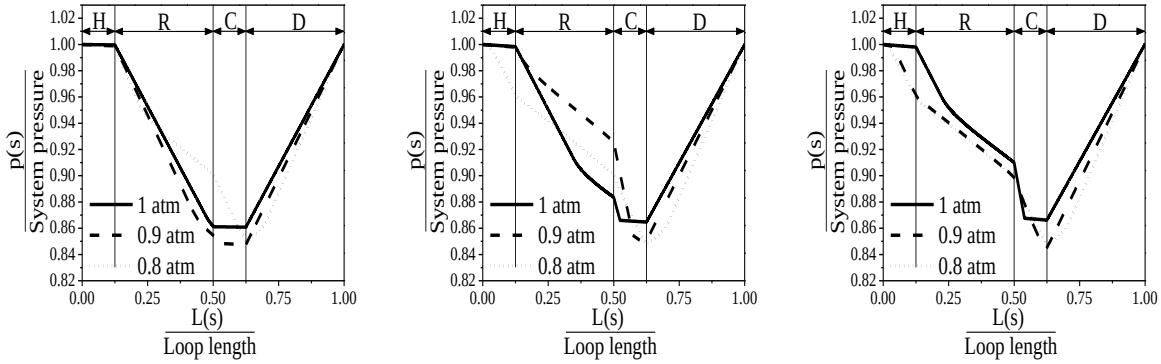

a. Inlet temp 90^{o}C , heat flux 40 kW/m^2 b. Inlet temp 90^{o}C , heat flux 60 kW/m^2 c. Inlet temp 90^{o}C , heat flux 120 kW/m^2

Fig. 3.26 Variation of local pressure along the loop

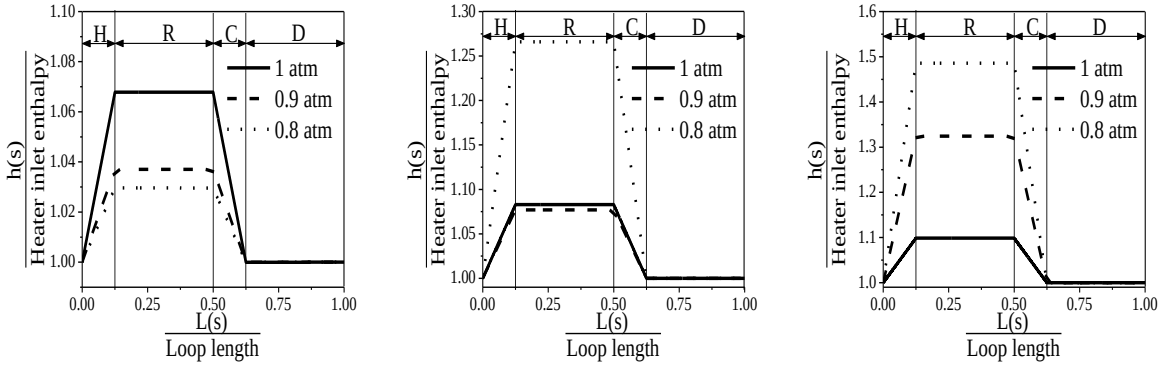

a. Inlet temp 90^{o}C , heat flux 40 kW/m^2 b. Inlet temp 90^{o}C , heat flux 60 kW/m^2 c. Inlet temp 90^{o}C , heat flux 120 kW/m^2

Fig. 3.27 Variation of local enthalpy along the loop

Enthalpy

Figure 3.27 (a) to (c) shows the variation of enthalpy along the loop length over a pressure range of 0.8–1 atm for the heater inlet temperature of 90 ^{O}C and heat fluxes of 40, 60 and 120kW/m^2, respectively. The enthalpy variation along the different sections in the loop is already described in Fig. 3.7 for atmospheric loop. As heat flux varies, the local enthalpy profiles at different pressures show significant variation. At the lower heat flux the loop fluid mass flow rate increases with decrease of pressure that can be observed in Fig. 3.25. Change in the enthalpy in the heater section is inversely proportional to the mass flow rate. So, the local enthalpy profiles along the loop length follow reverse trend to the mass flow rates. By increasing the heat flux, the loop fluid circulating at lower pressures will quickly reach the critical mass flow rate. It can be observed from Fig. 3.27 (a) to (c) for different pressures. As the heater inlet temperature decreases, the corresponding heater exit enthalpy in the loop fluid also decreases. This happens because of the increased sensible heat in the heater section.

Temperature

The variation of local temperature along the loop length is shown in Fig. 3.28 (a) to (c) for a heater inlet temperature of 90 ^{O}C and heat fluxes of 40, 60 and 120kW/m^2, respectively. The local temperature is expressed as a function of heat flux and system pressure. The variation of temperature for different sections in the loop with heat flux is already discussed in Figure 3.8 for atmospheric loop. Similar variation is observed for the sub-atmospheric loops. It is observed from Fig. 3.28 (a) to (c) that the loop operating at 0.8 atm and 90 _C heater inlet temperature, the downcomer has two-phase mixture as well. From Zahang et.al. [119] it is noticed that the downcomer is not always having a single-phase flow, and it depends on the local loop fluid condition. The local pressure in the downcomer increases with the favour of gravitational head and the two-phase mixture changes to single-phase fluid, i.e. liquid. As system pressure decreases the corresponding saturation temperature decreases. For a particular inlet temperature to the heater, the sensible heat region is less. However, the given heat input may or may not be sufficient for the loop fluid to undergo phase change in the heater. Thereafter, the loop fluid experiences flashing in the adiabatic riser. At all heat fluxes, as pressure decreases from 1 to 0.8 atm, the fluid experiences flashing or boiling early in the loop. This happens for all inlet conditions.

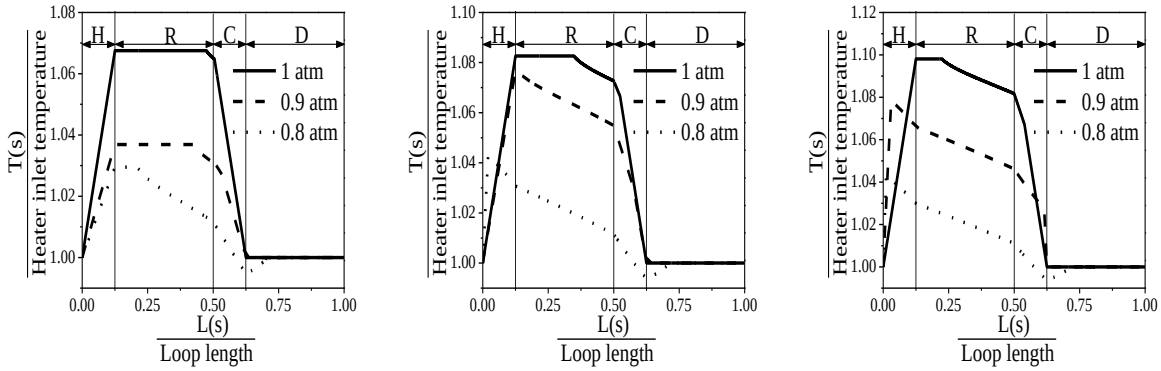

a. Inlet temp 90°C , heat flux 40 kW/m^2 b. Inlet temp 90°C , heat flux 60 kW/m^2 c. Inlet temp 90°C , heat flux 120 kW/m^2

Fig. 3.28 Variation of local temperature along the loop

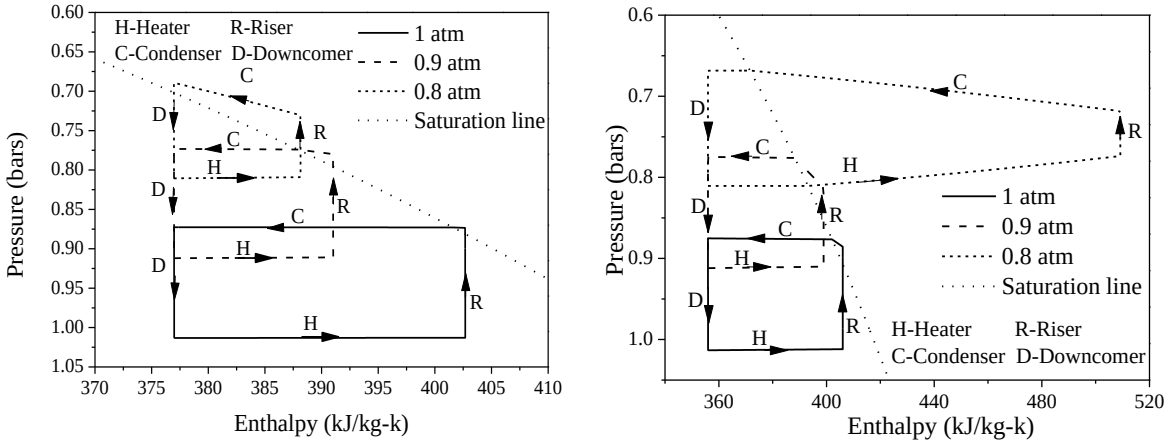

a. At heater inlet temp. 90°C and heat flux 40kW/m^2 b. At heater inlet temp. 85°C and heat flux 170kW/m^2

Fig. 3.29 p-h chart for the loop

Figure 3.29 shows the local pressure and enthalpy variation in the loop at a pressure range of 1–0.8 atm. The region is divided into single phase and two phases by a saturated line. The subcooled liquid absorbs the heat from the heater and increases its enthalpy. Based on the given heat input the loop fluid either in two-phase or single-phase mixture. In the adiabatic riser the enthalpy remains same and the pressure decreases. The decrement in local pressure along the riser increases the quality of the fluid. Thereafter the two-phase mixture enters into condenser and rejects the heat and its enthalpy decreases. The local pressure in the condenser has significant variation up to loop fluid phase change occurs. In the adiabatic downcomer sections, the enthalpy remains same and local pressure increases.

Figure 3.29 (a) is a p–h chart of NCL at lower heat input. In the heater section as system pressure decreases, there is no local pressure variation which means the loop is in single phase

and it undergoes flashing in riser. Similarly Fig. 3.29 (b) shows the NCLs at high heat flux. Loop operating at system pressure of 0.8 atm experiences boiling whereas for 0.9 and 1 atm NCLs have single-phase fluid at heater exit and undergoes phase change in riser. For the same amount of heat input, enthalpy variation is significant as system pressure varies, and it is dependent on the mass flow rate. For the same amount of heat input, the mass flow rate and enthalpy are inversely related.

3.5.2 Influence of Al_2O_3 particle concentration

The influence of nanoparticle concentration on loop behaviour is presented in this section. The nanoparticle concentrations considered in this study are 0.001%, 0.005% and 0.01% respectively. Such low concentrations are considered because of the particle deposition phenomena at higher concentrations during the nanofluid boiling. By fixing the loop fluid heater inlet condition at 95 ^{o}C and 1atm, Al_2O_3 nanoparticles concentration is varied.

Mathematical Modelling

In the nanofluid boiling the nanoparticles are assumed to stay with liquid phase only. Therefore same equations presented in section 3.1 for two phase NCL are used here. The thermo-physical properties correlations of the nanofluid are presented in table 3.3.

Table 3.3: Nanofluid thermo-physical properties correlations

Property	**Correlation**
Density	$\rho_{nf} = \emptyset\rho_{np} + (1-\emptyset)\rho_{bf}$
Specific heat	$Cp_{nf} = \frac{\emptyset\rho_{np}\rho Cp_{np}+(1-\emptyset)\rho_{bf}Cp_{bf}}{\rho_{nf}}$
Viscosity	$\mu_{nf} = (1 + 2.5\emptyset + 6.5\emptyset^2)\mu_{bf}$

Fig.3.30 (a, b, and c) depicts the effect of nanoparticles concentration on density, specific heat and viscosity respectively. The considered particle concentrations are less so the variation on thermos-physical properties is insignificant that can be observed in Fig.3.30 (a, b, and c).

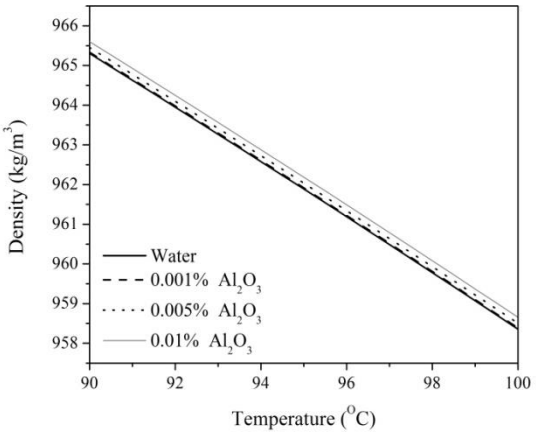

Fig. 3.30 (a) Variation of density with temperature

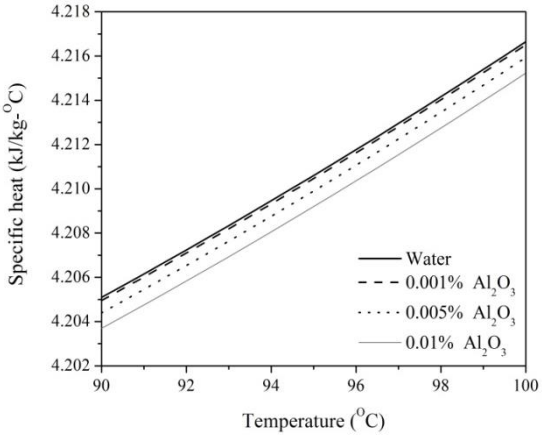

Fig. 3.30 (b) Variation of specific heat with temperature

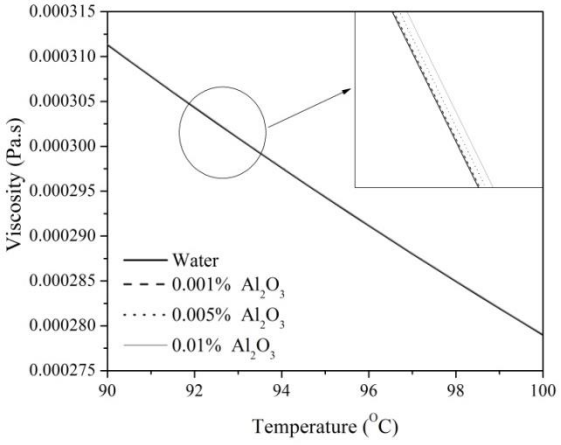

Fig. 3.30 (c) Variation of viscosity with temperature

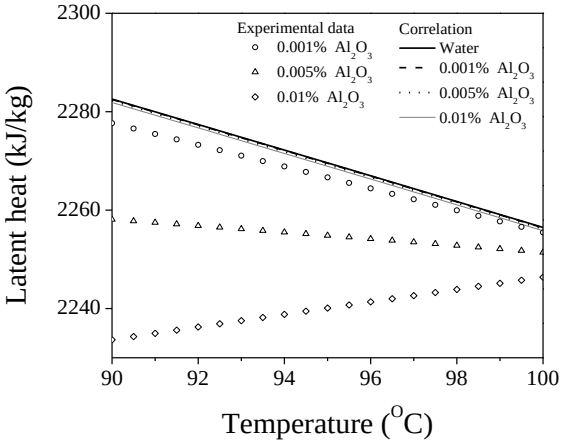

Fig. 3.30 (d) Variation of latent heat with temperature

Enthalpy and latent heat of nanofluid are the remaining parameters to estimate. The enthalpy of the nanofluid is expressed as function of specific heat and temperature. In order to estimate the latent heat of nanofluid across the loop as per the fluid state there is a need of data. So in the present work latent heat of nanofluids is obtained by the data interpolation of C.Y. Tso and C.Y.H. Chao [120]. The data interpolation is done under the temperature limits of 85 ^{O}C to 100 ^{O}C and for the concentration of 0 to 0.01%. Fig.3.30 (d) shows the variation of latent heat of Al_2O_3 nanofluids at different concentrations.

Steady state analysis

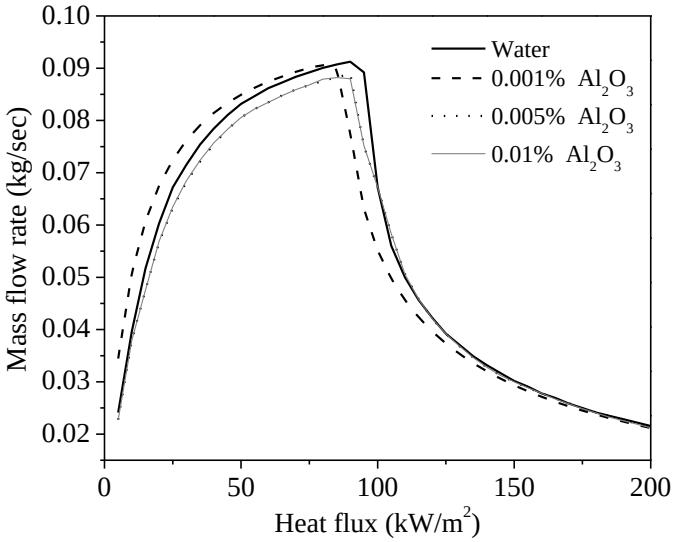

Fig.3.31 Variations of mass flow rate with heat flux

Fig. 3.31 depicts the mass flow rate variation with respect to heat for different nanofluids. The mass flow rate behaviour w.r.to heat flux is same for both nanofluids and water. The mass flow rate of the 0.001% Al_2O_3 nanofluid is high as compared with water and other two nanofluids. The average enhancement in mass flow rate as compared with water is 9.01% up to the critical heat flux. The 0.005% and 0.01% Al_2O_3 nanofluids have low mass flow rate as compared with water. The addition of nanoparticles in the base fluid does not have much influence on the thermo-physical properties like density, specific heat. But the latent heat of nanofluid is significantly reduced resulting in increased vapour quality in the riser section. So the buoyancy forces in riser section increases which results in increased mass flow rate. However, increase of nanoparticles concentration to 0.01% in the loop fluid results in further increase in vapour quality for the same heat flux. The increased vapour quality offers drag in the riser section and mass flow rate decreases.

3.6 Conclusions

In chapter 3, a 1D numerical model is developed to analyse the steady-state analysis of two phase rectangular NCL. The influence of various parameters such as heater and condenser orientation, aspect ratio, diameter of the various sections in the loop, pressure and nanoparticle

concentration is studied. The following major conclusions have been drawn from the numerical analysis.

1. The proposed model is validated with Vijayan's [57] correlation. The maximum error obtained is ±5%.
2. Two phase NCLs performance is affected by different parameters such as heater and condenser orientation, heater inlet temperature, heat flux, aspect ratio, diameter, pressure and type of the loop fluid.
3. Heater and condenser orientations and positions are considered as per the design and constructional constraints. However it is better to place the condenser in a horizontal orientation.
4. As aspect ratio increase, the loop height increases and mass flow rate increases. This is due to high pressure gradient across the riser and downcomer sections.
5. NCL performance is strongly affected by loop riser diameter. An increment in riser diameter leads to reduce the two-phase frictional pressure drop which leads to a higher mass flow rate and lower quality in the loop. Whereas varying the downcomer diameter has insignificant effect on loop performance.
6. As the system pressure decreases from atmospheric to sub-atmospheric, the loop fluid experiences early flashing or boiling. Hence, at lower heat fluxes the loop exhibits higher density gradients. So, NCLs operating at sub-atmospheric pressure have high mass flow rates at lower heat fluxes as compared to NCL operating at atmospheric pressure.
7. For a particular heater inlet temperature and fixed heat flux, the decrement in system pressure decreases the sensible heat capacity of the loop fluid and remaining heat is used as enthalpy of vaporisation which leads to the increase of loop fluid quality (void fraction). Further decrement in local pressure situates high quality fluid in riser and offers more drag/frictional forces resulting in lower mass flow rate.

Chapter 4

Experimental studies on flow boiling of alumina nanofluid

Chapter 4

Experimental studies on flow boiling of alumina nanofluid

This chapter describes the vertical flow boiling behaviour of alumina/water nanofluids under subcooling and saturated boiling conditions. The procedure to prepare nanofluid and estimation of thermo-physical properties is explained below with complete details of the experimental set-up. The test section (main heater) is made up of borosilicate glass tube to observe the flow patterns/regimes of the working fluid. Uncertainty analysis is carried out and presented briefly. Finally the flow boiling behaviour of alumina nanofluids with special emphasis on flow pattern transitions are discussed.

4.1 Nanofluid preparation

Nanofluids can be prepared by two methods i.e. single step method and two step method.

4.1.1 Single step method

In Single step method, nanoparticle preparation and dispersion in a base fluid is carried out in one ago [46], [143]. This method is suitable for high thermal conductive metals to avoid oxidation. Uniform dispersions of nanoparticles in the base fluid and consequently high stability can be attained by using this method. Additionally, tedious sequence of steps such as drying, storing, dispersing of the nanoparticles can be avoided. The main drawback of this method is that the nanofluids cannot be manufactured on a commercial scale and it is not a cost effective method for large scale nanofluids production..

4.1.2 Two step method

In the two-step method, nanoparticles are preparation and suspension in a base fluid take place sequentially. Desired concentrations of fluids can be prepared easily. The primary advantage of this method is that the thermo-physical properties can be controlled comparatively in a better way than single-step method. An important feature of this method is that nanoparticles can be prepared commercially and economically at large scale. However, the inevitable agglomeration of such particles is a major problem due to the cohesive and van der Waal forces between the nanoparticles. This agglomeration can be controlled by using the appropriate surfactant or

dispersant at critical micellar concentration. Agglomeration can also be reduced by the use of appropriate mechanical dispersion devices such as ultrasonic bath, magnetic stirrer, high-pressure homogenizer and ultrasonic disrupter.

4.1.3 Nanofluid preparation for the current research work

In the present work two step method is used to prepare the Al_2O_3/water nanofluid. Distilled water was used as base fluid for nanofluid preparation. The specifications of the received nanoparticles provided by reliable manufacturer is summarized in Table 4.1.

Table 4.1: specifications of the nanoparticles

Vendor	**SISCO Research laboratory Pvt Ltd**
Particle size (nm)	20-30
Particle thermal conductivity (W/m K)	40
Particle density (kg/m^3)	3950

The mass of the nanoparticles required for a particular particle concentration is estimated by using eq.4.1.

$$\emptyset = \frac{\left(\frac{m}{\rho}\right)_{np}}{\left(\frac{m}{\rho}\right)_{np}+\left(\frac{m}{\rho}\right)_{bf}} \tag{4.1}$$

A digital electronic balance (Figure 4.1) is used to weigh the nanoparticles. First surfactant (CTAB, 10% by wt. of nanoparticles) is added to the base fluid and sonicated for 30 minutes using a sonicator (Figure 4.2). The addition of surfactant to base fluid improves the stabilization of the nanofluids and the distribution of suspended nanoparticles. Then after, the weighted alumina nanoparticles are added to base fluid, and sonicated by a sonicator for 5 hours with a cycle time of 10 min sonication and 2 min idle time. A well-dispersed stable alumina nanofluid is obtained at the end as shown in Figure 4.3.

Fig.4.1 Electronic Weighing measuring device

Fig.4.2 Ultra sonicator

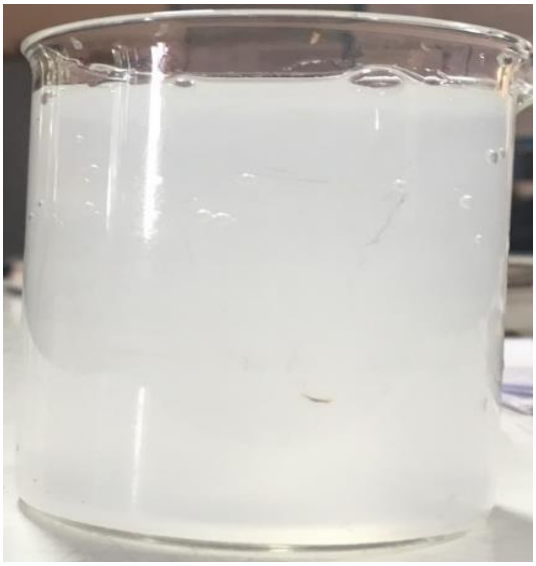

Fig.4.3 0.005% Al_2O_3 nanofluid (sample).

In the present study nanofluids having particle concentrations of 0.001%, 0.005%, and 0.01%. are prepared for experimentation.

4.2 Estimation of thermo-physical properties of nanofluids

For better understanding of the boiling behaviour of nanofluid the precise estimation of thermo-physical properties such as thermal conductivity, specific heat and density are required. This parameters are used to calculate the heat transfer coefficient (HTC), superficial gas and liquid velocities. The estimation of these parameters is discussed in the below section.

4.2.1 Estimation of density (theoretical)

In this study very low concentrations of nanoparticles are dispersed in water. Hence it is expected that the density of the nanofluids is negligibly differ from that of water. The density of nanofluid is estimated based on the principle of the mixture rule and it can be calculated by using eq. 4.2. [121].

$$\rho_{nf} = \left(\frac{m}{V}\right)_{nf} = \frac{m_{bf}+m_{np}}{V_{bf}+V_{np}} = \frac{\rho_{bf}V_{bf}+\rho_{np}V_{np}}{V_{bf}+V_{np}} = \emptyset\rho_p + (1-\emptyset)\rho_{bf} \quad (4.2)$$

4.2.2 Estimation of thermal conductivity and specific heat (Experimental).

Thermal conductivity and specific heat of all the working fluids (water and nanofluids) considered in the current work were measured experimentally using thermal conductivity analyzer (TPS 500S, Therm. Test Inc., Fredericton, Canada), which is shown in Fig. 4.4(a). The instrument is equipped with different types of sensors with a software module interface to measure the thermal conductivity and specific heat of different materials like bulk materials, powders, thin films, and wide range of liquids including nanofluids. This instrument measures thermal diffusivity and specific heat is estimated. The apparatus works based on transient plane source principle and follows ISO 22007-2.2 standards. In the current work, 7552 Kapton sensor of 2 mm diameter was used to measure thermal conductivity and thermal diffusivity of nanofluids for different particle concentrations. The equipment was supported with a thermostatic bath to facilitate the measurement of the thermal conductivity over a wide range of temperatures, from -20 °C to 200 °C.

To measure the thermal conductivity and thermal diffusivity of nanofluid, Kapton sensor was immersed in the nanofluid filled attachment, so that both sides of the sensor had identical environment. The arrangement was kept idle for 20 min to attain thermal equilibrium state and then thermal conductivity and thermal diffusivity were measured from the software interface module. Each sample was tested three times under identical temperature conditions and average of the readings were considered for the further analysis. The sensor-sample arrangement is as shown in Fig. 4.4 (b).

Fig. 4.4 (a) Thermal conductivity Analyzer

Fig. 4.4 (b) Conductivity measuring sensor

For the flow boiling experiment the working fluid enters the heater section at ≈ 95 ^{O}C. So the thermal conductivity and specific heat of the working fluid (water and nanofluids) is estimated at 90 ^{O}C and 95 ^{O}C and presented in Table 4.2.

Table 4.2: Thermo-physical properties of nanofluids

Temperature	Fluid	Density (kg/m^3)	Specific heat (kJ/kg-K)	Thermal conductivity (kW/m-K)
90 ^{o}C	0.001% Al_2O_3/water	965.35	4.1838	0.7056
	0.005% Al_2O_3/water	965.47	4.1622	0.7234
	0.01% Al_2O_3/water	965.63	4.1405	0.7791
	Water	965.32	4.2058	0.6735
95 ^{o}C	0.001% Al_2O_3/water	961.93	4.1893	0.7007
	0.005% Al_2O_3/water	962.08	4.1678	0.7197
	0.01% Al_2O_3/water	962.19	4.1461	0.7695
	Water	961.90	4.2106	0.6755

4.3 Details of the experimental setup, data reduction and uncertainty

4.3.1 Experimental setup

Schematic and pictorial view of the flow boiling experimental apparatus for the present study is shown in Figure 4.5 (a) and (b).The test facility consists of a fluid flow control system and data acquisition system. The reservoir tank [1] is equipped with immersion heaters [2] to maintain the temperature required in the liquid control system. Fluid circulation is achieved by using a centrifugal pump [3] and flow rate in the test section is adjusted by a bypass valve [4]. The fluid enters into the pre heater [5] to attain the required subcooling. The pre heater is made of SS-316 steel pipe with I.D and O.D 16 and 20 mm, respectively. A nichrome wire of resistance 53.5 Ω is uniformly wound around the pipe. Then the subcooled fluid is made to enter into the main heater (test section) [6]. In order to visualize the flow boiling at heater exit, borosilicate glass of 7.5mm ID and 12mm OD is used. Similar to pre heater, the main heater consists of nichrome wire of resistance 41.5 Ω uniformly wound along a length of 0.2 m.

A glass wool of 50mm thickness is wound around both the heaters to reduce the heat loss to the ambient. Variac transformer [7] is used to vary the heat flux in the main heater section. After the main heater, the loop fluid enters into the condenser [8] and undergoes condensation, finally returns to the reservoir. The mass flow rate of the loop fluid is measured using a calibrated rotameter [9]. While temperatures are measured with K type thermocouples and recorded by using Agilent data acquisition system [10]. The fluid temperatures are measured at inlet and outlet sections of the main heater and the reservoir tank. The heater wall temperature is measured at outer surface at three different axial locations, as shown in Figure 4.6 (a). To get accurate wall temperature three thermocouples are placed radially at every axial location as shown in Figure 4.6 (b).These thermocouples are electrically insulated to avoid short circuiting. The parameters such as pre-heater heat flux, condenser cold fluid temperature and mass flow rate are controlled in order to achieve a stable state condition in the loop.

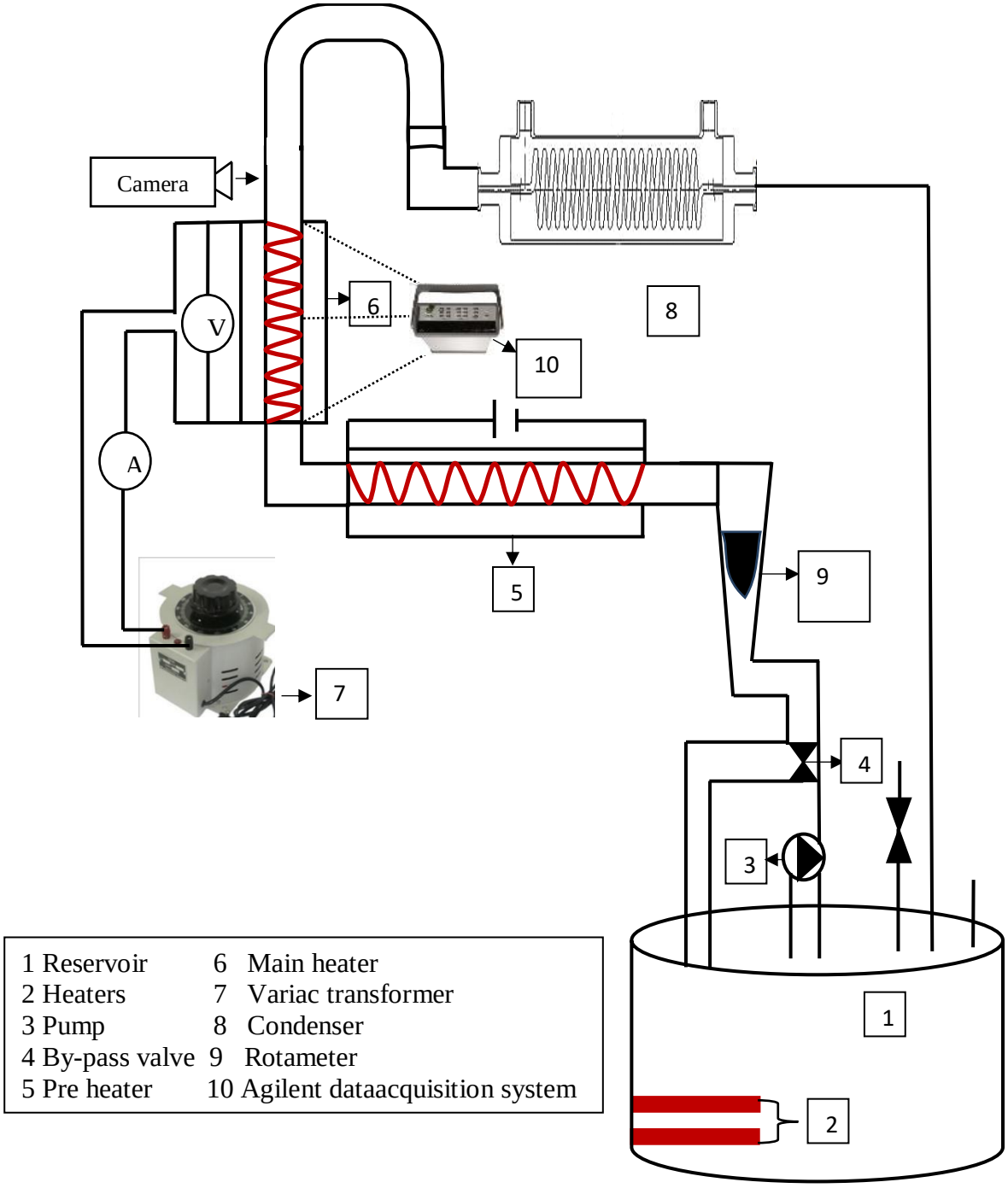

Fig.4.5 (a) Schematic view of flow boiling experimental apparatus

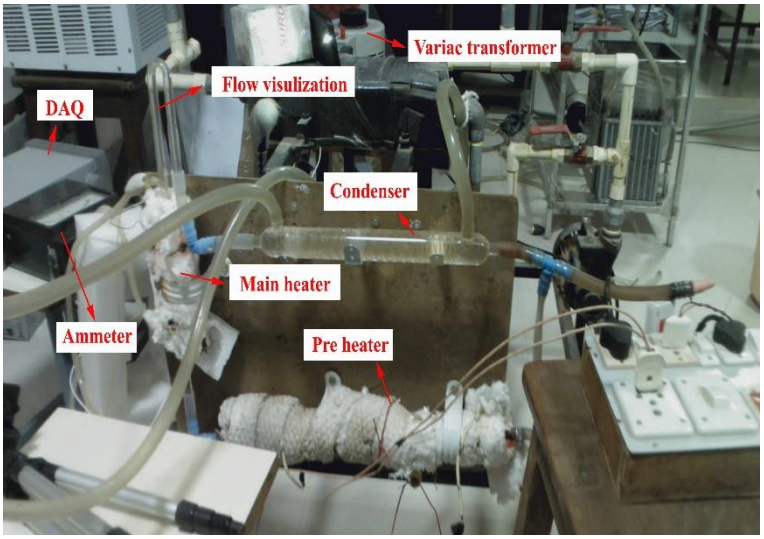

Fig.4.5 (b) Pictorial view of flow boiling experimental apparatus

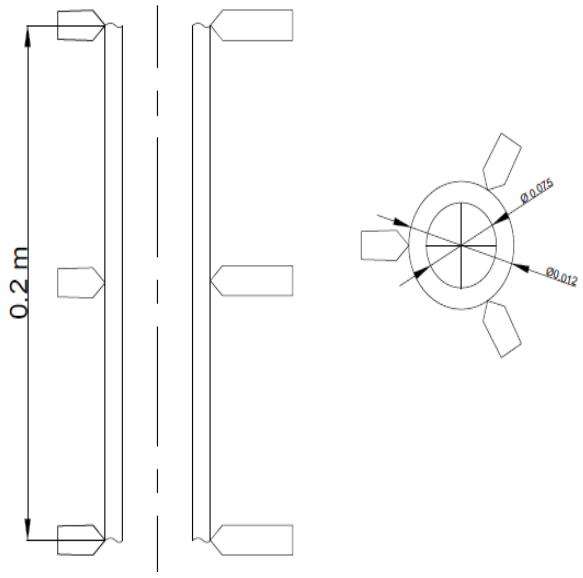

Fig. 4.6 (a &b) Thermocouple location on main heater

4.3.2 Experimental Procedure

The influence of dissolved gases strongly affects the flow boiling heat transfer and pressure drop [122]. Hence, before the start of each experiment, the fluid was degassed by boiling it in the reservoir tank rigorously using an immersed heater for more than one hour. While boiling, the fluid was kept in circulation by using a pump in order to reduce the deposition of nanoparticles at the heater outer surface. After degassing, power supply was given to the required components in order to control the reservoir temperature. Once the desired inlet

subcooling conditions at the main heater was achieved, the main heater was switched on to impose constant heat flux and constant flow rate throughout the experiment. Experiments were conducted at steady state condition which was ensured by checking the temperature at different locations. Heat flux was increased by using variac transformer and then the condenser coolant conditions (mass flow rate and temperature) were adjusted in order to achieve constant heater inlet conditions. Experiments were conducted for different mass flux values of 905.42, 679.06 and 452.71 kg/sec-m^2 at fluid inlet temperature of 95 ^{O}C by varying the heat flux from 73.60 to 247.45 kW/m^2.

4.3.3 Data reduction and uncertainty analysis

Heat transfer data reduction

The heat supplied to the main heater (test section) is given by

$$Q = V.I \tag{4.3}$$

Where V is voltage and I is current measured by the voltmeter and ammeter respectively, which have uncertainty of 0.28 % and 0.15% respectively.

After accounting for the losses (convection and radiation), the net heat absorbed by the fluid is given by

$$Q_{net} = Q - Q_{loss} \tag{4.4}$$

where; $Q_{loss} = Q_{convection} + Q_{radiation}$

The convection losses are evaluated by using eq. 4

$$Q_{convection} = h_{air} A_{surface} \left(T_{surf} - T_{amb}\right) \tag{4.5}$$

where h_{air} is convective HTC for the air , A_{surf} outer surface area of the pipe after insulation and it is estimated by ($A_{surf} = \pi D_{surf} L$), T_{surf} is insulation temperature and T_{amb} is ambient temperature.

The radiation losses is evaluated by using eq. 5

$$Q_{rad} = \sigma A_{surf} \left(T_{surf}^4 - T_{amb}^4 \right) \tag{4.6}$$

Where σ is Stefan Boltzmann constant and the value is 5.67 $\times 10^{-8}$ W/m^2-K^4

The net heat flux obtained inside the test section (main heater) is given by

$$q_{net} = \frac{Q_{net}}{\pi D_{in} L} \tag{4.7}$$

The loop fluid enters the test section at sub-cooled state ($T_{f,i} < T_{sat}$) for all experiments. As per the given heat input, the fluid may exist in a sub-cooled state or saturated state along the test section during the flow. Therefore the test section is virtually divided into two regions (single phase region and two phase region). The length of the single phase region in the test section is estimated by using eq.4.8 [28]

$$Z_{sc} = \frac{G(h_{sat} - h_{in}) D_{in}}{4 q_{net}} \tag{4.8}$$

where h_{sat} is saturation enthalpy calculated based on the inlet pressure.

If $Z_{sc} > L$ the fluid is either in single phase or in sub cooled boiling phase. The sub cooled boiling is observed by visualising bubble formation at the test section outlet. While, if $Z_{sc} < L$ the test section is in single phase region and the saturated region as well. The local HTC (h) is estimated by using eq.4.9 [37]with inputs of local fluid temperature, wall temperature and the given heat flux.

$$h_i = \frac{q_{net}}{T_{wall,i} - T_{fluid,i}} \tag{4.9}$$

where 'i' is axial location along the pipe. For the present study, heat transfer coefficients are obtained at the exit of the test section. $T_{wall,i}$ is the inner surface wall temperature. As, provision to measure inside wall temperature $T_{wall,i}$ is not available in the test rig, thermocouples are located at the outer surface of the test section pipe. Inner wall temperature is obtained by using

steady state one-dimensional heat conduction equation of cylindrical co-ordinates and is given by eq.4.10 [35]

$$T_{wall,inner} = T_{wall,outer} + \frac{Q_{net}}{4\pi k_{gp} L}\left(\frac{\xi(1-ln\xi)-1}{\xi-1}\right) \quad (4.10)$$

Where ξ is given by $\left(\frac{D_o}{D_{in}}\right)^2$

The thermodynamic vapour quality at the exit of the test section (x) is estimated from the energy balance and is given by eqn. 4.11.

$$x = \frac{q_{net}\pi D_{in}(L-Z_{sc})}{GA_{cs}h_{fg}} \quad (4.11)$$

4.3.4 Uncertainty analysis

This uncertainty analysis is to assess the errors associated with the experiments. The uncertainties of the instruments used in this test rig are summarized in Table 4.3.

Uncertainties of surface area, heat flux, mass flux and HTC have been evaluated based the procedure mentioned by J. R. Taylor et.al. [123]. The maximum possible uncertainties involved in the experiments are estimated and summarized in Table 4.4

Table 4.3: Uncertainties of the instruments

Measuring parameter	**Measuring unit**	**Uncertainty**
Voltage	Voltmeter	0.8 %
Current	Ammeter	3 %
Length	Verniercaliper	± 0.02 mm
Diameter	Multimeter	± 0.02 mm
Temperature	Thermocouple	± 0.5 ^{O}C
Mass flow rate	Rotameter	1.5%

Table 4.4: Uncertainties of the estimated data

S.No	Variable name	Uncertainty (%)
1	Surface area	0.27
2	Heat flux	3.12
3	Mass flux	1.59
4	Heat transfer coefficient	8.31

4.4 Result and discussion

This section describes the heat transfer characteristics of water and Al_2O_3/water nanofluids by considering sub cooled and saturated flow boiling at the heater exit. The concentrations of Al_2O_3 are 0.001%, 0.005% and 0.01% by volume. Experiments were conducted over a heat flux range of 65-250 kW/m^2, for mass fluxes of 905.42, 679.06 and 452.71 kg/s-m^2 at atmospheric pressure. The operating parameters were same for all working fluids (water and Al_2O_3 nanofluid). The aim of the present experimental work is to study the effects of imposed wall heat flux and mass flux on flow boiling heat transfer coefficient (HTC) and the corresponding flow regimes for the nanofluid (Al_2O_3/water).

4.4.1 Vertical flow boiling regimes for water and nanofluid

Flow visualization study was done to better understand the boiling heat transfer mechanism. Flow regime was observed at the heater exit using a camera with a frame rate of 240fps. The flow regimes observed from the experimental data were plotted on Kaichiro Mishima [124] flow regime map. The KaichiroMishima [124] flow regime map is well suited for boiling flows (steam water flows) and the same method is used for nanofluids. The experimental data corresponding to the saturated region is drawn on the flow regime map.

Figure 4.7 (a) depicts the flow map for water and Fig.4.7 (b, c and d) depicts the flow map for nanofluids for mass fluxes of 905.42, 679.06 and 452.71 kg/s-m^2 respectively. As per the imposed heat flux and mass flux, the experimental data points of the water lie in bubbly flow, slug flow, churn flow and annular flow regimes. For the nanofluids, most of the experimental data points lie in slug flow and annular flow regimes that can be observed in

Fig.4.7 (b, c and d). That means nanofluids don't exhibit churn flow regime. In the experimental observation, churn flow regime is very rare for nanofluids and it appears for water especially at low mass fluxes (452.71 kg/s-m^2). At high mass fluxes (905.42 kg/s-m^2) water exhibits slug flow and annular flow regimes (Fig 4.7 (a)). The bubbly flow and slug flow appears either at high superficial liquid velocities or low superficial vapour velocities.

At low heat fluxes, water and nanofluids have lower superficial vapour velocities in which flow exhibits either bubbly flow or slug flow. Further increase of superficial vapour velocity by means of increasing imposed heat flux results in flow transitions from either bubbly to slug or slug to annular.

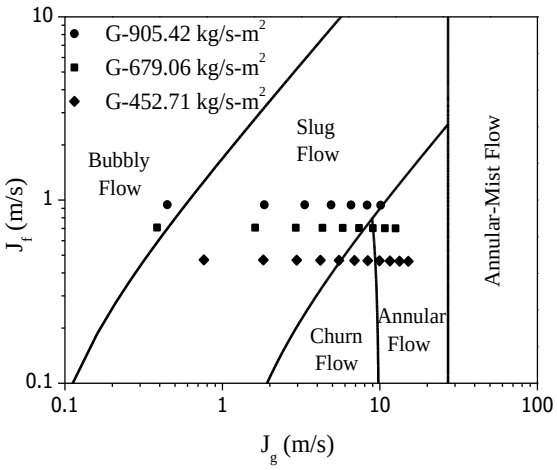

Fig.4.7 (a). Flow map for water

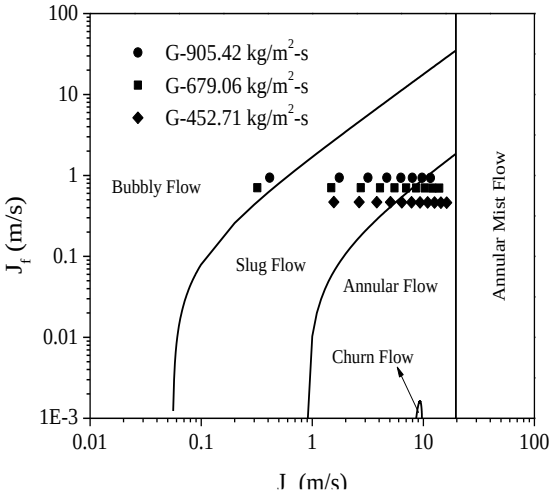

Fig.4.7 (b). Flow map for 0.001% Al_2O_3/water nanofluid

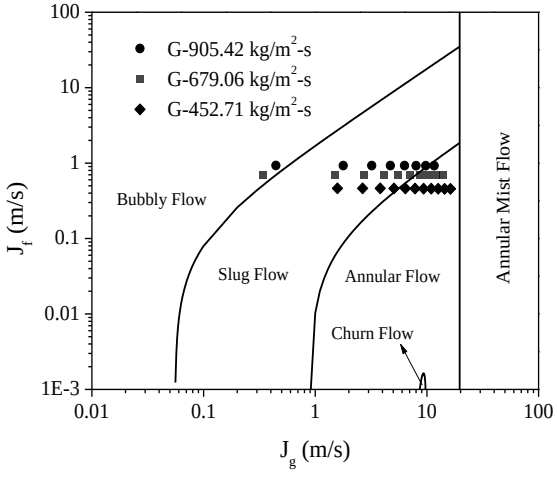

Fig.4.7 (c). Flow map for 0.005% Al_2O_3/water nanofluid

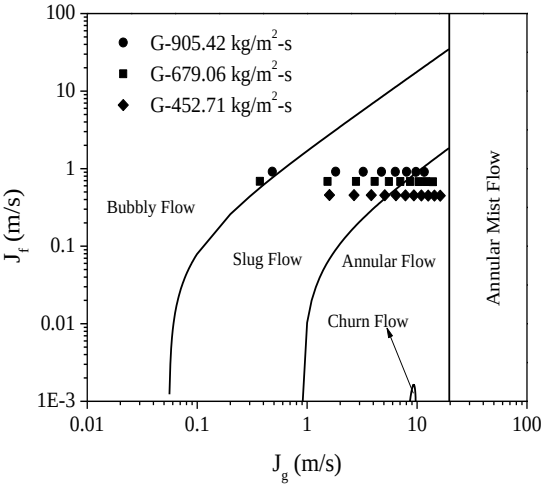

Fig.4.7 (d). Flow map for 0.01% Al_2O_3/water nanofluid

The photographic views of the flow are used to validate the flow map. The nanofluids have poor transparency and hence it is hard to visualize the patterns. However, for lower concentration of 0.001% an attempt was made to capture the flow regimes. The different flow regimes that are observed in the present study are discussed in subsequent section.

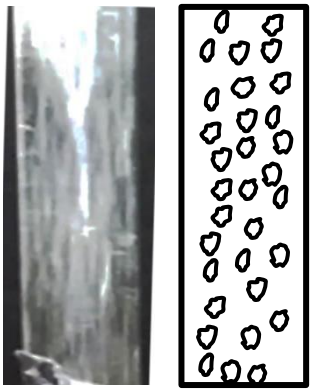

Mass flux= 905.42 kg/s-m^2,
Heat flux = 130.87 kW/m^2

Fig.4.8 (a) Bubble flow regime for water

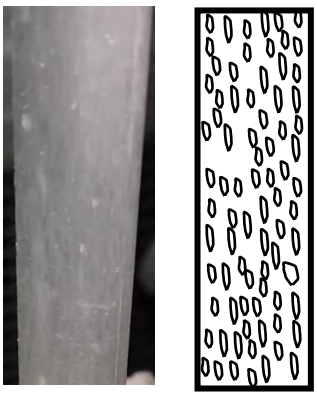

Mass flux= 905.42kg/s-m^2,
Heat flux = 130.87 kW/m^2

Fig.4.8 (b) Bubble flow regime for 0.001% Al_2O_3/water nanofluid

Bubbly flow

During sub cooled boiling, once the required superheat is achieved by the wall, bubble nucleation starts. The generated bubbles detach from the heater surface and collapse in bulk fluid thereby causing an increase in bulk fluid temperature. Increase of heat flux results in more active nucleation sites which results in increase of bubble departure population. These departed bubbles can be sustained in the main stream because of low local subcooling and this phenomena is indicated as onset of significant void (OSV). As the heat flux further increases, vapour quality increases with the nucleation sites and the bubbles grow and detach from the heater surface and these bubbles travel along the liquid phase which is known as bubbly flow (evident from Fig.4.8).The line diagram drawn based on the video observations is provided for better understanding. Bubbly flow regime is observed in water and all nanofluids for the mass fluxes of 905.42. & 679.06 kg/s-m^2 over a heat flux range of 68- 130.87 kW/m^2 and 68-100kW/m^2 respectively. Heat transfer is taking place in this regime majorly with single phase forced convection. The bubble behaviour (bubble formation, growth at nucleation sites, slide and detachment from the heater surface) is the same for water and all Al_2O_3 nanofluids. Similar behaviour was observed by N.Patra et.al. [125]. However, from the experimental observation,

it is noticed that bubble size for all the nanofluids is smaller as compared to water. But the bubble detachment frequency for nanofluids is more compared to water. The reason may be attributed to altered heater surface characteristics. While nanofluid boiling takes place, the fluid leaves the nanoparticles at the heater surface as a result of evaporation. The deposition of nanoparticles on the heater surface forms a porous layer [102] and alters the heater surface characteristics such as roughness, nucleation sites and thermal resistance, which have a strong influence on bubble behaviour.

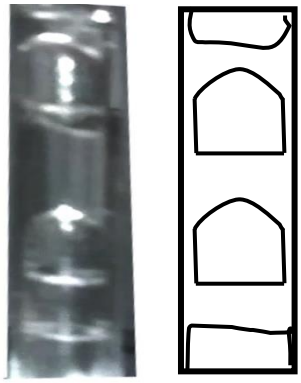

Mass flux= 679.06kg/s-m^2,

Heat flux = 147.74kW/m^2

Fig.4.9 (a) Slug flow regime for water

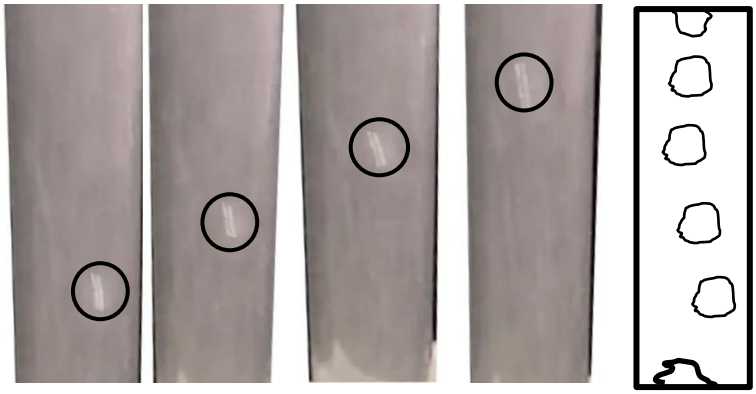

Mass flux= 679.06 kg/s-m^2,

Heat flux = 147.74 kW/m^2

Fig.4.9 (b) Slug flow regime for 0.001% Al_2O_3/water nanofluid

Slug flow

As the heat flux was further increased, the size of detached bubbles and their population from the heater surface also increased. In pure water, bubble growth rate was more and very large sized bubbles were formed. The time period before bubble detachment from the heater was high. However, for nanofluid the time period before bubble detachment was low. The bubble departure radius is also low for nanofluid. This is due to low surface tension and also as a result of variation in net force acting at the interface (triple line [126]). These detached bubbles continued to grow and coalesce with other bubbles and formed larger bubbles (bullet shaped). This flow regime is treated as slug flow. The photographic view of slug flow for water and nanofluid is shown in Fig.4.9a and Fig. 4.9b respectively, and this flow regime existed in all mass fluxes. In this regime, the major portion of heat transfer is achieved by nucleate boiling. Compared with water, the slug size is smaller for nanofluids which can be observed in Fig.4.9 (b). It is also observed that slug shape was almost circular for nanofluid.

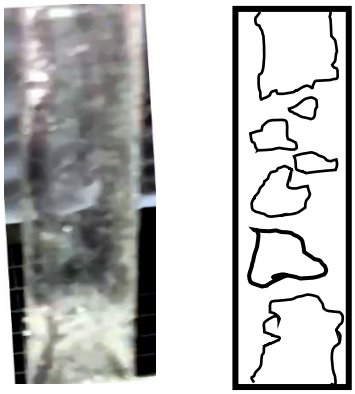

Mass flux= 452.71 kg/s-m^2,
Heat flux = 165.64 kW/m^2

Fig.4.10 Churn flow regime for water

Churn flow

On increasing the heat flux further heater surface area was covered with more active nucleation sites and hence bigger bubbles were detached which grow and coalesce with other bubbles and form large bullet shaped bubble (Taylor bubble). The relative parity between the gravitational and frictional forces acted in opposite direction on liquid Taylor bubble. So, these bubbles are unstable, fragile and rearrange themselves to form either irregular small bubbles or cap shaped bubbles [127]. Hence flow transits from slug to churn flow. In churn flow the vapour and liquid interface is chaotic in nature while the net flow moves upwards. Due to chaotic flow oscillations, the heater surface undergoes local burn out, which should be prohibited to protect the heater. The churn flow regime in the nanofluids is rarely observed. Sometimes, churn flow was observed for a very short duration of time. The bubbles are small sized compared to water. These small sized bubbles coalesced and transited to slug flow. In water, for mass flux of 452.71 kg/s-m^2, it exhibited churn flow at the heat flux range of130.87 to 165.64 kW/m^2.A sample photographic view is shown for the heat flux of 147.74 kW/m^2 in Fig, 4.10.

Annular flow

On increasing the heat flux further, the small sized bullet shaped bubbles coalesce and form annular flow regime at the heater exit. The photographic view of annular flow for water and nanofluid is shown in Fig.4.11 (a, b and c). From the flow regime map (Fig.4.7), it is observed that in nanofluids, the transition from slug to annular flow happens without churn flow. It is

evident from the nanofluid flow regime map that churn flow occurs at very low superficial liquid velocities.

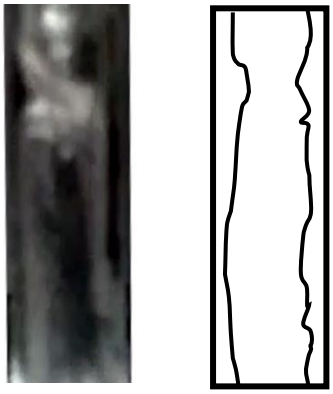

Mass flux= 679.06kg/s-m^2,
Heat flux = 225.46 kW/m^2

Fig.4.11 (a) Annular flow regime for water

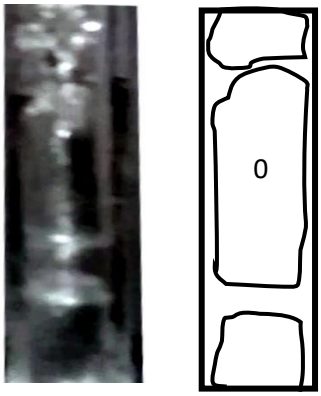

Mass flux= 905.42 kg/s-m^2,
Heat flux = 247.45 kW/m^2

Fig.4.11 (b) Slug-annular flow regime for water

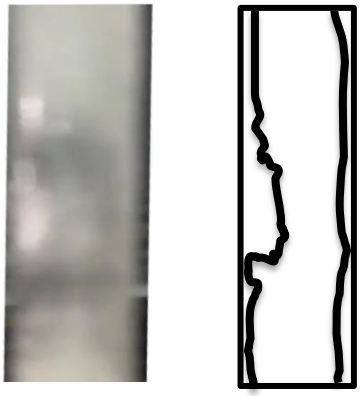

Mass flux= 679.06 kg/s-m^2,
Heat flux = 184.56 kW/m^2

Fig.4.11 (c) Annular flow regime for 0.001% Al_2O_3/water nanofluid

The annular flow regime in nanofluids is different from water in the following ways;. In water, for mass flux of 452.71 kg/s-m^2, after the heat flux of 184.56 kW/m^2, annular flow regime is observed and the sample photographic view is shown in Fig. 4.11 (a). However, for mass fluxes of 905.42 & 679.06 kg/s-m^2, the transition from slug to annular flow happens without churn flow (Fig. 4.11 (b)). The Taylor bubbles in slug flow elongate further and meet other vapour slug and coalesce into slug annular flow. This can be observed for the mass flux of 679.06 kg/s-m^2 over a heat flux range of 204.50 to 247.45kW/m^2. For the mass flux of 905.42, 679.06 and 452.71 kg/s-m^2 and concentrations of 0.001%, 0.005% & 0.01%, nanofluids exhibit annular flow regimes after heat fluxes of 225.47, 165.64 and 115.01 kW/m^2 respectively.

4.4.2 Flow boiling characteristics of water and Al_2O_3/water nanofluids

Initially, fluid condition at the heater inlet is in sub cooled state. Depending on the imposed heat flux and mass flux, the fluid condition at heater exit is either in sub cooled boiling state or in saturated boiling state. In sub cooled boiling, the fluid closer to the wall is in saturation state and the bulk fluid which is away from wall is in sub cooled state. In sub cooled boiling, heat transfer takes place by forced convection and nucleation which depends on heat

flux and mass flux. In saturated boiling, heat transfer takes place by nucleation which depends on heat flux only.

Flow boiling curve

Fig. 4.12 (a, b and c) depicts the flow boiling curve for Al_2O_3/water nanofluid at three different mass fluxes of 905.42, 679.06 & 452.71 kg/s-m^2. The boiling curve (Fig. 4.12 (a, b and c)) plots are shown between the imposed wall heat flux to the wall superheat. The wall superheat is considered at heater exit location. The wall superheat is low for both water and Al_2O_3 nanofluid at the higher mass flow rates. Convective boiling dominant heat transfer mechanism is the reason for such low values.

The nanofluid boiling curve is similar to the boiling curve of water with a shift towards left, which indicates a reduction in wall superheat. Shifting of boiling curve towards left also indicates the enhancement of boiling performance. Good boiling performance implies that, for the same heat flux, use of nanofluid lowers the surface temperature compared to water. The shift of boiling curve towards left is more rapid with increase of volume concentration at all mass flow rates of the nanofluids. In the boiling process, the deposition of nanoparticles creates more number of active nucleation sites on the heater surface. More heat transfer in the case of nanofluids is attributed to different heat transfer mechanisms such as nucleate boiling, single phase forced convection, particle driven natural convection and conduction between nanoparticles. The average reduction of wall superheat at mass flux of 905.42 kg/s-m^2 for 0.001%, 0.005% & 0.01% Al_2O_3/water nanofluids are 10.8%, 21.34% and 26.97% respectively. Similar trend of reduction in wall superheat is observed at 679.06 kg/s-m^2 and 452.71 kg/s-m^2 mass fluxes as well.

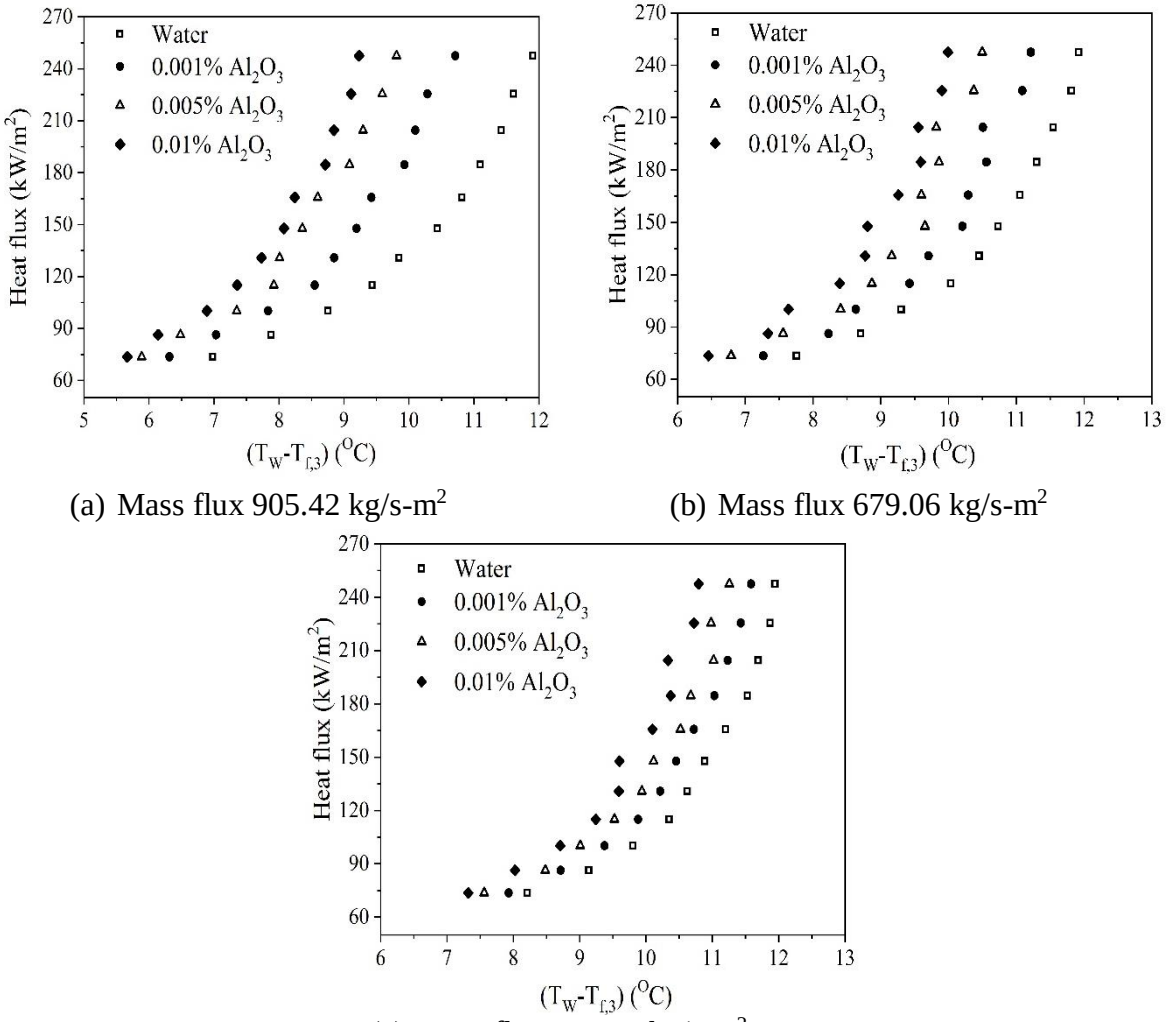

(a) Mass flux 905.42 kg/s-m^2 (b) Mass flux 679.06 kg/s-m^2

(c) Mass flux 452.71 kg/s-m^2

Fig.4.12 Flow boiling curve for water

From Fig.4.12 (a, b and c), it can be observed that slope of every boiling curve changed at a particular heat flux. The change in slope indicates transition from sub cooled boiling to saturated boiling. Occurrence of slope change is observed at low heat fluxes in case of nanofluid compared to water. For example, at the mass flux of 905.42 kg/s-m^2, change of slope for water occurred at a heat flux of 130.87 kW/m^2, whereas for 0.001% particle concentration of Al_2O_3/water nanofluid slope change is observed at the heat flux of 115.01 kW/m^2. Similarly, at 0.01% Al_2O_3/water nanofluid slope change occured at 100.19 kW/m^2 heat flux. Similar behaviour is noticed at the mass flux 679.06 kg/s-m^2. However, it needs to be noticed that at a mass flux of 452.71 kg/s-m^2, the heater exit is in a saturated boiling region for both water and nanofluids.

Flow boiling heat transfer coefficient

The variation of flow boiling HTC with the thermodynamic quality for water and Al_2O_3/water nanofluid is illustrated in Fig. 4.13 (a, b and c). HTC and thermodynamic quality is estimated at heater exit. The meaning of the term thermodynamic quality is same as mass quality, but differs by a negative sign in the sub cooled boiling region. Sub cooled boiling and saturated boiling regions are separated by zero quality, which can be observed Fig. 4.13 (a and b). For a particular mass flux, HTC increases with increase of thermodynamic quality, which is directly proportional to the imposed wall heat flux. From Fig. 4.13 (a, b and c) it is noticed that, the rate of increase of HTC is higher in saturated boiling region compared with sub cooled boiling region. In sub cooled boiling region, heat transfer takes place by nucleate boiling and single phase forced convection. Further increase of heat flux increases active nucleation sites. This leads to increase of bubble formation and thereby increases thermodynamic quality (> 0). At this condition, heater exit is in the saturated boiling region while heat transfer takes place by nucleate boiling mechanism. HTC is high during nucleate boiling. During nucleate boiling, bubbles are formed at active nucleation sites and depart from the heater surface. This situation induces considerable fluid mixing near the wall surface, which substantially increases the convective heat transfer coefficient.

For a particular mass flux and heat input, nanofluid exhibits more vapour quality than pure water. The variation in latent heat is the sole reason for the quality enhancement. The variation of thermodynamic quality with volume concentration of nanofluid is insignificant at a particular heat flux and mass flux. However, for the same quality, boiling HTC increases with volume concentration.

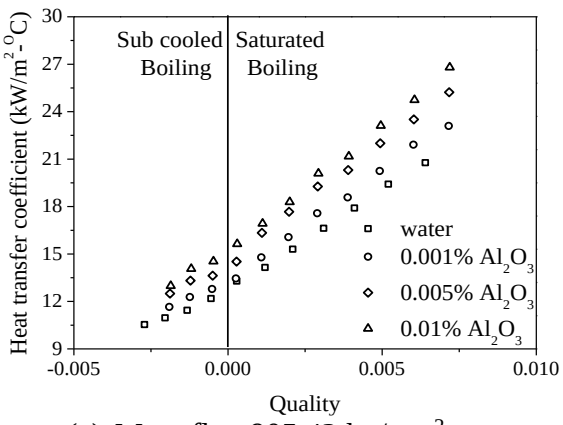

(a) Mass flux 905.42 kg/s-m^2

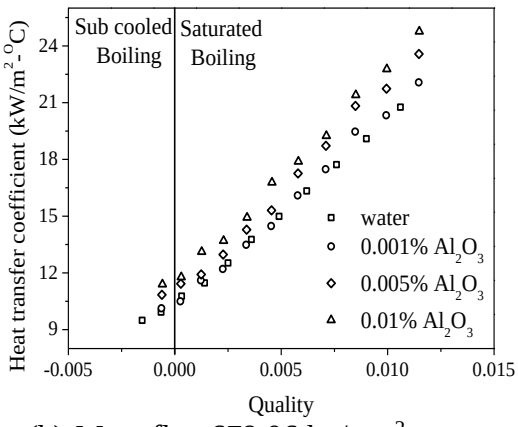

(b) Mass flux 679.06 kg/s-m^2

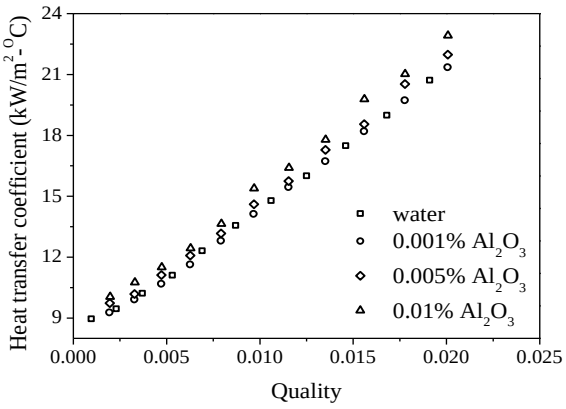

(c) Mass flux 452.71 kg/s-m^2

Fig.4.13 Variation of HTC with exit vapour quality.

Fig. 4.14 (a, b and c) depicts the relation between HTC and heat flux for water and Al_2O_3/water nanofluids. From Fig.4.14 (a, b and c) it is observed that nanofluid possesses high HTC at a given heat flux range for all mass flow rates considered in the present study. The average enhancement in HTC for various concentration and corresponding mass flux is shown in table 4.5.

Table 4.5: Average enhancement of HTC

Mass flux (kg/s-m^2)	**Nanoparticle concentration**		
	0.001%	**0.005%**	**0.01%**
905.42	12.11 %	21.75 %	27.97 %
679.06	6.98 %	13.91 %	19.78 %
452.71	4.18 %	7.56 %	11.94 %

During the boiling of nanofluids, nanoparticles got deposited on the heater surface, which influences the bubble dynamics parameters such as nucleation site density, bubble departure diameter, departure frequency and evaporation of the micro- and macro-layer beneath the growing bubbles. Likewise, the presence of nanoparticles in the liquid phase of the fluid also modifies bubble formation mechanism. At the interface of solid, liquid and vapour which is termed as triple line [126], the net force balance is different compared to nanofluids. The change in the net balance strongly influences the bubble dynamics by varying the contact angle, bubble departure volume and frequency [128]. All the above phenomenon has a strong

influence on the boiling characteristics of nanofluids which makes it different from boiling characteristics of water.

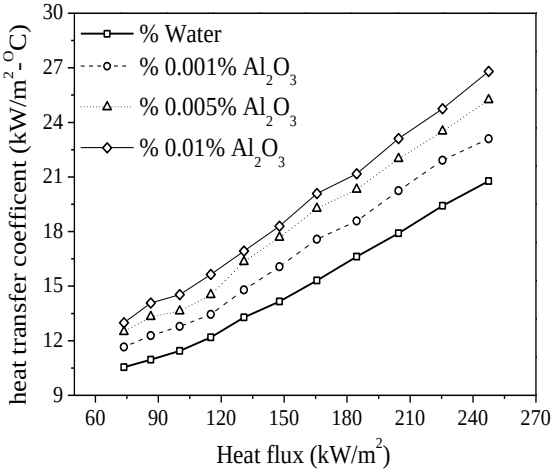

(a) Mass flux 905.42 kg/s-m^2

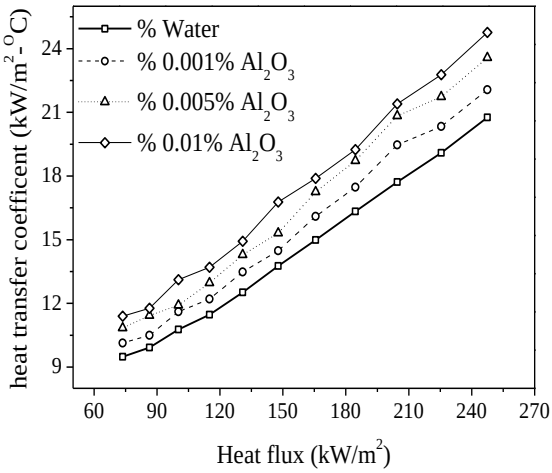

(b) Mass flux 679.06 kg/s-m^2

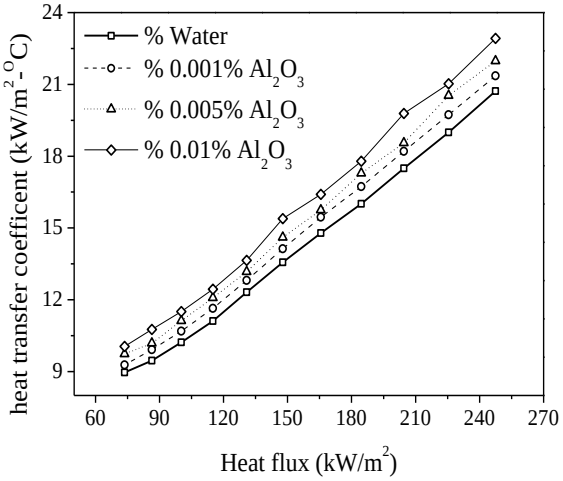

(c) Mass flux 452.71 kg/s-m^2

Fig.4.14. Effect of heat and mass flux on the local heat transfer coefficient

4.4.3 Comparison of heat transfer coefficient data with classical correlations and propose a new correlation for nanofluid boiling heat transfer coefficient

The HTC data acquired in the above experiments are compared with the predictions from three classical two-phase heat transfer correlations namely those due to Chen [75], Shah [76] [77] and Gungor and Winterton [78]. The details of these three correlations are provided in the appendix. Predictions of the local saturated flow boiling HTC from these three correlations are compared in Fig.4.15 against the experimental data for the mass flux of 452.71 kg/m^{2}s. From Fig. 4.15 it is clear that the HTC of water was well matched with the Shah correlation, the rest

of the two correlations are over predicting, especially Chen correlation. Shah distinguished the boiling heat transfer by three regions, namely pure nucleate boiling, convective boiling and bubble suppression regions. In bubble suppression region, both nucleate boiling and convective boiling mechanisms are significant. By comparing experimental data with Shah correlation predicted data, it is observed that at low vapour qualities, the heat transfer had taken place by nucleate boiling. Increase of vapour quality, heat transfer transits from nucleate boiling to bubble suppression and next convective boiling mechanisms.

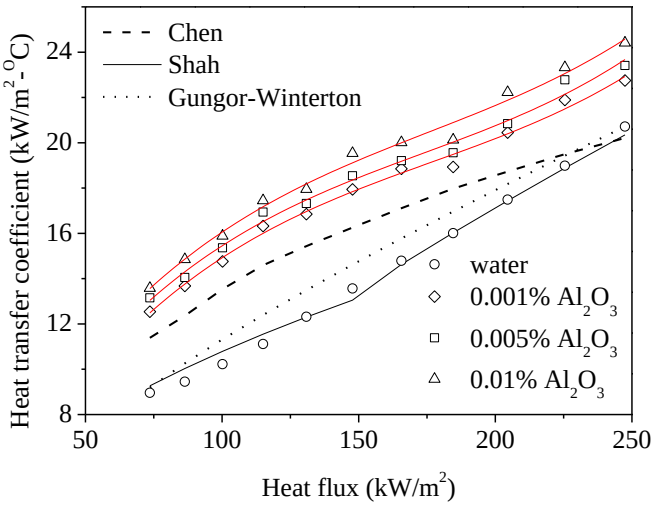

Fig. 4.15 Comparison of classical two-phase heat transfer correlations with experimental data(G=452.71 kg/m^2-s)

In the open literature, the empirical correlations for nanofluid boiling heat transfer coefficient are quite scarce. Some researchers [129]give the correlation to predict the boiling HTC; However, the correlation did not distinguish the various heat transfer regions. So, the shortages of previous correlations highlight the need for developing new correlations that are applicable for low concentration alumina nanofluid. In this study, a new correlation is proposed to predict the nanofluid boiling heat transfer coefficient in vertical flows at very low concentrations. It is observed from Fig. 4.14, nanofluid HTC behaviour is same as that of water. So, it is assumed that heat transfer mechanism in nanofluid is similar to water, hence new correlation developed by modifying the Shah correlation and is given by

$$\psi_{cbd} = 3.33 N_s^{-0.8} \tag{4.12}$$

$$\psi_{nbd} = 304.22 Bo^{0.5} \tag{4.13}$$

$$\psi_{bs} = 15.4Bo^{0.5}e^{\left(2.92N_s^{-0.1}\right)} \tag{4.14}$$

For $1 > N_s > 0.1$

$$\psi = Max(\psi_{cbd}, \psi_{bs}) \tag{4.15}$$

For $N_s > 1$

$$\psi = Max(\psi_{cbd}, \psi_{nbd}) \tag{4.16}$$

Where

$$\psi = \frac{h_{tp}}{h_f} \tag{4.17}$$

$$h_f = 0.023\left(\frac{k_f}{D}\right)Re_f^{0.8}Pr_f^{0.4} \tag{4.18}$$

The terms Bo and N_s are given in the appendix.

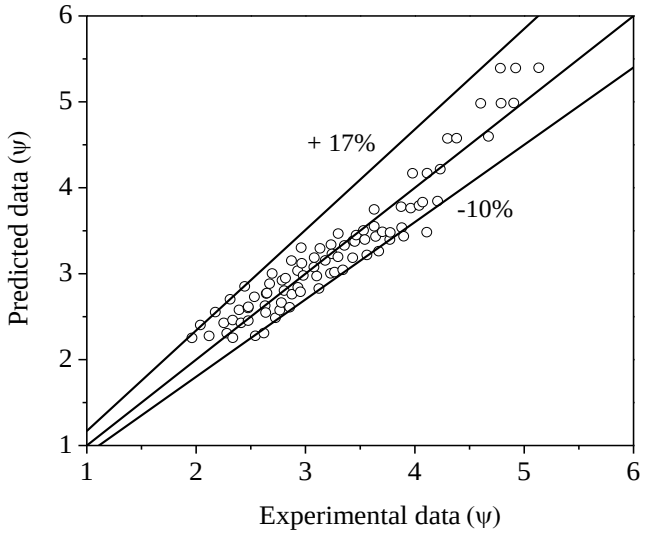

Fig.4.16 Comparisons between the predicted and experimental ψ

Fig. 4.16 assesses the new correlation using the experimental data. It is shown that all the data are captured within an accuracy of +17% to -10%. The mean absolute error (MAE) and root mean square error (RMSE) of the new correlation are 12.12 % and 23.75%, respectively. It is found that 91.95 % of the data fall within the range of ±10%. The new

correlation are validated in the range of, G = 452.71– 905.42 kg/m^2 s, q = 65-250 kW/m^2, and particle concentrations 0.001% - 0.01%.

4.5. Conclusion

An experimental study was carried out to investigate the flow boiling heat transfer in a vertical pipe of I.D 7.5 mm with water and Al_2O_3/water. Al_2O_3 nanoparticles with 20-30 nm size were used in this study and water was used as base fluid. Experiments were carried out at atmospheric pressure and constant inlet subcooling condition at heater inlet. Flow visualization study was carried out to understand the flow boiling regimes and the corresponding heat transfer mechanisms. The major conclusions are as follows:

1. The flow boiling heat transfer coefficient (HTC) increases with mass flux for both water and nanofluids. However, the magnitudes are different.
2. The boiling curve of the nanofluids shifts towards left as compared with water because of the reduction in wall superheat. The average reduction of wall superheat at mass flux of 905.42 kg/s-m^2 for 0.001%, 0.005% and 0.01% Al_2O_3 nanofluids are 10.8%, 21.34% and 26.97% respectively.
3. Nanofluids have high boiling HTC compared to water and the HTC increases with the increase of volume concentration. For example, the average enhancement in HTC for concentrations of 0.001 %, 0.005 % & 0.01 % nanofluids at the mass flux of 905.42 kg/s-m^2 are 12.11%, 21.75 % & 27.97 % respectively.
4. The Al_2O_3/water nanofluid boiling HTC is enhanced due to the improved heater surface characteristics and amendment in bubble formation mechanism.
5. The flow boiling behaviour of nanofluid differs from water as follows:

(i) In nanofluid boiling, nanoparticles are deposited on heater surface and modify the heater surface such that more nucleation sites are created.

(ii) Al_2O_3/water nanofluid exhibits early transition of flow regimes compared to water.

(iii) Water exhibits flow regime in the sequence given below:

Bubble flow → Slug flow → Churn flow → Annular flow.

On the other hand, Al_2O_3/water nanofluids exhibit the following sequence:

Bubble flow ► Slug flow ► Annular flow.

6. A new empirical correlation has been proposed to predict the flow boiling heat transfer coefficient of nanofluids.

Chapter 5

Experimental studies on nanofluid based NCL

Chapter 5

Experimental studies on nanofluid based NCL

The previous chapter presented the flow boiling behaviour of alumina/water nanofluid. From the experimental studies, it is concluded that nanofluids can transfer more heat during flow boiling as compared with water. Although, there are several studies available in the open literature on natural circulation loop (NCL) with water as a working fluid, studies on nanofluid based two phase NCL are almost scarce. Hence, in the present chapter, experimental studies have been conducted to understand the nanofluid behaviour in two phase NCL with heater as a heat source and heat exchanger as a heat sink. The experimental data is also used to validate the numerical model described in chapter 3. Experiments were carried out in an in-house test facility that was designed and fabricated to conduct experimental studies on two phase NCL.

5.1 Experimental facility

Figure 5.1 shows the schematic diagram of the experimental set up used in this study. The pictorial view of the actual setup is shown in Fig. 5.2. In the experimental test facility, the rectangular NCL consists of heater (heat source) at the bottom and tube-in-tube heat exchanger (heat sink/condenser) at the top. These two are connected with two parallel vertical legs named as riser and downcomer. Sight glasses were placed at the middle of the vertical legs (riser and downcomer) to visualize the flow. A smooth stainless steel tube with 12 mm external diameter and10 mm internal diameter was chosen to construct the loop. The entire loop was insulated with 5 mm thick glass wool to prevent the heat leak from or to the ambient. The geometrical specifications and operating parameters considered in this study are given in table 5.1. The temperatures of the loop fluid (T_1 to T_4), external fluid (T_5 and T_6) and the heater wall surface (T_7 to T_{12}) were measured by using K- type thermocouples as shown in Fig. 5.1. These thermocouples were connected to a computer integrated data acquisition system (Agilent-34972A) to log the temperature data at regular intervals. The pressure drop between the riser and downcomer sections in the NCL was measured using U-tube manometers, as shown in Fig. 5.1. A rotameter connected between condenser and thermostatic bath outlet was used to measure the condenser coolant flow rate. The classic scientific made thermostatic bath was used to control the coolant temperature which is sent to condenser.

Table 5.1: Geometrical specifications and operating parameters

Parameter	**Value**
Loop pipe inner diameter	0.010 m
Loop width	0.35 m
Loop height	0.7 m
Length of heater	0.19 m
Length of Condenser	0.19 m
Inner diameter of condenser external tube	0.4 m
Heat flux	22.01-136.61 kW/m^2
External fluid inlet temperature	10 °C to 20 °C
Pipe wall thickness	0.001 m
Cold fluid mass flow rate	0.12-0.04 kg/s
Particle volume concentration (ϕ) vol./vol.	0.001 % , 0.005 % and 0.01 %
Pipe wall material	Stainless steel
Working/loop fluid	Distilled water and Al_2O_3-water nanofluid

5.2 Experimental procedure

Experimental studies on rectangular NCL were conducted with distilled water and Al_2O_3/water nanofluid. Nanofluid volume concentrations of 0.001%, 0.005% and 0.01% were considered for the study. During the experimentation, the effects of heat flux, particle concentration, condenser coolant flow rate and its temperature on the loop fluid behaviour were analysed. The sequence of steps followed during the experimentation is given below:

- The NCL was filled with working fluid.
- Air bubbles were drained out by giving continuous pulses while filling the loop.

- Sufficient time was given to the loop fluid to obtain thermal equilibrium with room temperature without heating.
- The cold fluid temperature at CHE was set at a desired value.
- The DAQ system was switched on and the initial readings were taken.
- After ensuring the thermal equilibrium, thermostatic bath and heater were started simultaneously.
- Repeatability of the data was ensured for a given set of input parameters.
- The same procedure was repeated for all the experiments.

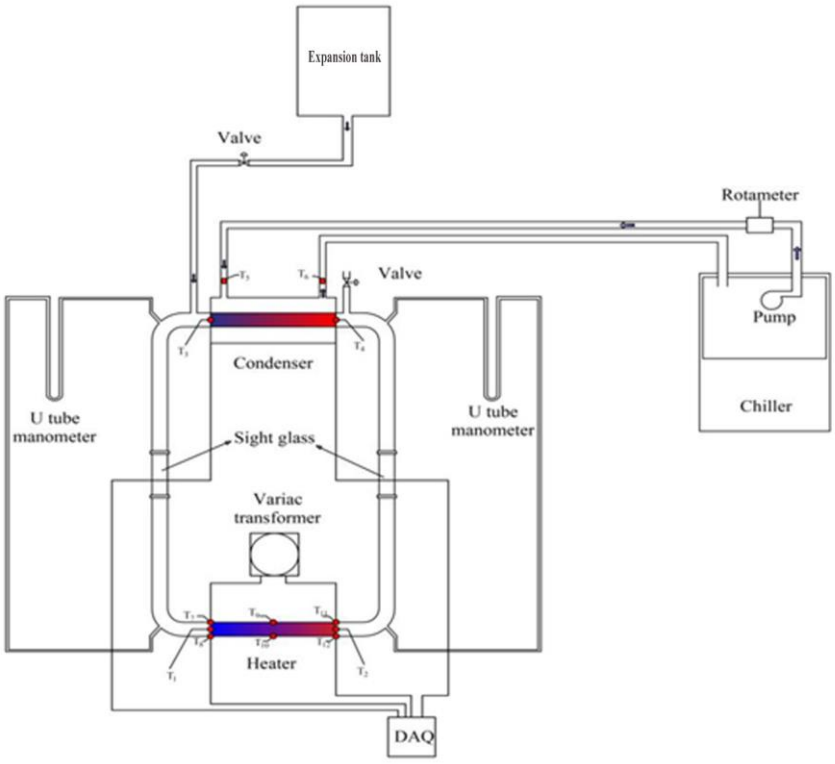

Fig.5.1 Schematic diagram of the experimental setup

Fig.5.2 Photographic view of the experimental test rig

5.3 Data Reduction

The steady-state condition in NCL is attained when the buoyancy and frictional forces were balanced. The steady-state mass flow rate ($\dot{m}$) and average heat transfer coefficient ($\bar{h}$) of the working fluid are calculated by using the following equations.

Heat transfer coefficient

The net heat flux given to the heater section is estimated by using the eq. 4.3 to eq. 4.7.

The average heat transfer coefficient of the loop fluid at heater section is given by eq. 5.1

$$\bar{h} = \frac{q_{net}}{(\overline{T_{wall}} - \overline{T_{fluid}})} \qquad 5.1$$

Where $\overline{T_{wall}}$ is the inner surface wall temperature (average of temperature recorded by thermocouples from 7 to 12) and is estimated by using eq. 5.2

$$\overline{T_{wall}} = \sum_{i=7}^{12} \frac{T_i}{6} \qquad 5.2$$

As, provision to measure inside wall temperature T_i is not available in the test rig, thermocouples are located at the outer surface of the test section pipe. Inner wall temperature is obtained by using steady state one-dimensional heat conduction equation of cylindrical co-ordinates and is given by eq. 4.10 [35]

$\overline{T_{fluid}}$ is the average loop fluid temperature and it is given by eq. 5.3

$$\overline{T_{fluid}} = \frac{T_1+T_2}{2} \quad 5.3$$

The thermodynamic vapour quality at the exit of the heater section (x) is estimated by using eq. 4.11.

Mass flow rate

The mass flow rate of the working fluid is estimated by using the single phase frictional pressure drop in the downcomer section and is given by

$$\Delta P = \frac{2}{D} C_f G^2 \vartheta_f L \quad 5.4$$

where C_f is the single phase frictional factor and is given by

$C_f = \frac{16}{Re}$ for laminar flow

$C_f = \frac{0.079}{Re^{0.25}}$ for turbulent flow

5.4 Results and Discussion

In the present study, the effect of particle concentration, heat flux and heat sink condition (condenser coolant flow rate and temperature) on the thermal performance of the NCL was experimentally investigated. Al_2O_3/water nanofluid was used at different particle concentrations (0.001%, 0.005% and 0.01%) and the results are compared with water. The heat flux at heater was varied from 22 kW/m^2 to 136.61 kW/m^2. The heat sink condition, i.e. inlet temperature of condenser coolant was varied from 10 °C to 20 °C with a step size of 5 °C, and flow rate was varied from 0.12 kg/s to 0.04 kg/s with a step size of 0.04 kg/s.

5.4.1 Comparison of experimental results with proposed numerical model

Figure 5.3 shows the comparison of experimental results with numerical results. It is observed that a good agreement is obtained between the proposed model and the experimental data. The proposed model under-predicts the NCL mass flow rate with an average deviation of 9%.

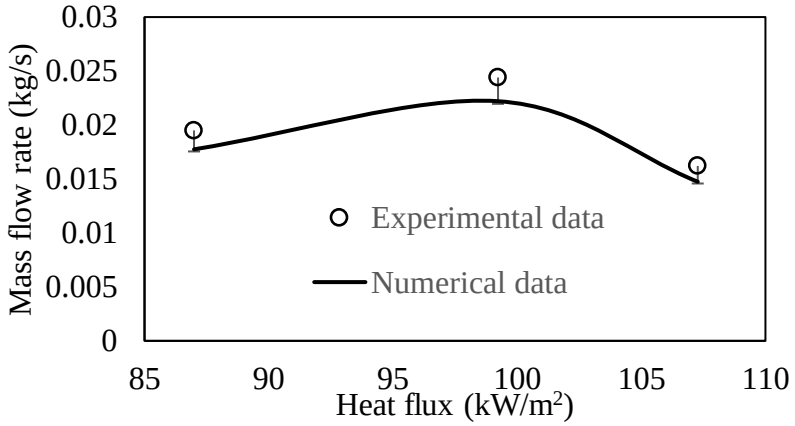

Fig.5.3 Validation

5.4.2 Transient characteristics of NCL

The loop fluid temperature at heater and condenser exits were recorded by using the DAQ for every second. During the experimentation the loop fluid in the riser could be either single phase or two phase state depending upon the heat flux at the heater section. Figure 5.4 (a, b, c and d) shows the variation of working fluid temperature with time at different locations in the loop for different heat fluxes. These results were taken at external fluid flow rate of 0.12 kg/s and 10 °C inlet temperature. Table 5.2 provides the details of imposed heat fluxes and steady-state reaching time. It is to be noted that up to 265s, heat flux is not imposed and loop is kept idle in order to achieve thermal equilibrium with the ambient. From the 265th second, the heat flux of 22.01 kW/m^2 is imposed on the heater. Time taken to reach steady state is given in table 5.2. The steady state condition was ensured by observing the temperature data. The imposed condition was maintained for 15 minutes even after reaching the steady state. Afterwards, imposed heat flux was increased in steps up to 136.61 kW/m^2. Same steps were followed for all the tests. It is observed from Fig.5.4 that the transient response of both working fluids (water

and nanofluids) is similar. However, the temperature values at measured locations are not the same. Table 5.3 provides steady-state temperature data at the heater inlet and outlet for all the working fluids. The bulk fluid temperature of the water at different locations in NCL is lower than the bulk fluid temperature of nanofluid at same locations. The reason behind this is specific heat of nanofluid is lower as compared to water (Table: 4.2). It is also observed that increasing the particle concentration increases the temperature at the heater inlet. Therefore, the increase of working fluid temperature at the heater inlet and increasing the heat input (increasing heat flux at heater section) leads to subcooled boiling/flashing or saturated boiling in the loop. The subcooled boiling/flashing phenomena is observed for water, 0001% Al_2O_3, 0.005% Al_2O_3 nanofluids at 87.07 kW/m^2 heat flux, while for 0.01% Al_2O_3 nanofluid at 70.56 kW/m^2. The subcooled boiling/flashing phenomena was confirmed by the flow visualization in the riser (bubbly flow) meanwhile, the working fluid temperature at heater outlet was below the saturation temperature. Further increase of imposed heat flux causes saturated boiling in the heater section. The saturated boiling in the heater section was observed at 99.2 kW/m^2 for water, 0001% Al_2O_3, 0.005% Al_2O_3 nanofluids; for the 0.01% Al_2O_3 nanofluid the same is observed 87.07 kW/m^2.

It is also observed Fig.5.4 (d) that there is early initiation of boiling for 0.01% Al_2O_3 nanofluid which can be explained from the reduction in specific heat capacity of nanofluid as compared to water [130], [131]. Hence for the same heat addition rate, the rise in temperature in Al_2O_3 nanofluid is higher as compared to water. Besides, the presence of nanoparticles may give rise to additional nucleation sites for bubble creation resulting in early initiation of boiling.

Table 5.2: Transient data for imposed heat flux and steady state reaching time

Working fluid/ Time	**Heat flux (kW/m^2)**													
	22.01		**34.59**		**49.99**		**70.56**		**87.07**		**99.2**		**107.7**	
	t_{hi} (s)	**t_{ss} (s)**	**t_{hi} (s)**	**t_{ss} (s)**	**t_{hi} (s)**	**t_{ss} (s)**	**t_{hi} (s)**	**t_{ss} (s)**	**t_{hi} (s)**	**t_{ss} (s)**	**t_{hi} (s)**	**t_{ss} (s)**	**t_{hi} (s)**	**t_{ss} (s)**
Water	265	990	2260	895	4150	860	6010	755	7765	685	9450	590	11040	465
0.001% Al_2O_3	265	990	2260	870	4130	800	5930	715	7645	575	9220	415	10635	455
0.005% Al_2O_3	265	990	2250	850	4075	780	5850	685	7535	560	9090	495	10450	395
0.01% Al_2O_3	265	960	1600	825	2880	770	3950	690	5015	585	6735	295	-	-

t_{hi} = Heat flux imposed time

t_{ss} = Time to reach steady state

Table 5.3: Transient data for imposed heat flux and steady state reaching time

Working fluid/ Time	**Heat flux (kW/m^2)**													
	22.01		**34.59**		**49.99**		**70.56**		**87.07**		**99.2**		**107.7**	
	T_{in} (^oC)	**T_{out} (^oC)**	**T_{in} (^oC)**	**T_{out} (^oC)**	**T_{in} (^oC)**	**T_{out} (^oC)**	**T_{in} (^oC)**	**T_{out} (^oC)**	**T_{in} (^oC)**	**T_{out} (^oC)**	**T_{in} (^oC)**	**T_{out} (^oC)**	**T_{in} (^oC)**	**T_{out} (^oC)**
Water	51.92	55.06	62.70	66.92	75.07	80.38	84.46	91.10	90.04	96.34	93.30	98.56	94.56	98.56
0.001% Al_2O_3	52.78	55.83	63.86	67.93	76.68	81.76	86.67	93.01	90.56	96.58	93.34	97.85	95.68	97.85
0.005% Al_2O_3	53.86	56.86	64.82	68.76	77.55	82.55	87.48	93.64	91.86	96.86	94.57	97.85	95.68	97.85
0.01% Al_2O_3	55.43	58.32	66.41	70.12	79.18	83.97	90.23	91.16	92.34	97.85	96.86	97.85	-	-

T_{in} = Loop fluid temperature at heater inlet

T_{out}= Loop fluid temperature at heater outl

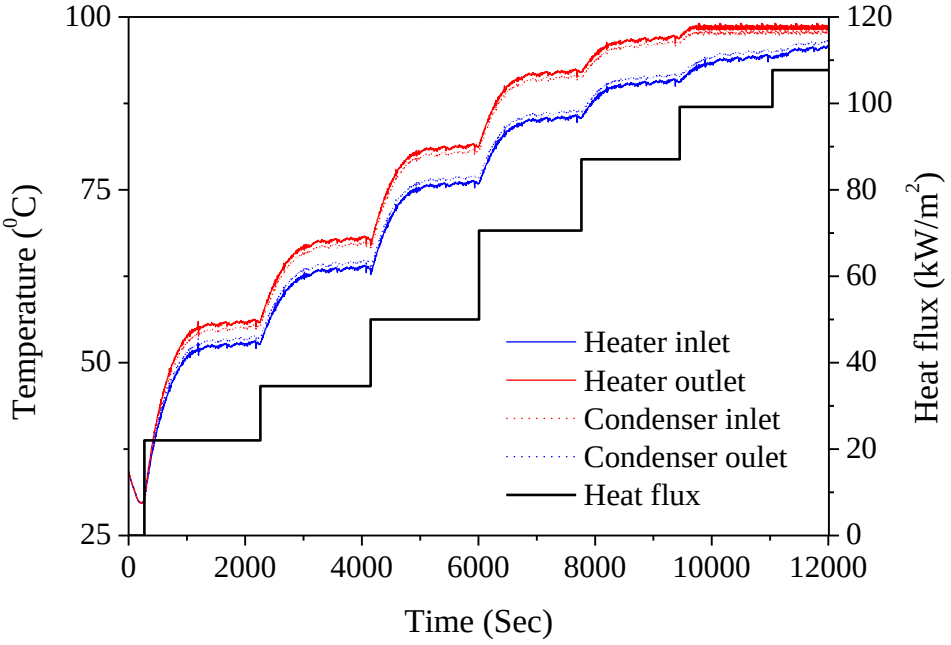

(a) Water

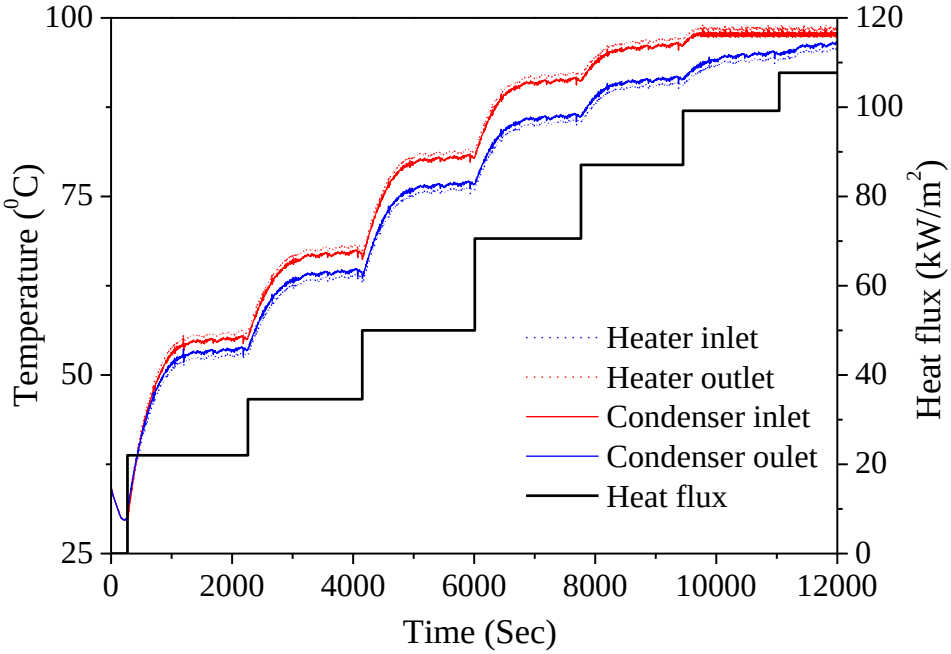

(b) 0.001% Al_2O_3/water nanofluid

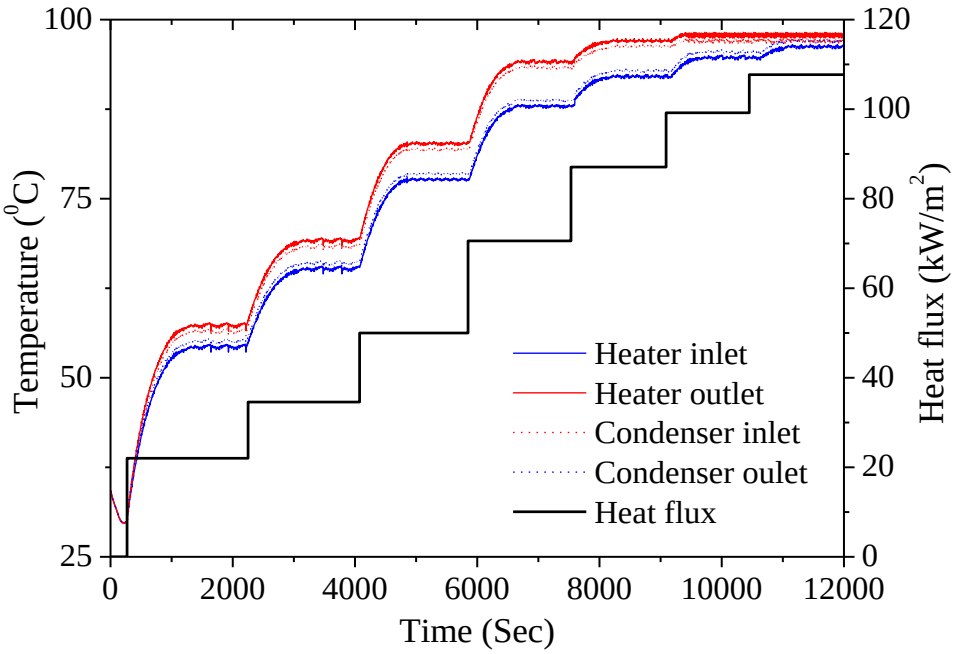

(c) 0.005% Al_2O_3/water nanofluid

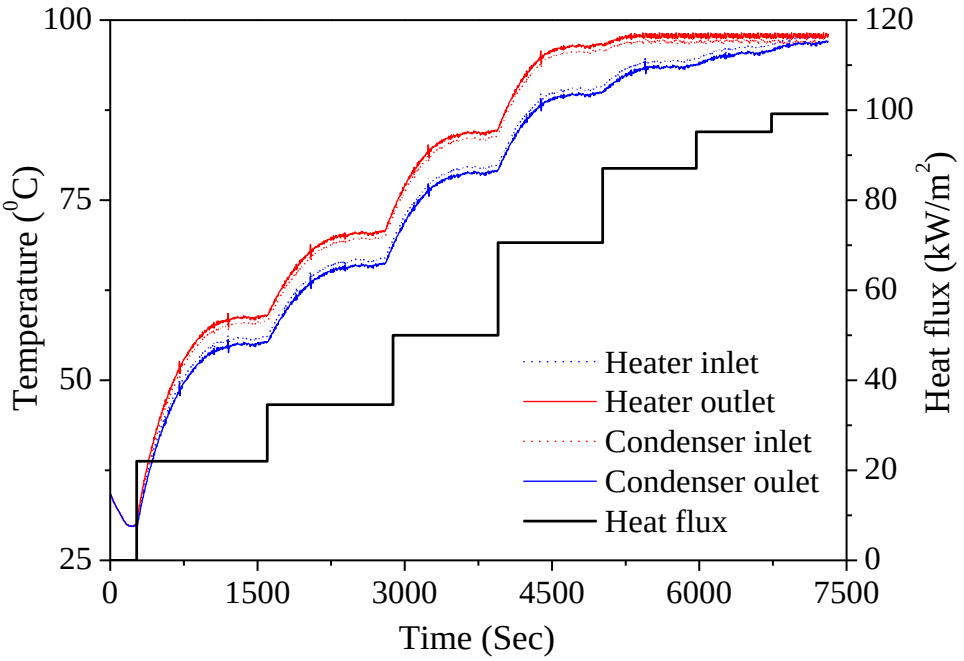

(d) 0.01% Al_2O_3/water nanofluid

Fig.5.4. Transient behaviour of NCL for different working fluids

With further increase in heat flux, the loop exhibits oscillatory behaviour. The loop exhibits oscillatory behaviour after the heat flux 107.7 kW/m^2 for water, 0.001% Al_2O_3 and 0.005% Al_2O_3 nanofluids, while for the 0.01% Al_2O_3 nanofluid oscillatory behaviour was

observed after the heat flux of 99.2 kW/m^2. This oscillatory behaviour was observed in terms of heater outlet temperature data, as shown in Fig. 5.5. The oscillations are very much high for water as seen in Fig 5.5a, and it is in order of ± 8 ^{O}C. By having a small concentration of Al_2O_3 nanofluid in water (0.001% - 0.01% by volume), the amplitudes of oscillations are found to be strongly dampened, which can be observed in Fig.5.5 (b, c and d). It is also observed that the frequency of heater outlet temperature was significantly decreased by adding the nanoparticles in to base fluid.

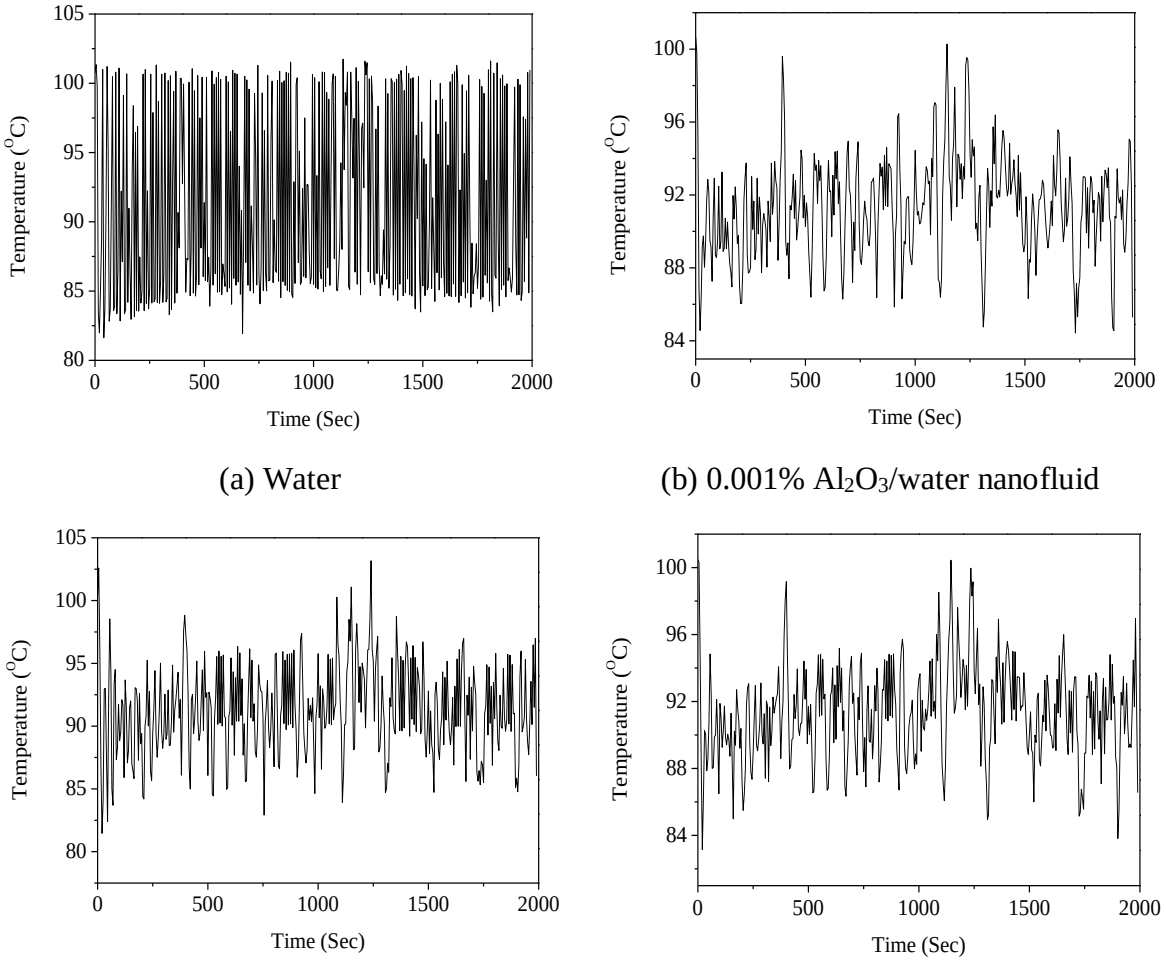

(a) Water (b) 0.001% Al_2O_3/water nanofluid

(c) 0.005% Al_2O_3/water nanofluid (d) 0.01% Al_2O_3/water nanofluid

Fig.5.5 Oscillatory behaviour of NCL at 136.61 kW/m^2 heat flux

5.4.3 Steady state characteristics of NCL

Effect of heat flux and particle concentration on mass flow rate

Figure 5.6 depicts the steady-state mass flow rate of NCL for different heat fluxes and different working fluids at condenser coolant flow rate of 0.12 kg/s and 10 °C inlet temperature. The mass flow rate of the NCL is estimated by using the single phase liquid pressure drop in the downcomer. For the given heat flux range, loop is operated either in single-phase or two-phase mode in heater and/or riser But, working fluid is in single phase in downcomer due to the complete condensation in condenser. It is observed from Fig.5.6, the mass flow rate of the loop is initially low and increases with heat flux. At this stage loop is operated in single-phase mode. The loop is operated in single phase mode (Single phase NCL) up to the heat flux of 70.56 kW/m^2 for water, 0.001% Al_2O_3 and 0.005% Al_2O_3 nanofluids and 49.99 kW/m^2 heat flux for 0.01% Al_2O_3 nanofluid. In single phase NCL, it is well known that the mass flow rate of the loop fluid increases with heat flux. By increasing the heat flux at the heater, the density gradient developed across the heater and condenser sections was high, which causes buoyancy forces, that subsequently increases the mass flow rate. For a given heat flux, the mass flow rate of nanofluids is higher than that of water, and it increases with particle concentration. By suspending the nanoparticles in the base fluid, the net specific heat decreases. This decrement in specific heat gives more significant rise in temperature in the fluid for given heat flux. The temperature rise gives a substantial increase in the density gradient between the heater and condenser, which increases the steady state mass flow rate in the loop. In addition to this, the thermal expansion coefficient of the nanofluid is another important parameter for mass flow rate enhancement. By dispersing nano-sized particles in water, the thermal expansion coefficient was enhanced [132]–[135], and this enhancement, improved the driving force.

From Fig. 5.6 it is also observed that the mass flow rate of NCL increases suddenly for water, 0.001% Al_2O_3 and 0.005% Al_2O_3 nanofluid at 70.56 kW/m^2 heat flux and for 0.01% Al_2O_3 nanofluid at 49.99 kW/m^2 heat flux respectively. The sudden increase in the mass flow rate is due to the significant rise in buoyancy force with the initiation of subcooled boiling/flashing. In two phase NCLs the mass flow rate increases with heat flux and reaches a peak value and then after it decreases. This sudden drop in mass flow rate is because of the increased drag due to increased void fraction in the riser section. This phenomenon was

followed by all the working fluids. It is also observed that 0.01% Al_2O_3 nanofluid exhibit two phase flow in NCL at 70.56 kW/m^2 heat flux whereas 0.001% Al_2O_3, 0.005% Al_2O_3 nanofluids and water exhibit two phase flow in NCL at 87.07 kW/m^2 heat flux. This indicates that the initiation of boiling happens earlier in 0.01% Al_2O_3 nanofluid compared to all other working fluids considered. The attributed reason for this behaviour is the presence of more nanoparticles which give rise to additional sites for bubble nucleation.

Therefore, in a two phase NCL for given heat flux, the mass flow rate of nanofluids is not always higher than that of water, and it depends on the vapour quality available in the riser section, which depends upon the particle concentration of the nanofluid. The average enhancement in mass flow rate as compared with water are 4.48%, 9% and 8.7% for 0.001% Al_2O_3, 0.005% Al_2O_3 and 0.01% Al_2O_3 nanofluids respectively.

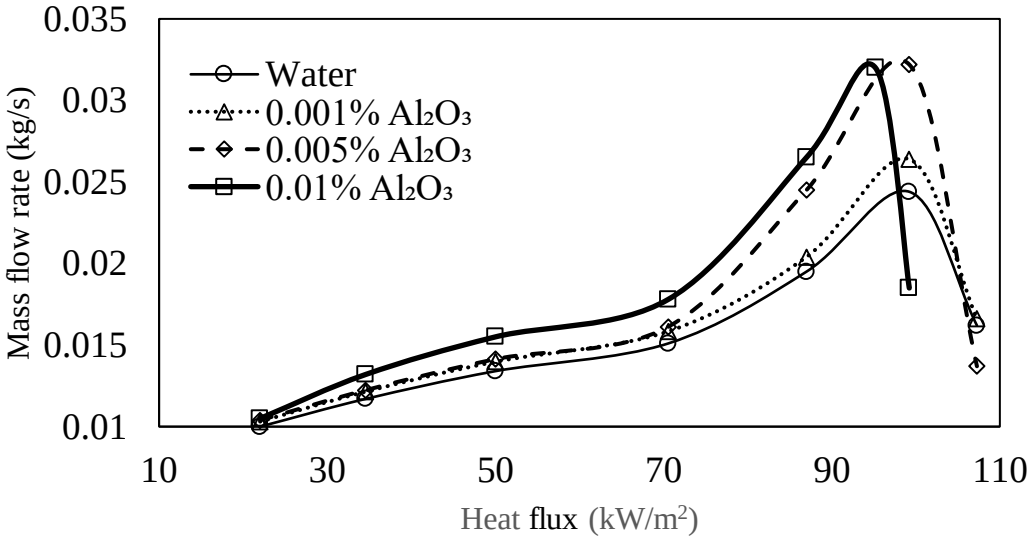

Fig.5.6 Variation of mass flow rate with heat flux

Effect of heat flux and particle concentration on average HTC

Figure 5.7 shows the variation of average HTC with heat flux for different working fluids at condenser coolant flow rate of 0.12 kg/s and 10 °C inlet temperature. The average HTC of the working fluid at the heater section is estimated using eq. (5.1). As illustrated in Fig. 5.7, for a given working fluid, the average HTC increases with heat input, and it is very much high in two phase condition. It is noticed from Fig. 5.7 that for the heat flux range of 22.01 kW/m^2 – 70.56 kW/m^2. the average single phase HTC is enhanced by 4.18%, 6.85% and 9.09% for

0.001% Al_2O_3, 0.005% Al_2O_3 and 0.01% Al_2O_3 nanofluids respectively when compared with water. . Further increase in heat flux loop is operated in two phase condition. The average two phase HTC enhancement by 0.001% Al_2O_3, 0.005% Al_2O_3 and 0.01% Al_2O_3 nanofluids when compared with water are 8.73%, 11.22% and 91.01% respectively. The 0.01% Al_2O_3 nanofluid has higher enhancement in HTC compared with water and other nanofluids at the heat flux of 99.2 kW/m^2. The attributed reason is heat transfer is dominated by nucleate boiling mechanism in 0.01% Al_2O_3 nanofluid whereas in other working fluids heat transfer is combination convective and nucleate boiling mechanism.

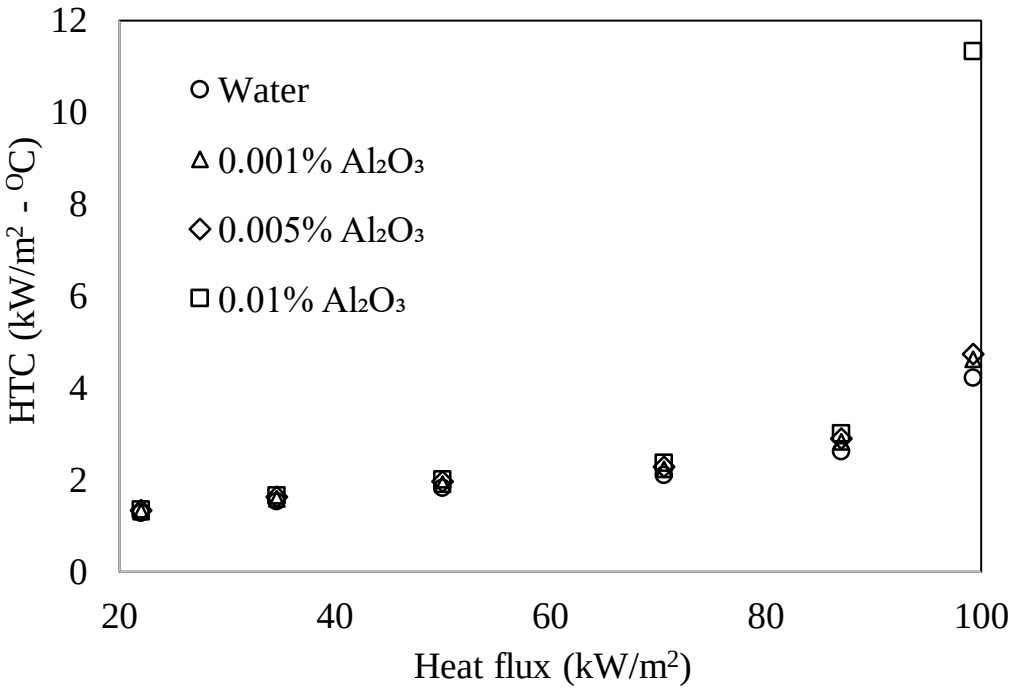

Fig.5.7 Variation of HTC with heat flux

5.4.4 Flow regimes in two phase NCL

Figure 5.8 shows the photographic views of the flow captured through the sight glass. The nanofluids have poor transparency, and hence it is hard to visualize the patterns. However, for a lower concentration of 0.001%, an attempt was made to capture the flow regimes. The different flow regimes observed in the nanofluid are bubbly flow, slug flow and annular flow. It is observed that churn flow is missing in nanofluid. The bubble formation and growth phenomena for water and nanofluid was already discussed in section 4.4.1. In Fig 5.8, supporting line diagrams are drawn beside each photographic view for better understanding.

Bubbly flow

Both water and nanofluids exhibited the bubbly flow pattern that was shown in Fig. 5.8 (a and b). The loop exhibits bubbly flow for water, 0.001% Al_2O_3 and 0.005% Al_2O_3 nanofluids at 87.07 kW/m^2 heat flux and for 0.01% Al_2O_3 nanofluid at 70.56 kW/m^2 heat flux respectively. At these heat fluxes, the working fluid is below saturation temperature, but still bubbles were observed through the sight glass. That means subcooled boiling/flashing exists. The heat transfer has taken place by majorly with single phase convection, so the average HTC is also low (Fig. 5.7). It is also observed from Fig. 5.8 (a) and (b) the departed bubble diameter is low for the nanofluid.

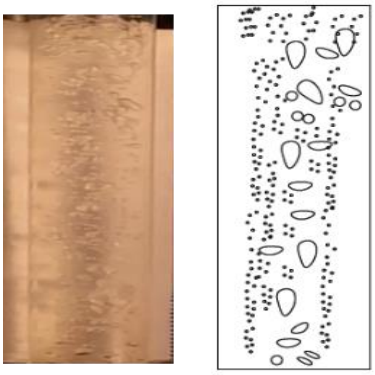

Heat flux = 87.07 kW/m^2

Fig. 5.8(a) Bubble flow for water

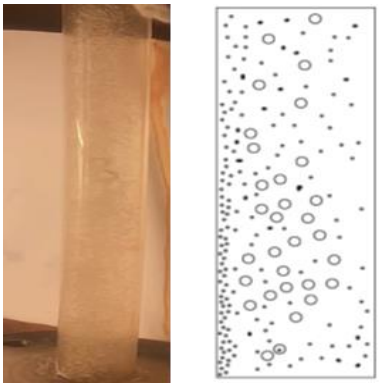

Heat flux = 87.07 kW/m^2

Fig.5.8(b) Bubble flow for 0.001% Al_2O_3 nanofluid

Slug flow

Figure 5.8 (c and d) depicts the photographic view of the slug flow for water and nanofluid. As the heat flux further increases, the loop fluid reaches saturation temperature, and the detached bubble population from the heater surface also increases. These detached bubbles continue to grow and coalesce with other bubbles to form bullet shaped bubbles (vapour slug). The slug flow pattern was exhibited by water, 0.001%, 0.005% Al_2O_3 nanofluids at 99.2 kW/m^2 heat flux and 0.01% Al_2O_3 nanofluid at 87.07 kW/m^2 heat flux. In this regime, the major portion of heat transfer is by nucleate boiling; hence the average HTC is increased significantly.

Heat flux = 99.2 kW/m^2

Fig.5.8 (c) Slug flow for water

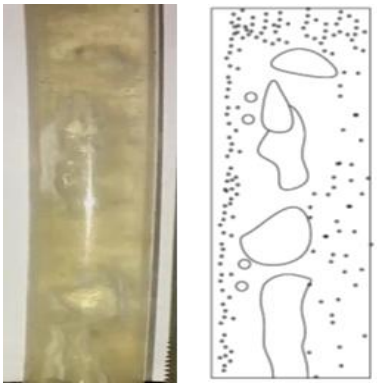

Heat flux = 99.2 kW/m^2

Fig.5.8(d) Slug flow for 0.001% Al_2O_3 nanofluid

Churn flow

With further increase in heat flux, water exhibits churn flow in the loop whereas nanofluid exhibit slug flow/slug annular flow. This is because the heat surface area is covered with more active nucleation sites and hence many bubbles grow, detach from the surface, and they coalesce with other bubbles to form a large bullet-shaped bubble (Taylor bubble). In water the relative parity between the gravitational and frictional forces act in opposite direction on liquid Taylor bubble and so Taylor bubbles are unstable, fragile and reform to small bubbles, cap shaped bubbles and the flow transits to churn flow. However, in the nanofluid, these small bubbles coalesce and form slug or slug annular flow. Fig.5.8 (e) depicts the photographic view of churn flow of the water.

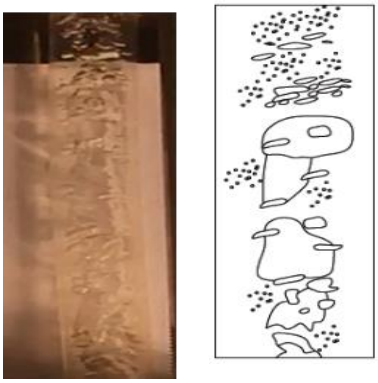

Heat flux = 107.27 kW/m^2

Fig.5.8 (e) Churn flow for water

Annular

With further increase in heat flux, the vapour quality increases in the loop and the flow became oscillatory. In the oscillatory flow, the annular regime is observed for both water and nanofluid as depicted in Fig.5.8 (f and g).

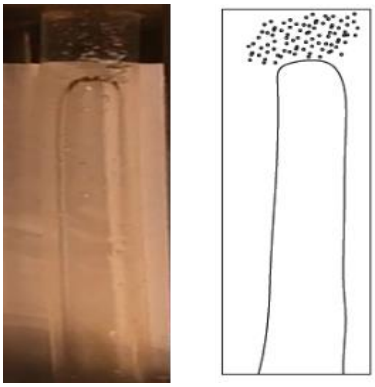

Heat flux = 136.61 kW/m^2

Fig.5.8 (f) Annular flow for water

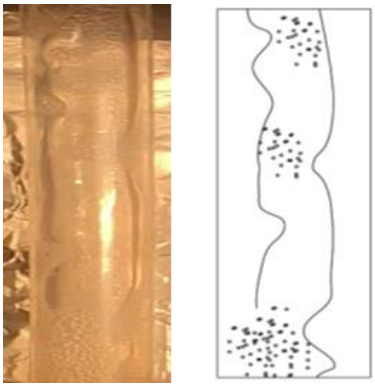

Heat flux = 136.61 kW/m^2

Fig.5.8(g) Annular flow for 0.001% Al_2O_3 nanofluid

5.4.5 Influence of heat sink condition

It is now quite evident that the flow stream condition at heater exit or condenser inlet can be controlled by either imposed heat flux at the heater section or heat sink condition (condenser coolant flow rate and temperature). Both condenser coolant flow rate and it inlet temperature are important control variables for an NCL. So, the experiments were conducted by varying the condenser coolant flow rate from 0.04 kg/s to 0.12 kg/s in steps of 0.04 kg/s and inlet temperature from 10 ^{O}C to 20 ^{O}C with a step of 5 ^{O}C. The influence of heat sink condition on NCL mass flow rate is similar for all the working fluids. Therefore, the results are presented for water and 0.005% nanofluid.

Fig.5.9 (a and b) depicts the influence of external fluid flow rate on NCL mass flow rate. As can be seen from Fig. 5.9, with a change in external fluid flow rate, there is significant variation in loop mass flow rate for water and 0.005% nanofluid. It is observed that, with increase in external fluid flow rate the maximum mass flow rate occurs at high heat fluxes, and also there is slight increment in maximum mass flow rate. With further increase in heat flux, oscillatory behaviour is observed in the loop. . For example, for working fluids (water and

0.005% Al_2O_3) at 0.04 kg/s of condenser coolant flow rate, the maximum loop mass flow rate appears at 87.07 kW/m^2 and oscillation behaviour was observed after 99.2 kW/m^2 heat flux. In contrast, for 0.12 kg/s of condenser coolant flow rate, the corresponding values are 99.2 kW/m^2 and 107.7 kW/m^2 respectively. Hence, it is not possible to operate at very high heat fluxes with low condenser coolant flow rates. It is also observed that initially with increase in heat flux, the loop mass flow rate is high for lower external fluid flow rate as compared with high external fluid flow rate. However, this phenomenon is reversed at high heat fluxes. The attributed reason is, for a given heat flux and a lower value of condenser coolant flow rate in the loop, condenser fluid exit temperature is high, which results in higher fluid temperature on the downcomer side and accordingly higher temperature or higher two phase mixture fluid at heater exit. This leads to either increase/decrease buoyancy force or oscillatory behaviour in the system.

Similar behaviour was observed with an increase in external fluid inlet temperature (Fig. 5.10). Higher condenser coolant inlet temperature results in smaller average temperature difference with the loop fluid at the condenser, leading to lower energy transfer. This situates high temperature loop fluid in the downcomer and accordingly increase the temperature or vapour quality of the loop fluid at the heater exit. Consequently increase in the driving force and results enhancement in mass flow rate. This phenomenon observed at initial heat fluxes. With an additional increase in heat flux, the loop fluid vapour quality increases and offers drag hence mass flow rate decreases. Hence, for a higher condenser coolant inlet temperature the maximum loop mass flow rate appears at a lower value of heat flux. So it is noted that, loop operating at high heat fluxes with high condenser coolant inlet temperature is not feasible. Therefore, it concluded that for favourable sink conditions, i.e., high condenser coolant flow rate or low inlet temperature, the system can be operated over wider ranges of heat flux.

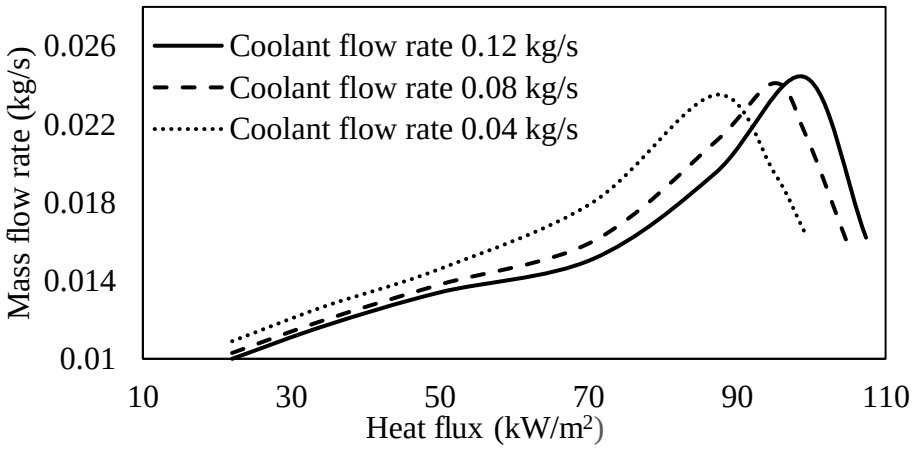

(a) Water

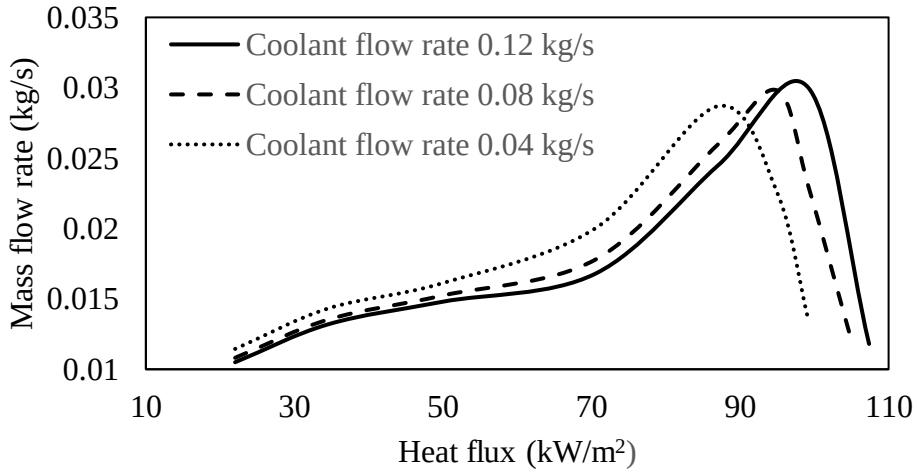

(b) 0.005% Al_2O_3 nanofluid

Fig.5.9 Influence of condenser coolant flow rate on loop mass flow rate at 10 ^{O}C coolant inlet temperature

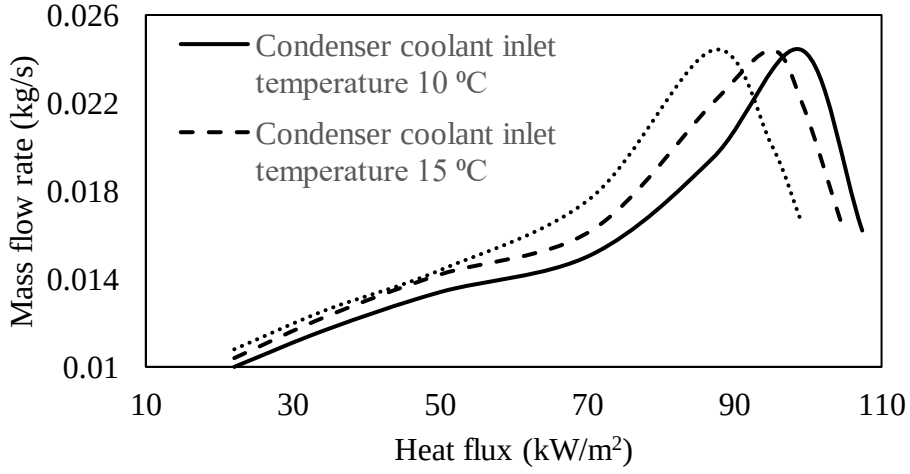

(a) Water

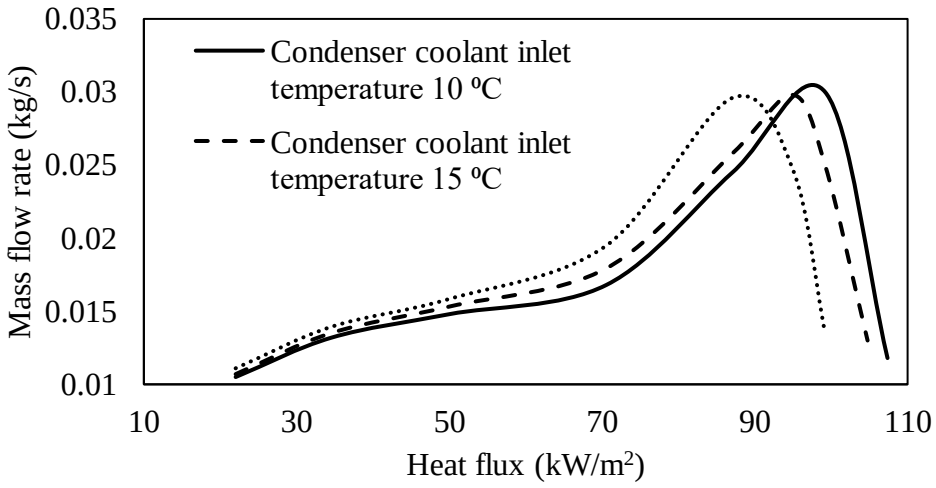

(b) 0.005% Al_2O_3 nanofluid

Fig.5.10 Influence of condenser coolant inlet temperature on loop mass flow rate at 0.12 kg/sec flow rate

5.5 Conclusions

The performance of a rectangular natural circulation loop filled with water and nanofluids was experimentally investigated and the results are presented in this chapter. The conclusions from experimental results can be summarized as follows:

1. Natural circulation loop operated with nanofluid quickly reaches steady state condition compared to water.
2. The steady state mass flow rate increase with heat flux. Also, the fluid mass flow rate is further enhanced by adding nanoparticles to the working fluid. The average enhancement in mass flow rate for 0.01% Al_2O_3 based NCL is 8.7% as compared with water based NCL.
3. It is also observed that, the nanofluid based NCL early reaches boiling as compared with water based NCL.
4. The average enhancement of HTC for 0.01% Al_2O_3 based NCL as compared with water based NCL operated in single phase condition is 9.09 % and in two phase condition is 99.2% respectively.
5. With decrease in condenser coolant inlet temperature and increase in coolant flow rate, the NCL mass flow rate increases for water and nanofluids.
6. The water based NCL exhibits flow regime in the sequence given below:

Bubbly flow → Slug flow → Churn flow → Annular flow

7. The nanofluid based NCL exhibits flow regime in the sequence given below:

   Bubbly flow → Slug flow → Annular flow

Chapter 6

General conclusions and scope of future work

Chapter – 6

General conclusions and scope of future work

6.1 General conclusions

In the present work, first, a detailed literature survey on two phase natural circulation loops (NCL) and their applications was carried out. Following the survey, numerical studies on the steady state performance of the nanofluid based natural circulation loops were carried out. Then after, experimental studies were carried out on in-house developed flow boiling test rig in order to understand the flow boiling behaviour of nanofluid by varying different parameters such as particle concentration, heat flux and mass flux. The results obtained were compared with deionised water. Finally, based on the numerical results, an instrumented nanofluid based natural circulation loop with heater as a heat source and heat exchanger as heat sink was designed, fabricated and experimentation was done on this test rig.

The following are the important conclusions drawn based on the present study.

6.1.1 Based on numerical studies on two phase NCL

1. The proposed model is validated with Vijayan's [57] correlation. The maximum error obtained is ±5%.
2. Two phase NCLs performance is affected by different parameters such as heater and condenser orientation, heater inlet temperature, heat flux, aspect ratio, diameter, pressure and type of the loop fluid.

3. Heater and condenser orientations and positions are considered as per the design and constructional constraints. However it is better to place the condenser in a horizontal orientation.

4. As aspect ratio increase, the loop height increases and mass flow rate increases. This is due to high pressure gradient across the riser and downcomer sections.
5. NCL performance is strongly affected by loop riser diameter. An increment in riser diameter leads to reduce the two-phase frictional pressure drop which leads to a higher

mass flow rate and lower quality in the loop. Whereas varying the downcomer diameter has insignificant effect on loop performance.

6. As the system pressure decreases from atmospheric to sub-atmospheric, the loop fluid experiences early flashing or boiling. Hence, at lower heat fluxes the loop exhibits higher density gradients. So, NCLs operating at sub-atmospheric pressure have high mass flow rates at lower heat fluxes as compared to NCL operating at atmospheric pressure.
7. For a particular heater inlet temperature and fixed heat flux, the decrement in system pressure decreases the sensible heat capacity of the loop fluid and remaining heat is used as enthalpy of vaporisation which leads to the increase of loop fluid quality (void fraction). Further decrement in local pressure situates high quality fluid in riser and offers more drag/frictional forces resulting in lower mass flow rate.

6.1.2 Based on experimental study on nanofluid flow boiling

8. The flow boiling heat transfer coefficient (HTC) increases with mass flux for both water and nanofluids. However, the magnitudes are different.

9. The boiling curve of the nanofluids shifts towards left as compared with water because of the reduction in wall superheat. The average reduction of wall superheat at mass flux of 905.42 kg/s-m^2 for 0.001%, 0.005% and 0.01% Al_2O_3 nanofluids are 10.8%, 21.34% and 26.97% respectively.

10. Nanofluids have high boiling HTC compared to water and the HTC increases with the increase of volume concentration. For example, the average enhancement in HTC for concentrations of 0.001 %, 0.005 % & 0.01 % nanofluids at the mass flux of 905.42 kg/s-m^2 are 12.11%, 21.75 % & 27.97 % respectively.

11. The Al_2O_3/water nanofluid boiling HTC is enhanced due to the improved heater surface characteristics and amendment in bubble formation mechanism.

12. The flow boiling behaviour of nanofluid differs from water as follows:

    i. In nanofluid boiling, nanoparticles are deposited on heater surface and modify the heater surface such that more nucleation sites are created.

ii. Al_2O_3/water nanofluid exhibits early transition of flow regimes compared to water.

iii. Water exhibits flow regime in the sequence given below:

Bubble flow → Slug flow → Churn flow → Annular flow.

On the other hand, Al_2O_3/water nanofluids exhibit the following sequence:

Bubble flow → Slug flow → Annular flow.

13. A new empirical correlation has been proposed to predict the flow boiling heat transfer coefficient of nanofluids.

6.1.3 Based on experimental studies on two phase NCL

14. Natural circulation loop operated with nanofluid quickly reaches steady state condition compared to water.

15. The steady state mass flow rate increase with heat flux. Also, the fluid mass flow rate is further enhanced by adding nanoparticles to the working fluid. The average enhancement in mass flow rate for 0.01% Al_2O_3 based NCL is 8.7% as compared with water based NCL.

16. It is also observed that, the nanofluid based NCL early reaches boiling as compared with water based NCL.

17. The average enhancement of HTC for 0.01% Al_2O_3 based NCL as compared with water based NCL operated in single phase condition is 9.09 % and in two phase, condition is 99.2% respectively.

18. With decrease in condenser coolant inlet temperature and increase in coolant flow rate, the NCL mass flow rate increases for water and nanofluids.

19. The water based NCL exhibits flow regime in the sequence given below:

Bubbly flow → Slug flow → Churn flow → Annular flow

20. The nanofluid based NCL exhibits flow regime in the sequence given below:

    Bubbly flow ⟶ Slug flow ⟶ Annular flow

6.2 Future scope

Future research directions are identified upon observing trend of results and some deficiencies of the existing models/correlations and experimental data. Although the current study covered a wide range of parameters in numerical studies, several additional parameters still need to be identified experimentally. In addition, the designing of two phase system is a challenging task due to the enormous promise and intricate thermal-hydraulic phenomena of two phase flows especially for cooling applications like nuclear reactor core cooling and electronic chip cooling which requires a critical zero tolerance while they are in use. So, suggested research topics for future work are numerated as follows:

1. Numerical model developed by imposing the realistic boundary conditions like conjugate heat transfer condition at heat sink.
2. Nanofluids boiling heat transfer phenomena has to be investigated/studied briefly over broader range of thermodynamic conditions with different nanoparticles.
3. Theoretical and experimental investigation of two-phase NCL behaviour under steady sate and transient conditions with different nanofluids over a broad range of operating conditions.

Finally prioritizing the addressed topics will promote the idea of utilizing the emerged outcomes from this study. First, a simple numerical model developed to understand the thermo-hydraulic behaviour of two phase NCL. The proposed model successfully estimate the performance of two phase NCL for various operating and geometrical conditions. On the other hand, imposed constant heat flux boundary condition at heat sink is unrealistic manner and a small penalty is observed in estimated parameters. Therefore the future research effort should be focused on develop more realistic numerical model of two phase NCL.

Second, experimental studies conducted to analyse the boiling heat transfer phenomena of alumina nanofluids. Results is believed to be very inclusive (e.g., Wall superheat, nucleation site density bubble dynamics and heat transfer coefficient). Based on results a

new correlation is developed by using the existing models to estimate the boiling heat transfer coefficient. However, the embedded approach of coupling own experimental data with existing models was not very effective in predicting the measured HTC data. This because of experiments conducted by varying parameters are limited and hence use of proposed correlation is own limiting constraints. Therefore, a more research effort is needed to obtain a more accurate heat transfer model in nanofluids over a broader range of thermodynamic conditions. Moreover, use of alumina nanofluids in boiling heat transfer applications in practicality needed. Therefore, direct use of nanofluids in NCL is experimentally analysed. The use of nanofluids in NCL increases the performance and decreases the instability characteristics and that was presented in this thesis work. Meanwhile, more experiments has to be carried out over a wide range of operating conditions with various other nanofluids such as CuO, SiO_2, and TiO_2.

Publications

International Journals:

S.No.	Title of the paper	Name of the Journal and Publisher	Status
1	Two-phase natural circulation loop behaviour at atmospheric and sub-atmospheric conditions.	Published: Part E: Journal of Process Mechanical Engineering, (SCI).	Published
2	Experimental studies of heat transfer and flow regimes during flow boiling of water and alumina nanofluids at different heat and mass fluxes.	Published: Part C: Journal of Mechanical Engineering Science, (SCI).	Published
3	Effect of Loop Diameter on Two Phase Natural Circulation Loop Performance.	Lecture notes in Mechanical engineering, Springer (SCOPUS).	Published
4	Effect of riser and downcomer diameter variation on the performance of two-phase natural circulation loop.	International Journal of Mechanical and Production Engineering Research and Development (IJMPERD) (SCOPUS).	Published
5	Steady State Performance of Two Phase Natural Circulation Loop: Two Vertical Branches with Point Heat Source and Sink.	International Journal of Advanced Trends in Computer Applications.	Published

International/ National Conferences:

S.No.	**Title of the paper**	**Name of the Conference**	**Status**
1	Analysisoftwophase rectangular natural circulationloop	NSMERS 2016, NIT Warangal 7th Oct, 2016. India	Presented
2	Numericalstudyon performance oftwophase natural circulationloop at sub-atmosphericconditions	International Conference on Recent Trends in Engineering, Science and Technology, 27-28th October 2016, Hyderabad, India	Presented.
3	Numericalanalysisof rectangular twoPhase Natural circulationLoop	TSME, Bangkok, December 12-15, 2017	Presented

4	Experimental investigationonflowboilingheat transfer characteristicsthrough vertical tube	INCEEE, NIT Warangal, February 15-16, 2019.	Presented

References

[1] R. Greif, “Natural circulation loops,” J. Heat Transfer, vol. 110, no. 4, pp. 1243–1259, 1988.

[2] H. Bieliński and J. Mikielewicz, “Natural circulation in single and two phase thermosyphon loop with conventional tubes and minichannels,” Heat Transf. - Math. Model. Numer. Methods Inf. Technol., vol. 19, 2011.

[3] M. Misale, “Experimental study on the influence of power steps on the thermohydraulic behavior of a natural circulation loop”, International journal of heat and mass transfer,” Int. J. Heat Mass Transf., vol. 99, pp. 789–791, 2016.

[4] Michael P. Heisler, “Development of scaling requirements for natural convection liquid-metal fast breeder reactor shutdown heat removal test facilities,” Nucl. Sci. Eng., vol. 80, pp. 347–359, 1982.

[5] D. E. Kim, M. H. Kim, J. E. Cha, and S. O. Kim, “Numerical investigation on thermal – hydraulic performance of new printed circuit heat exchanger model,” Nucl. Eng. Des., vol. 238, pp. 3269–3276, 2008.

[6] A. Mertol, W. Place, and T. Webster, “Detailed loop model (DLM) analysis of liquid solar thermosiphons with heat exchangers,” Sol. Energy, vol. 27, no. 5, pp. 367–386, 1981.

[7] Hugh R. McKee, “Thermosiphon reboilers-A review,” Ind. Eng. Chem., vol. 62, no. 12, pp. 76–82, 1970.

[8] N. V. L. . Sarma, P. J. Reddy, and P. S. Murti, “A computer design method for vertical thermosyphon reboilers,” Ind. Eng. Chem. Process Des. Dev., vol. 12, no. 3, pp. 278–290, 1973.

[9] F. J. B. Cohen., Henry., “Heat-transfer problems of liquid-cooled gas-turbine blades,” Proc. Inst. Mech. Eng., vol. 169, no. 1, pp. 1063–1080, 1955.

[10] D. Japikse, “Advances in thermosyphon technology,” Adv. Heat Transf., vol. 9, no. C, pp. 1–111, 1973.

[11] P. K. Vijayan and A. K. Nayak, “Natural circulation systems: Advantages and

challenges," Proc. NUTHOS-6, no. May, pp. 1–12, 2004.

[12] H. F. Creveling, J. F. de Paz, J. Y. Baladi, and R. J. Schoenhals, "Stability characteristics of a single-phase free convection loop," J. Fluid Mech., vol. 67, no. 1, pp. 65–84, 1975.

[13] P. Welander, "On the oscillatory behaviour of a differentially heated fluid loop," J. Fluid Mech., vol. 29, no. 1967, pp. 17–30, 1967.

[14] N. M. Rao, B. Maiti, and P. K. Das, "Dynamic performance of a natural circulation loop with end heat exchangers under different excitations," Int. J. Heat Mass Transf., vol. 48, no. 15, pp. 3185–3196, 2005.

[15] H. H. Bau, "Transient and steady behavior of an open, symmetrically-heated, free convection loop," vol. 24, no. 4, pp. 597–609, 1981.

[16] M. A. Bernier and B. R. Baliga, "A 1-D/2-D model and experimental results for a closed-loop thermosyphon with vertical heat transfer sections," Int. J. Heat Mass Transf., vol. 35, no. 11, pp. 2969–2982, 1992.

[17] D. J. Close, "The performance of solar water heaters with natural circulation," Sol. Energy, vol. 6, no. 1, pp. 33–40, 1962.

[18] K. S. Ong, "A finite-difference method to evaluate the thermal performance of a solar water heater," Sol. Energy, vol. 16, no. 3–4, pp. 137–147, 1974.

[19] A. Shitzer, D. Kalmanoviz, Y. Zvirin, and G. Grossman, "Experiments with a flat plate solar water heating system in thermosyphonic flow," Sol. Energy, vol. 22, no. 1, pp. 27–35, 1979.

[20] Y. Zvirin, A. Shitzer, and G. Grossman, "The natural circulation solar heater-models with linear and nonlinear temperature distributions," Int. J. Heat Mass Transf., vol. 20, no. 9, pp. 997–999, 1977.

[21] H. D. Koca, S. Doganay, and A. Turgut, "Thermal characteristics and performance of Ag-water nanofluid: Application to natural circulation loops," Energy Convers. Manag., vol. 135, pp. 9–20, 2017.

[22] D. B. Kreitlow, G. M. Reistad, C. R. Miles, and G. G. Culver, "Thermosyphon models for downhole heat exchanger applications in shallow geothermal systems," J. Heat Transfer, vol. 100, no. 4, pp. 713–719, 1978.

[23] P. E. Tuma and H. R. Mortazavi, “Indirect thermosyphons for cooling electronic devices,” Electron. Cool., vol. 12, no. 1, pp. 26–32, 2006.

[24] J. B. Joshi, “Computational flow modelling and design of bubble column reactors,” Chem. Eng. Sci., vol. 56, no. 21–22, pp. 5893–5933, 2001.

[25] K. K. Kumar and M. R. Gopal, “Carbon dioxide as a secondary fluid in natural circulation loops,” Proc. Inst. Mech. Eng. Part E J. Process Mech. Eng., vol. 223, pp. 189–194, 2009.

[26] S. Gumus, H. Ozcan, M. Ozbey, and B. Topaloglu, “Aluminum oxide and copper oxide nanodiesel fuel properties and usage in a compression ignition engine,” Fuel, vol. 163, pp. 80–87, 2016.

[27] J. Zambrana, T. J. Leo, and P. Perez-del-Notario, “Vertical tube length calculation based on available heat transfer coefficient expressions for the subcooled flow boiling region,” Appl. Therm. Eng., vol. 28, no. 5–6, pp. 499–513, 2008.

[28] J. G. Collier and J. R. Thome, Convective boiling and condensation, 3rd ed. Newyork: McGraw-Hill, 1994.

[29] S. J. Kim, T. McKrell, J. Buongiorno, and L. wen Hu, “Subcooled flow boiling heat transfer of dilute alumina, zinc oxide, and diamond nanofluids at atmospheric pressure,” Nucl. Eng. Des., vol. 240, no. 5, pp. 1186–1194, 2010.

[30] T. Il Kim, W. J. Chang, and S. H. Chang, “Flow boiling CHF enhancement using Al2O3 nanofluid and an Al2O3 nanoparticle deposited tube,” Int. J. Heat Mass Transf., vol. 54, no. 9–10, pp. 2021–2025, 2011.

[31] S. U. S. Choi and J. A. Eastman, “Enhancing thermal conductivity of fluids with nanoparticles,” in Proceedings of the ASME International Mechanical Engineering Congress and Exposition, 1995, pp. 99–106.

[32] A. K. Nayak, P. P. Kulkarni, and P. K. Vijayan, “Study on the transient and stability behaviour of a boiling two-phase natural circulation loop with Al_2O_3nanofluids,” Appl. Therm. Eng., vol. 31, no. 10, pp. 1673–1681, 2011.

[33] S. Doganay and A. Turgut, “Enhanced effectiveness of nanofluid based natural circulation mini loop,” Appl. Therm. Eng., vol. 75, pp. 669–676, 2015.

[34] K. B. Rana, A. K. Rajvanshi, and G. D. Agrawal, “A visualization study of flow boiling heat transfer with nanofluids,” J. Vis., vol. 16, no. 2, pp. 133–143, 2013.

[35] Owhaib W, “Experimental heat transfer pressure drop and flow visualization of R-134a in vertical mini/micro tubes,” Royal Institute of Technology, KTH Stockholm, 2007.

[36] V. Nikkhah, “Application of spherical copper oxide (II) water nano-fluid as a potential coolant in a boiling annular heat exchanger,” Chem. Biochem. Eng. Q., vol. 29, no. 3, pp. 405–415, 2016.

[37] M. M. Sarafraz and F. Hormozi, “Convective boiling and particulate fouling of stabilized CuO-ethylene glycol nanofluids inside the annular heat exchanger,” Int. Commun. Heat Mass Transf., vol. 53, pp. 116–123, 2014.

[38] E. Salari, M. Peyghambarzadeh, M. M. Sarafraz, and F. Hormozi, “Boiling heat transfer of alumina nano-fluids: Role of nanoparticle deposition on the boiling heat transfer coefficient,” Period. Polytech. Chem. Eng., vol. 60, no. 4, pp. 252–258, 2016.

[39] M. M. Sarafraz and F. Hormozi, “Forced convective and nucleate flow boiling heat transfer to alumnia nanofluids,” Period. Polytech. Chem. Eng., vol. 58, no. 1, pp. 37–46, 2014.

[40] M. M. Sarafraz, S. M. Peyghambarzadeh, S. A. Alavi Fazel, and N. Vaeli, “Nucleate pool boiling heat transfer of binary nano mixtures under atmospheric pressure around a smooth horizontal cylinder,” Period. Polytech. Chem. Eng., vol. 57, no. 1–2, pp. 71–77, 2013.

[41] M. M. Sarafraz and S. M. Peyghambarzadeh, “Nucleate pool boiling heat transfer to Al_2O_3 - water and TiO_2 - water nanofluids on horizontal smooth tubes with dissimilar homogeneous materials,” Chem. Biochem. Eng., vol. 26, no. 3, pp. 199–206, 2012.

[42] S. J. Kim, T. McKrell, J. Buongiorno, and L. wen Hu, “Subcooled flow boiling heat transfer of dilute alumina, zinc oxide, and diamond nanofluids at atmospheric pressure,” Nucl. Eng. Des., vol. 240, no. 5, pp. 1186–1194, 2010.

[43] B. Sun and D. Yang, “Flow boiling heat transfer characteristics of nano-refrigerants in a horizontal tube,” Int. J. Refrig., vol. 38, no. 1, pp. 206–214, 2014.

[44] S. W. Lee et al., “Critical heat flux enhancement in flow boiling of Al_2O_3 and SiC

nanofluids under low pressure and low flow conditions," Nucl. Eng. Technol., vol. 44, no. 4, pp. 429–436, 2012.

[45] Om Shankar Prajapati and Nirupam Rohatgi, "Flow boiling heat transfer enhancement by using ZnO-water Nanofluids," Sci. Technol. Nucl. Install., vol. 2014, pp. 1–7, 2014.

[46] M. M. Sarafraz, H. Arya, M. Saeedi, and D. Ahmadi, "Flow boiling heat transfer to MgO-therminol 66 heat transfer fluid: Experimental assessment and correlation development," Appl. Therm. Eng., vol. 138, no. January, pp. 552–562, 2018.

[47] Y. ZVIRIN, "A review of natural circulation loops in pressurized water reactors and other systems," Nucl. Eng. Des., vol. 67, pp. 203–225, 1981.

[48] R. Greif, "Natural circulation loops," J. Heat Transfer, vol. 110, pp. 1243–1258, 1988.

[49] H. R. McKEE, "Thermosiphon reboilers-A review," Ind. Eng. Chem., vol. 62, no. 12, pp. 76–82, 1970.

[50] N. Goswami and S. Paruya, "Progress in nuclear energy advances on the research on nonlinear phenomena in boiling natural circulation loop," Prog. Nucl. Energy, vol. 53, no. 6, pp. 673–697, 2011.

[51] D. N. Basu, S. Bhattacharyya, and P. K. Das, "A review of modern advances in analyses and applications of single-phase natural circulation loop in nuclear thermal hydraulics," Nucl. Eng. Des., vol. 280, pp. 326–348, 2015.

[52] S. S. A. and H. A. Mohd. Kamil, "Prediction of circulation rates in vertical tube thermosiphon reboiler," Int. J. heat mass Transf., vol. 38, no. 4, pp. 745–748, 1995.

[53] A. I. Johnson, "Circulation rates and overall temperature driving forces in a vertical thermosiphon reboiler," Chem. Eng. Prog. Symp. Ser., vol. 52, pp. 37–43, 1956.

[54] J. V. Smith, "Improving the performance of vertical thermosiphon reboilers," Chem. Engng Prog, vol. 70, pp. 68–70, 1974.

[55] G. C. Shah, "Trouble shooting reboiler systems," Chem. Engng Prog., vol. 75, no. 7, pp. 53–58, 1979.

[56] D. L. J. and Y. Yukawa, "Vertical thermosyphon reboilers in vacuum service," Chem. Eng. Prog., vol. 75, no. 7, pp. 47–52, 1979.

[57] M. R. Gartia, P. K. Vijayan, and D. S. Pilkhwal, “A generalized flow correlation for two-phase natural circulation loops,” Nucl. Eng. Des., vol. 236, no. 17, pp. 1800–1809, 2006.

[58] Y. Lee and U. Mital, “A two-phase closed thermosyphon,” Int. J. Heat Mass Transf., vol. 15, no. 9, pp. 1695–1707, 1972.

[59] K. S. Chen and Y. R. Chang, “Steady-state analysis of two-phase natural circulation loop,” Int. J. Heat Mass Transf., vol. 31, no. 5, pp. 931–940, 1988.

[60] C. Feroz Md and F. Kaminaga, “Boiling heat transfer characteristics of R-113 in a vertical small diameter tube under natural circulation condition,” Int. J. Heat Mass Transf., vol. 45, no. 24, pp. 4823–4829, 2002.

[61] H. Ali and S. S. Alam, “Circulation rates in thermosiphon reboiler,” Int. J. Heat Fluid Flow, vol. 13, no. 1, pp. 86–92, 1992.

[62] K. Kiran Kumar and M. Ram Gopal, “Steady-state analysis of CO_2 based natural circulation loops with end heat exchangers,” Appl. Therm. Eng., vol. 29, no. 10, pp. 1893–1903, 2009.

[63] K. Kiran Kumar and M. Ram Gopal, “Effect of system pressure on the steady state performance of a CO_2 based natural circulation loop,” Appl. Therm. Eng., vol. 29, no. 16, pp. 3346–3352, 2009.

[64] K. Kiran Kumar and M. Ram Gopal, “Experimental studies on CO_2 based single and two-phase natural circulation loops,” Appl. Therm. Eng., vol. 31, no. 16, pp. 3437–3443, 2011.

[65] N. M. Rao, S. Yadav, T. V. Kumar, and P. Yadav, “Theoretical investigation on the steady state of two phase natural circulation loop (NCL) with end heat exchangers,” Int. J. Sci. Eng. Res., vol. 8, no. 2, pp. 63–67, 2017.

[66] S. W. Chang, D. C. Lo, K. F. Chiang, and C. Y. Lin, “Sub-atmospheric boiling heat transfer and thermal performance of two-phase loop thermosyphon,” Exp. Therm. Fluid Sci., vol. 39, pp. 134–147, 2012.

[67] S. W. Chang and C. Y. Lin, “Thermal performance improvement with scale imprints over boiling surface of two-phase loop thermosyphon at sub-atmospheric conditions,”

Int. J. Heat Mass Transf., vol. 56, no. 1–2, pp. 294–308, 2013.

[68] D. Wang, J. Jiang, D. Zhan, X. Zhang, and X. Liu, “Annals of nuclear energy design and analysis of improved two-phase natural circulation systems with thermoelectric generator,” Ann. Nucl. Energy, vol. 139, pp. 1–10, 2020.

[69] Y. Liu, Z. Li, Y. Li, Y. Jiang, and D. Tang, “Heat transfer and instability characteristics of a loop thermosyphon with wide range of fi lling ratios,” Appl. Therm. Eng., vol. 151, no. January, pp. 262–271, 2019.

[70] H. Cao, T. Ding, Z. He, and Z. Li, “Research on the refrigerant column height in the downcomer of a two-phase loop thermosyphon,” Int. J. Refrig., vol. 94, pp. 40–48, 2018.

[71] L. Zhu and J. Yu, “Experimental investigation on startup performances of a separator assisted two-phase loop thermosyphon,” Int. J. Heat Mass Transf., vol. 148, pp. 1–10, 2020.

[72] P. Zhang, W. Shi, X. Li, B. Wang, and G. Zhang, “A performance evaluation index for two-phase thermosyphon loop used in HVAC systems,” Appl. Therm. Eng., vol. 131, pp. 825–836, 2017.

[73] I. A. Furzer, “Vertical thermosiphon reboilers, maximum heat flux and separation efficiency,” Ind. Eng. Chem. Res., vol. 29, no. 7, pp. 1396–1404, 1990.

[74] G. m. Hughmark, “Designing thermosiphon reboilers-I,” Chem. Enyny Proy., vol. 57, pp. 43–47, 1961.

[75] G. A. Hughmark, “Designing thermosiphon reboilers-II,” Chem. Engng. Prog., vol. 60, pp. 59–61, 1969.

[76] J. W. and R. W. Bowring, “Methods for detailed thermal and hydraulic analysis of water-cooled reactors,” Nuel. Sci. Engng, vol. 57, pp. 255–276, 1975.

[77] A. Knaani and Y. Zvirin, “Bifurcation phenomena in two-phase natural circulation,” Int. J. Multiph. Flow, vol. 19, no. 6, pp. 1129–1151, 1993.

[78] R.B. Duffey and J. P. Sursock, “Natural circulation phenomena relevant to small breaks and transients,” Nucl. Eng. Des., vol. 102, pp. 115–128, 1987.

[79] E. Ramos, M. Sen, and C. Treviño, “A steady-state analysis for variable area one- and two-phase thermosyphon loops,” Int. J. Heat Mass Transf., vol. 28, no. 9, pp. 1711–

1719, 1985.

[80] N. M. Rao, C. C. Sekhar, B. Maiti, and P. K. Das, “Steady-state performance of a two-phase natural circulation loop,” Int. Commun. Heat Mass Transf., vol. 33, no. 8, pp. 1042–1052, 2006.

[81] A. K. Nayak, P. Dubey, D. N. Chavan, and P. K. Vijayan, “Study on the stability behaviour of two-phase natural circulation systems using a four-equation drift flux model,” Nucl. Eng. Des., vol. 237, no. 4, pp. 386–398, 2007.

[82] L. Lin and A. Faghri, “Steady-state performance in a thermosyphon with tube separator,” Appl. Therm. Eng., vol. 17, no. 7, pp. 667–679, 1997.

[83] D. N. Basu, S. Bhattacharyya, and P. K. Das, “Steady-state behavior of a two-phase natural circulation loop with thermodynamic nonequilibrium,” J. Heat Transfer, vol. 131, pp. 1–12, 2009.

[84] N. Goudarzi and S. Talebi, “Improving performance of two-phase natural circulation loops by reducing of entropy generation,” Energy, vol. 93, pp. 882–899, 2015.

[85] S. Bodjona, E. Videcoq, R. Saurel, A. Chinnayya, A. M. Benselama, and Y. Bertin, “Transient simulation of a two-phase loop thermosyphon with a model out of thermodynamic equilibrium,” Int. J. Heat Mass Transf., vol. 108, pp. 474–496, 2017.

[86] F. A. Braz, G. Sabundjian, G. B. Ribeiro, and A. D. Caldeira, “Annals of nuclear energy assessment of RELAP5 matrix solvers for a two-phase natural circulation loop,” Ann. Nucl. Energy, vol. 105, pp. 249–258, 2017.

[87] P. K. Vijayan, A. P. Patil, D. S. Pilkhwal, D. Saha, and V. Venkat Raj, “An assessment of pressure drop and void fraction correlations with data from two-phase natural circulation loops,” Heat Mass Transf., vol. 36, pp. 541–548, 2000.

[88] B. Chexal, J. Maulbetsch, J. Harrison, C. Petersen, P. Jensen, and J. Horowitz, “Understanding void fraction in steady and dynamic environments,” Hillview Avenue,Palo Alto, California, 1996.

[89] P. Saha and N. Zuber, “Point of net vapour generation and void fraction in subcooled boiling,” in Proceedings of 5th International Heat Transfer Conference, 1974, pp. 175–179.

[90] V. Chatoorgoon, “SPORTS - A simple non-linear thermalhydraulic stability code,” Nucl. Eng. Des., vol. 93, no. 1, pp. 51–67, 1986.

[91] A. A. Avdeev, “Self-boiling of a two-phase coolant in the case of upwards motion,” J. Chem. Inf. Model., vol. 53, no. 9, pp. 1689–1699, 2019.

[92] F. Inada and T. Ohkawa, “Thermo-hydraulic instability of natural circulation BWRs (explanation on instability mechanisms at start-up by homogeneous and thermo-dynamic equilibrium model considering flashing effect),” in International Conference on New Trends in Nuclear System Thermohydraulics, 1994, pp. 187–193.

[93] D. D. B. Van Bragt, W. J. M. De Kruijf, A. Manera, T. H. J. J. Van Der Hagen, and H. Van Dam, “Analytical modeling of flashing-induced instabilities in a natural circulation cooled boiling water reactor,” Nucl. Eng. Des., vol. 215, pp. 87–98, 2002.

[94] K. K. Dewangan and P. K. Das, “Assessing the effect of flashing on steady state behavior and Ledinegg instability of a two phase rectangular natural circulation loop,” Int. J. Heat Mass Transf., vol. 116, pp. 218–230, 2018.

[95] S. V. S. Sudheer, K. K. Kumar, and K. Balasubramanian, “Two-phase natural circulation loop behaviour at atmospheric and subatmospheric conditions,” vol. 233, no. 4, pp. 687–700, 2018.

[96] K. Tanimoto, M. Ishii, and S. Yong, “Examination of transient characteristics of two-phase natural circulation within a Freon-113 boiling / condensation loop,” Nucl. Eng. Des., vol. 183, pp. 77–95, 1998.

[97] X. Wang and X. Xu, “Thermal conductivity of nanoparticle - fluid mixture,” J. Thermophys. Heat Transf., vol. 13, no. 4, pp. 474–480, 2008.

[98] E. De Robertis et al., “Application of the modulated temperature differential scanning calorimetry technique for the determination of the specific heat of copper nanofluids,” Appl. Therm. Eng., vol. 41, pp. 10–17, 2012.

[99] M. V. Narayanan and S. G. Rakesh, “Nanofluids: A review on current scenario and future prospective,” in IOP Conference Series: Materials Science and Engineering, 2018, vol. 377, pp. 1–9.

[100] I. M. Mahbubul, R. Saidur, and M. A. Amalina, “Latest developments on the viscosity

of nanofluids," Int. J. Heat Mass Transf., vol. 55, no. 4, pp. 874–885, 2012.

[101] M. M. Sarafraz, "Experimental investigation on pool boiling heat transfer to formic acid, propanol and 2-butanol pure liquids under the atmospheric pressure," J. Appl. Fluid Mech., vol. 6, no. 1, pp. 73–79, 2013.

[102] S. J. Kim, I. C. Bang, J. Buongiorno, and L. W. Hu, "Surface wettability change during pool boiling of nanofluids and its effect on critical heat flux," Int. J. Heat Mass Transf., vol. 50, no. 19–20, pp. 4105–4116, 2007.

[103] M. M. Sarafraz, F. Hormozi, M. Silakhori, and S. M. Peyghambarzadeh, "On the fouling formation of functionalized and non-functionalized carbon nanotube nano-fluids under pool boiling condition," Appl. Therm. Eng., vol. 95, pp. 433–444, 2016.

[104] H. Xie, J. Wang, T. Xi, Y. Liu, F. Ai, and Q. Wu, "Thermal conductivity enhancement of suspensions containing nanosized alumina particles," J. Appl. Phys., vol. 91, no. 7, pp. 4568–4572, 2002.

[105] V. Sajith, M. Mannoor, and C. B. Sobhan, "An experimental investigation of the boiling performance of water-based nanofluids," in ASME 2008 First International Conference on Micro/Nanoscale Heat Transfer, 2008.

[106] M. H. Shi, M. Q. Shuai, Z. Q. Chen, Q. Li, and Y. Xuan, "Study on pool boiling heat transfer of nano-particle suspensions on plate surface," J. Enhanc. Heat Transf., vol. 14, no. 3, pp. 223–231, 2008.

[107] J. S. Coursey and J. Kim, "Nanofluid boiling: The effect of surface wettability," Int. J. Heat Fluid Flow, vol. 29, no. 6, pp. 1577–1585, 2008.

[108] I. C. Bang and S. Heung Chang, "Boiling heat transfer performance and phenomena of Al2O 3-water nano-fluids from a plain surface in a pool," Int. J. Heat Mass Transf., vol. 48, no. 12, pp. 2407–2419, 2005.

[109] M. M. Sarafraz and F. Hormozi, "Scale formation and subcooled flow boiling heat transfer of CuO-water nanofluid inside the vertical annulus," Exp. Therm. Fluid Sci., vol. 52, pp. 205–214, 2014.

[110] H. Peng, G. Ding, W. Jiang, H. Hu, and Y. Gao, "Heat transfer characteristics of refrigerant-based nanofluid flow boiling inside a horizontal smooth tube," Int. J. Refrig.,

vol. 32, no. 6, pp. 1259–1270, 2009.

[111] K. B. Rana, G. D. Agrawal, J. Mathur, and U. Puli, “Measurement of void fraction in flow boiling of ZnO-water nanofluids using image processing technique,” Nucl. Eng. Des., vol. 270, pp. 217–226, 2014.

[112] J. R. T. John G. Collier, Convective Boiling and Condensation. 1996.

[113] R.K. Shah and A.L. London, Laminar forced convective in ducts. Newyork: Academic press, 1978.

[114] M. Al-Arabi, “Turbulent heat transfer in the entrance region of a tube,” Heat Transf. Eng., vol. 3, no. 3–4, pp. 76–83, 1982.

[115] S. G. Kandlikar, “A general correlation for saturated two-phase flow boiling heat transfer inside horizontal and vertical tubes,” J. Heat Transfer, vol. 112, no. 1, pp. 219–228, 1990.

[116] L. Chen, X.-R. Zhang, and B. Jiang, “Effects of heater orientations on the natural circulation and heat transfer in a supercritical CO_2 rectangular loop,” J. Heat Transfer, vol. 136, no. May 2014, pp. 052501: 1–12, 2014.

[117] B. T. Swapnalee, P. K. Vijayan, M. Sharma, and D. S. Pilkhwal, “Steady state flow and static instability of supercritical natural circulation loops,” Nucl. Eng. Des., vol. 245, pp. 99–112, 2012.

[118] V. Archana, A. M. Vaidya, and P. K. Vijayan, “Numerical modeling of supercritical CO2 natural circulation loop,” Nucl. Eng. Des., vol. 293, pp. 330–345, 2015.

[119] P. Zhang, B. Wang, W. Shi, X. Li, “Experimental investigation on two-phase thermosyphon loop with partially liquid-filled downcomer,” Appl. Energy, vol. 160, pp. 10–17, 2015.

[120] C. Y. Tso and C. Y. H. Chao, “Study of enthalpy of evaporation, saturated vapor pressure and evaporation rate of aqueous nanofluids,” Int. J. Heat Mass Transf., vol. 84, pp. 931–941, 2015.

[121] B. C. Pak and Y. I. Cho, “Hydrodynamic and heat transfer study of dispersed fluids with submicron metallic oxide particles,” Exp. Heat Transf., vol. 11, no. 2, pp. 151–170, 1998.

[122] T. Chen and S. V. Garimella, “Effects of dissolved air on subcooled flow boiling of a dielectric coolant in a microchannel heat sink,” J. Electron. Packag., vol. 128, pp. 398–404, 2006.

[123] J. R. Taylor, An introduction to error analysis the study of uncertainties in physical measurements, 2nd ed. Sausalito, Calif: University Science Books, 1997.

[124] M. Kaichiro and M. Ishii, “Flow regime transition criteria for upward two-phase flow in vertical tubes,” Int. J. Heat Mass Transf., vol. 27, no. 5, pp. 723–737, 1984.

[125] N. Patra, P. Ghosh, R. S. Singh, and A. Nayak, “Flow visualization in dilute oxide based nanofluid boiling,” Int. J. Heat Mass Transf., vol. 135, pp. 331–344, 2019.

[126] J. X. Li Xu, “Nanofluid stabilizes and enhances convective boiling heat transfer in a single microchannel,” Int. J. Heat Mass Transf., vol. 55, pp. 5673–5686, 2012.

[127] I. Henry, “Analysis of void fraction phase distribution of gas-liquid flow in a horizontal pipe using wire mesh sensor data,” The African University of Science and Technology, 2014.

[128] R. V. Pinto and F. A. S. Fiorelli, “Review of the mechanisms responsible for heat transfer enhancement using nanofluids,” Appl. Therm. Eng., vol. 108, pp. 720–739, 2016.

[129] P. K. Baburajan, G. S. Bisht, S. K. Gupta, and S. V. Prabhu, “Measurement of subcooled boiling pressure drop and local heat transfer coefficient in horizontal tube under LPLF conditions,” Nucl. Eng. Des., vol. 255, pp. 169–179, 2013.

[130] I. C. Bang and S. Heung Chang, “Boiling heat transfer performance and phenomena of Al2O3-water nano-fluids from a plain surface in a pool,” Int. J. Heat Mass Transf., vol. 48, no. 12, pp. 2407–2419, 2005.

[131] S. Q. Zhou and R. Ni, “Measurement of the specific heat capacity of water-based Al_2O_3 nanofluid,” Appl. Phys. Lett., vol. 92, no. 9, pp. 1–4, 2008.

[132] R. B. Bejjam, K. K. Kumar, and K. Balasubramanian, “Experimental Studies on Nanofluid-Based Rectangular Natural Circulation Loop,” J. Therm. Sci. Eng. Appl., vol. 11, no. August, pp. 041006: 1–10, 2019.

[133] K. Khanafer;, K. Vafai;, and M. Lightstone, “Buoyancy-driven heat transfer enhancemet

in a two dimensional enclosure utilizing nanofluid ," Int. J. Heat Mass Transf., vol. 46, pp. 3639–3653, 2003.

[134] I. Zahmatkesh and J. Ebrahimi, "Experimental Analysis of Thermal Expansion of Nanofluids," Majlesi J. Energy Manag., vol. 3, no. April, pp. 63–69, 2016.

[135] D. Saini and G. Das Agarwal, "Thermo-Physical Properties of Nano Fluids- A Review," Int. J. Adv. Eng. Sci. Technol., vol. 5, no. 1, pp. 39–45, 2016.

Appendix A: Correlations

Heat transfer correlations used in the thesis

1. Chen

$h_{tc3} = h_{mic} + h_{mac}$

$h_{mac} = h_f F(X)\, Pr_f^{0.296}$

$h_f = 0.023 \left(\frac{k_f}{D_h}\right) Re_f^{0.8} Pr_f^{0.4}$

$$Re_f = \frac{G(1-x)D_h}{\mu_f}$$

$$h_{mic} = 0.00122 \left[\frac{k_f^{0.79} c_{pf}^{0.45} \rho_f^{0.49}}{\sigma^{0.5} \mu_f^{0.29} h_{fv}^{0.24} \rho_g^{0.24}}\right] \times \left[T_w - T_{sat}(P_f)\right]^{0.24} \left[P_{sat}(T_w) - P_f\right]^{0.75} S$$

$$S = (1 + 2.56 \times 10^{-6}\, Re_{TP}^{1.17})^{-1}$$

$$Re_{TP} = Re_f\, [F(X)]^{1.25}$$

$$F(X) = 1 \qquad for \;\; X^{-1} \leq 0.1$$

$$F(X) = 2.35\left(0.213 + \frac{1}{X}\right)^{0.736} \qquad for\; X^{-1} > 0.1$$

$$X = \left(\frac{1-x}{x}\right)^{0.9} \left(\frac{\rho_g}{\rho_f}\right)^{0.5} \left(\frac{\mu_f}{\mu_g}\right)^{0.1}$$

2. Shah

$$\Psi = \frac{h_{tc3}}{h_f} = f(Co, Bo, Fr_{le})$$

$$Co = \left(\frac{1-x}{x}\right)^{0.8}\left(\frac{\rho_g}{\rho_f}\right)^{0.5} \quad ; Bo = \frac{q"}{Gh_{fg}} \quad ; Fr_{le} = \frac{G^2}{\rho_f^2 g D_h}$$

$N_s = Co$ $\quad for\ Fr_{le} \geq 0.04$

$N_s = 0.038\, Fr_{le}^{-0.3} Co$ $\quad for\ Fr_{le} < 0.04$

$F_{sh} = 14.7$ $\quad for\ Bo \geq 11 \times 10^{-4}$

$F_{sh} = 15.4$ $\quad for\ Bo < 11 \times 10^{-4}$

$\Psi_{cbd} = 1.8\, N_s^{-0.8}$

For $N_s > 1$*:*

$\Psi_{nbd} = 230\, Bo^{0.5}$ $\quad for\ Bo > 0.3 \times 10^{-4}$

$\Psi_{nbd} = 1 + 46\, Bo^{0.5}$ $\quad for\ Bo \leq 0.3 \times 10^{-4}$

Ψ=the greater of Ψ_{cbd} and Ψ_{nbd}

For $0.1 < N_s \leq 1$:

$\Psi_{bs} = F_{sh} Bo^{0.5} exp(2.74 N_s^{-0.1})$

Ψ=the greater of Ψ_{cbd} and Ψ_{bs}

For $N_s \leq 0.1$:

$\Psi_{bs} = F_{sh}\, Bo^{0.5} exp(2.74 N_s^{-0.15})$

Ψ=the greater of Ψ_{cbd} and Ψ_{bs}

3. Gungor-Winterton

$$h_{tc3} = h_f \left[1 + 3000 Bo^{0.86} + \left(\frac{x}{1-x}\right)^{0.75}\left(\frac{\rho_f}{\rho_g}\right)^{0.41}\right]$$

Appendix B: Sample Experimental Data

Table B1: Steady state temperature data with heat flux at heater section for water

Working fluid/ Temperature	Heat flux (kW/m^2)													
	22.01		34.59		49.99		70.56		87.07		99.2		107.7	
	T_{in} (^OC)	T_{out} (^OC)	T_{in} (^OC)	T_{out} (^OC)	T_{in} (^OC)	T_{out} (^OC)	T_{in} (^OC)	T_{out} (^OC)	T_{in} (^OC)	T_{out} (^OC)	T_{in} (^OC)	T_{out} (^OC)	T_{in} (^OC)	T_{out} (^OC)
Test run-1	52.01	55.21	62.83	67.17	75.13	80.59	84.57	91.39	90.11	96.62	93.39	98.43	94.63	98.43
Test run-2	51.92	55.06	62.70	66.92	75.07	80.38	84.46	91.10	90.04	96.34	93.30	98.56	94.56	98.56
Test run-3	51.81	54.90	62.58	66.73	74.93	80.15	84.33	90.86	89.96	96.18	93.22	98.62	94.43	98.62

Table B2: Steady state temperature data with heat flux at heater section for 0.005% Al_2O_3 nanofluid

Working fluid/ Temperature	Heat flux (kW/m^2)													
	22.01		34.59		49.99		70.56		87.07		99.2		107.7	
	T_{in} (^OC)	T_{out} (^OC)	T_{in} (^OC)	T_{out} (^OC)	T_{in} (^OC)	T_{out} (^OC)	T_{in} (^OC)	T_{out} (^OC)	T_{in} (^OC)	T_{out} (^OC)	T_{in} (^OC)	T_{out} (^OC)	T_{in} (^OC)	T_{out} (^OC)
Test run-1	53.27	57.53	63.95	68.28	77.11	81.38	86.98	91.26	91.21	95.49	94.23	97.55	95.06	98.43
Test run-2	53.86	56.86	64.82	68.76	77.55	82.55	87.48	93.64	91.86	96.86	94.57	97.85	95.68	97.85
Test run-3	54.11	58.28	65.25	69.48	77.95	82.12	88.12	92.31	92.34	96.53	94.98	98.11	96.08	98.62

T_{in} = Loop fluid temperature at heater inlet

T_{out}= Loop fluid temperature at heater outlet

Table B3: Test results on May 25th 2019 (loop fluid : Water)

Thermocouple positions are represented in figure 5.1 Units: Time-s; all Ts': ^{0}C												
Time	T1	T2	T3	T4	T5	T6	T7	T8	T9	T10	T11	T12
0	34.246	34.246	34.246	34.246	-	-	25.004	25.004	25.008	25.008	25.006	25.006
60	32.454	32.454	32.454	32.454	-	-	26.438	26.438	26.438	26.438	26.438	26.438
120	31.008	31.008	31.008	31.008	-	-	27.467	27.467	27.467	27.467	27.467	27.467
180	29.934	29.934	29.934	29.934	-	-	28.132	28.132	28.132	28.132	28.132	28.132
240	29.793	29.793	29.793	29.793	-	-	28.459	28.459	28.459	28.459	28.459	28.459
300	31.80944	32.22231	31.42231	32.60944	9.694	9.694	28.5	28.315	28.5	28.685	28.5	28.347
360	34.80937	35.71606	34.91606	35.60937	9.71	9.845	32.507	32.688	35.92	35.739	37.369	37.495
420	37.3646	38.66491	37.86491	38.1646	9.686	9.874	35.997	35.79	41.704	41.911	44.106	43.959
480	39.76769	41.39223	40.59223	40.56769	9.706	9.932	39.107	39.072	46.469	46.504	49.586	49.593
540	42.12074	44.0178	43.2178	42.92074	9.698	9.955	41.922	42.034	50.502	50.39	54.192	54.355
600	43.51216	45.64102	44.84102	44.31216	9.709	9.992	44.498	44.446	53.968	54.02	58.133	57.875
660	45.20573	47.533	46.733	46.00573	9.677	9.981	46.874	46.837	56.971	57.008	61.536	61.597
720	46.72711	49.22451	48.42451	47.52711	9.672	9.995	49.081	49.097	59.581	59.565	64.486	64.588
780	47.56092	50.20384	49.40384	48.36092	9.645	9.984	51.138	51.178	61.848	61.808	67.043	66.942
840	48.50811	51.27465	50.47465	49.30811	9.65	10.002	53.065	53.094	63.807	63.778	69.252	69.271
900	49.61282	52.48314	51.68314	50.41282	9.625	9.989	54.874	54.788	65.488	65.574	71.143	70.934
960	50.57704	53.53282	52.73282	51.37704	9.673	10.047	56.577	56.535	66.91	66.952	72.743	72.845
1020	50.84196	53.86606	53.06606	51.64196	9.743	10.125	58.183	58.235	68.09	68.038	74.07	74.114
1080	51.45933	54.53547	53.73547	52.25933	9.752	10.14	59.701	59.516	69.041	69.226	75.138	75.136
1140	51.81864	54.93119	54.13119	52.61864	9.738	10.131	61.136	61.317	69.771	69.59	75.958	75.838
1200	51.07026	54.204	53.404	51.87026	9.724	10.121	62.494	62.287	70.289	70.496	76.538	76.622
1260	51.96056	55.1005	54.3005	52.76056	9.772	10.171	63.78	63.745	70.597	70.632	76.884	76.798
1320	52.34756	55.4875	54.6875	53.14756	9.745	10.127	64.897	65.009	70.678	70.566	77.211	77.169

1380	52.34356	55.4835	54.6835	53.14356	9.755	10.143	64.949	64.897	70.626	70.678	77.159	77.211
1440	52.53656	55.6765	54.8765	53.33656	9.76	10.153	64.764	64.727	70.811	70.848	77.122	76.937
1500	52.37956	55.5195	54.7195	53.17956	9.777	10.174	64.945	64.961	70.63	70.614	77.138	77.319
1560	52.41156	55.5515	54.7515	53.21156	9.79	10.189	64.738	64.778	70.837	70.797	77.178	76.971
1620	52.53356	55.6735	54.8735	53.33356	9.829	10.211	64.703	64.732	70.872	70.843	77.207	77.172
1680	52.71456	55.8545	55.0545	53.51456	9.832	10.22	64.815	65.041	70.76	70.534	77.433	77.545
1740	52.27556	55.4155	54.6155	53.07556	9.883	10.276	64.763	64.6	70.812	70.975	77.27	77.218
1800	52.52356	55.6635	54.8635	53.32356	9.884	10.281	64.726	64.709	70.849	70.866	77.253	77.216
1860	52.81156	55.9515	55.1515	53.61156	9.898	10.297	64.742	64.844	70.833	70.731	77.355	77.371
1920	52.99056	56.1305	55.3305	53.79056	9.745	10.127	64.782	64.681	70.793	70.894	77.254	77.294
1980	52.66256	55.8025	55.0025	53.46256	9.755	10.143	64.811	64.83	70.764	70.745	77.273	77.302
2040	52.39456	55.5345	54.7345	53.19456	9.76	10.153	64.725	64.516	70.85	71.059	77.064	76.978
2100	52.98656	56.1265	55.3265	53.78656	9.777	10.174	64.683	64.785	70.892	70.79	77.166	77.124
2160	53.06256	56.2025	55.4025	53.86256	9.79	10.189	64.735	64.779	70.84	70.796	77.21	77.262
2220	52.91056	56.0505	55.2505	53.71056	9.829	10.217	64.55	64.548	71.025	71.027	77.208	77.023
2280	53.12932	56.41029	55.61029	53.92932	9.832	10.225	64.731	64.611	70.844	70.964	77.138	77.319
2340	54.68173	58.10147	57.30147	55.48173	9.109	9.499	65.125	65.209	70.844	70.76	77.088	76.881
2400	56.15232	59.69667	58.89667	56.95232	9.186	9.649	67.227	67.141	73.183	73.269	79.47	79.435
2460	57.24431	60.90032	60.10032	58.04431	9.188	9.711	69.127	69.085	75.296	75.338	81.625	81.737
2520	57.5495	61.30524	60.50524	58.3495	9.211	9.783	70.84	70.892	77.201	77.149	83.571	83.519
2580	58.94358	62.78793	61.98793	59.74358	9.201	9.815	72.381	72.196	78.913	79.098	85.322	85.285
2640	59.61732	63.53981	62.73981	60.41732	9.184	9.834	73.76	73.941	80.445	80.264	86.89	86.906
2700	60.51369	64.50442	63.70442	61.31369	9.192	9.873	74.985	74.778	81.806	82.013	88.285	88.325
2760	61.06203	65.11152	64.31152	61.86203	9.234	9.941	76.065	76.03	83.004	83.039	89.515	89.544
2820	61.47708	65.57623	64.77623	62.27708	9.201	9.931	77.005	77.117	84.048	83.936	90.586	90.812
2880	61.97508	66.11509	65.31509	62.77508	9.128	9.877	77.811	77.892	84.942	84.861	91.504	91.341
2940	62.25685	66.42915	65.62915	63.05685	9.1	9.865	78.486	78.463	85.691	85.714	92.274	92.257
3000	62.43376	66.62996	65.82996	63.23376	9.13	9.908	79.034	78.986	86.299	86.347	92.899	93.001

3060	62.85683	67.06867	66.26867	63.65683	9.178	9.965	79.458	79.259	86.769	86.968	93.382	93.281
3120	62.69072	66.91002	66.11002	63.49072	9.204	9.998	79.759	79.845	87.103	87.017	93.725	93.744
3180	63.14971	67.36968	66.56968	63.94971	9.174	9.972	79.94	80.267	87.303	86.976	93.931	93.722
3240	63.32671	67.54668	66.74668	64.12671	9.143	9.921	79.731	79.517	87.201	87.415	93.717	93.819
3300	63.35671	67.57668	66.77668	64.15671	9.145	9.932	79.833	79.703	87.157	87.287	93.587	93.631
3360	63.45971	67.67968	66.87968	64.25971	9.083	9.877	79.877	80.118	87.159	86.918	93.828	93.826
3420	63.03571	67.25568	66.45568	63.83571	9.154	9.952	79.875	79.685	87.279	87.469	93.638	93.518
3480	63.54271	67.76268	66.96268	64.34271	9.17	9.964	79.755	79.657	87.195	87.293	93.54	93.624
3540	63.62771	67.84768	67.04768	64.42771	9.204	10.002	79.839	79.916	87.281	87.204	93.617	93.531
3600	63.32871	67.54868	66.74868	64.12871	9.111	9.889	79.753	79.638	87.323	87.438	93.502	93.46
3660	63.43871	67.65868	66.85868	64.23871	9.097	9.884	79.711	79.852	87.271	87.13	93.643	93.695
3720	63.73871	67.95868	67.15868	64.53871	9.132	9.926	79.763	79.801	87.456	87.418	93.681	93.496
3780	63.58671	67.80668	67.00668	64.38671	9.091	9.885	79.578	79.392	87.275	87.461	93.495	93.676
3840	63.54471	67.76468	66.96468	64.34471	9.17	9.968	79.759	79.893	87.482	87.348	93.629	93.422
3900	63.71971	67.93968	67.13968	64.51971	9.159	9.937	79.552	79.374	87.517	87.695	93.451	93.416
3960	63.87571	68.09568	67.29568	64.67571	9.154	9.941	79.517	79.561	87.405	87.361	93.495	93.607
4020	63.85071	68.07068	67.27068	64.65071	9.07	9.864	79.629	79.636	87.324	87.317	93.502	93.583
4080	63.80671	68.02668	67.22668	64.60671	9.05	9.848	79.71	79.708	87.347	87.349	93.5	93.477
4140	63.69171	67.91168	67.11168	64.49171	9.087	9.881	79.687	79.567	87.395	87.515	93.38	93.332
4200	64.18749	68.54431	67.74431	64.98749	9.078	9.878	81.821	81.905	87.395	87.311	93.38	93.181
4260	65.99277	70.49821	69.69821	66.79277	9.105	9.963	83.76	83.72	90.186	90.226	96.482	96.568
4320	67.09651	71.73507	70.93507	67.89651	9.171	10.08	85.516	85.692	92.695	92.519	99.268	99.595
4380	68.83557	73.59294	72.79294	69.63557	9.133	10.086	87.1	86.962	94.945	95.083	101.76	101.55
4440	70.32187	75.18477	74.38477	71.12187	9.077	10.069	88.521	88.542	96.954	96.933	103.99	103.86
4500	70.90181	75.85775	75.05775	71.70181	9.123	10.149	89.788	90.368	98.737	98.157	105.96	106.2
4560	72.01352	77.05067	76.25067	72.81352	9.176	10.232	90.907	90.511	100.3	100.7	107.7	107.51
4620	72.80306	77.91016	77.11016	73.60306	9.128	10.209	91.882	91.978	101.66	101.57	109.21	109.11
4680	73.37661	78.54281	77.74281	74.17661	9.16	10.262	92.72	92.592	102.83	102.96	110.5	110.57

4740	73.87056	79.08538	78.28538	74.67056	9.227	10.347	93.422	93.588	103.81	103.64	111.58	111.46
4800	74.2276	79.48085	78.68085	75.0276	9.243	10.377	93.993	93.722	104.6	104.87	112.45	112.59
4860	74.65783	79.9395	79.1395	75.45783	9.263	10.408	94.435	94.444	105.21	105.2	113.13	113.17
4920	75.20873	80.50902	79.70902	76.00873	9.254	10.407	94.749	94.82	105.65	105.58	113.61	113.43
4980	74.93029	80.23946	79.43946	75.73029	9.275	10.433	94.937	95.1	105.91	105.75	113.9	114.03
5040	75.42061	80.73058	79.93058	76.22061	9.329	10.488	95.071	95.084	106.09	106.07	113.91	113.73
5100	75.59761	80.90758	80.10758	76.39761	9.278	10.42	94.893	95.008	106.04	105.93	114.03	114.07
5160	75.62761	80.93758	80.13758	76.42761	9.28	10.426	94.937	94.94	106.04	106.03	114.03	114.04
5220	75.73061	81.04058	80.24058	76.53061	9.311	10.469	94.944	94.992	106.04	105.99	114.08	114.08
5280	75.30661	80.61658	79.81658	76.10661	9.296	10.449	94.942	94.856	106.16	106.24	113.99	113.87
5340	75.81361	81.12358	80.32358	76.61361	9.364	10.52	94.822	94.78	106.07	106.12	113.95	114.03
5400	75.89861	81.20858	80.40858	76.69861	9.394	10.546	94.906	94.958	106.11	106.06	114	113.96
5460	75.59961	80.90958	80.10958	76.39961	9.418	10.568	94.866	94.681	105.94	106.12	113.82	113.99
5520	75.70961	81.01958	80.21958	76.50961	9.487	10.645	95.042	95.223	106.08	105.89	114	113.86
5580	76.00961	81.31958	80.51958	76.80961	9.519	10.659	94.904	94.697	106.05	106.26	113.79	113.81
5640	75.85761	81.16758	80.36758	76.65761	9.538	10.686	94.925	94.89	105.47	105.51	113.76	114.34
5700	75.81561	81.12558	80.32558	76.61561	9.512	10.667	95.505	95.617	105.87	105.76	113.87	113.47
5760	75.99061	81.30058	80.50058	76.79061	9.636	10.795	95.109	95.057	105.77	105.83	113.82	113.91
5820	76.14661	81.45658	80.65658	76.94661	9.599	10.743	95.205	95.307	105.9	105.8	113.92	113.79
5880	76.12161	81.43158	80.63158	76.92161	9.665	10.822	95.077	95.121	105.74	105.69	113.96	114.13
5940	76.07761	81.38758	80.58758	76.87761	9.725	10.884	95.243	95.241	106.01	106.01	113.96	113.69
6000	75.96261	81.27258	80.47258	76.76261	9.802	10.962	97.734	97.614	106.01	106.13	113.96	113.97
6060	77.04962	82.6521	81.8521	77.84962	9.737	10.972	99.971	100.05	108.54	108.46	115.71	115.78
6120	78.44606	84.22886	83.42886	79.24606	9.833	11.134	101.97	101.88	110.8	110.89	117.28	117.44
6180	79.17659	85.11983	84.31983	79.97659	9.966	11.325	103.74	103.56	112.81	112.99	118.68	118.7
6240	80.57268	86.65768	85.85768	81.37268	9.919	11.328	105.31	105.49	114.58	114.39	119.93	120.04
6300	81.74192	87.95103	87.15103	82.54192	9.109	10.563	106.67	106.46	116.11	116.32	121.01	121.02
6360	82.02719	88.34358	87.54358	82.82719	9.186	10.678	107.83	107.8	117.43	117.46	121.95	121.99

6420	82.8637	89.27123	88.47123	83.6637	9.188	10.714	108.81	108.92	118.53	118.42	122.73	122.64
6480	83.39512	89.87821	89.07821	84.19512	9.211	10.765	109.6	109.55	119.42	119.47	123.37	123.33
6540	83.72559	90.26908	89.46908	84.52559	9.201	10.778	110.21	110.18	120.11	120.15	123.86	123.91
6600	83.98979	90.57889	89.77889	84.78979	9.184	10.78	110.65	110.66	120.6	120.59	124.21	124.03
6660	84.12897	90.74913	89.94913	84.92897	9.192	10.821	110.91	110.95	120.9	120.86	124.42	124.61
6720	84.35197	90.9888	90.1888	85.15197	9.234	10.85	111.09	111.12	121.1	121.08	124.45	124.25
6780	84.82964	91.46959	90.66959	85.62964	9.201	10.821	110.88	110.8	121.14	121.23	124.37	124.33
6840	85.12964	91.76959	90.96959	85.92964	9.128	10.756	110.85	110.81	121.03	121.07	124.33	124.44
6900	84.97764	91.61759	90.81759	85.77764	9.1	10.725	110.96	111.01	121.08	121.03	124.38	124.33
6960	84.93564	91.57559	90.77559	85.73564	9.13	10.757	110.91	110.72	120.98	121.16	124.19	124.29
7020	85.11064	91.75059	90.95059	85.91064	9.178	10.802	111.01	111.19	120.93	120.75	124.37	124.42
7080	85.26664	91.90659	91.10659	86.06664	9.204	10.826	111.05	110.85	120.94	121.14	124.17	124.16
7140	85.24164	91.88159	91.08159	86.04164	9.174	10.803	111.05	111.02	121.06	121.09	124.13	124.01
7200	85.20364	91.84359	91.04359	86.00364	9.143	10.758	110.93	111.04	120.97	120.86	124.24	124.33
7260	85.00464	91.64459	90.84459	85.80464	9.145	10.766	111.02	110.96	121.06	121.11	124.19	124.11
7320	85.39164	92.03159	91.23159	86.19164	9.083	10.709	110.93	110.89	121.1	121.14	124.15	124.11
7380	85.38764	92.02759	91.22759	86.18764	9.154	10.783	110.89	110.9	121.05	121.03	124.17	124.22
7440	85.58064	92.22059	91.42059	86.38064	9.17	10.788	110.94	110.98	121.23	121.19	124.21	124.03
7500	85.42364	92.06359	91.26359	86.22364	9.204	10.831	110.75	110.78	121.05	121.02	124.24	124.42
7560	85.45564	92.09559	91.29559	86.25564	9.111	10.74	110.94	111.16	121.26	121.03	124.47	124.26
7620	85.57764	92.21759	91.41759	86.37764	9.097	10.726	110.73	110.57	121.29	121.46	124.3	124.27
7680	85.75864	92.39859	91.59859	86.55864	9.132	10.762	112.78	112.76	121.29	121.31	124.3	124.41
7740	85.31364	91.95359	91.15359	86.11364	9.091	10.791	114.62	114.72	122.21	122.11	125.21	125.16
7800	85.85648	92.40518	91.60518	86.65648	9.17	10.93	116.25	116.15	123.04	123.14	126.04	126
7860	86.5409	93.0429	92.2429	87.3409	9.159	10.972	117.7	117.72	123.77	123.75	126.77	126.79
7920	87.12656	93.58743	92.78743	87.92656	9.154	11.013	118.96	118.75	124.41	124.62	127.41	127.45
7980	87.82328	94.24823	93.44823	88.62328	9.07	10.967	120.05	120.15	124.97	124.87	127.97	128
8040	88.67862	95.07259	94.27259	89.47862	9.05	10.979	120.95	121	125.44	125.39	128.44	128.66

8100	88.74288	95.11057	94.31057	89.54288	9.087	11.042	121.69	121.69	125.82	125.82	128.82	128.66
8160	89.25219	95.5981	94.7981	90.05219	9.078	11.052	122.26	122.14	126.12	126.24	129.12	129.1
8220	89.71145	96.03992	95.23992	90.51145	9.105	11.093	122.67	122.75	126.33	126.24	129.33	129.43
8280	89.58938	95.90463	95.10463	90.38938	9.171	11.168	122.91	122.83	126.45	126.54	129.45	129.35
8340	89.67453	95.98069	95.18069	90.47453	9.133	11.131	122.9	122.85	126.43	126.48	129.41	129.43
8400	90.00127	96.3024	95.5024	90.80127	9.077	10.989	123.1	123.16	126.64	126.59	129.46	129.25
8460	89.86976	96.16977	95.36977	90.66976	9.123	11.057	123	122.82	126.54	126.73	129.28	129.38
8520	90.09676	96.39677	95.59677	90.89676	9.176	11.166	122.96	123.14	126.5	126.32	129.46	129.5
8580	90.18376	96.48377	95.68377	90.98376	9.128	11.096	122.96	122.75	126.5	126.71	129.25	129.25
8640	90.38676	96.68677	95.88677	91.18676	9.16	11.141	123	122.96	126.53	126.57	129.22	129.18
8700	90.24776	96.54777	95.74777	91.04776	9.227	11.188	122.88	123	126.42	126.31	129.33	129.44
8760	90.57776	96.87777	96.07777	91.37776	9.243	11.196	122.94	123.02	126.47	126.39	129.41	129.36
8820	90.60076	96.90077	96.10077	91.40076	9.263	11.256	122.97	122.95	126.51	126.53	129.39	129.35
8880	90.03276	96.33277	95.53277	90.83276	9.254	11.154	122.96	122.91	126.49	126.54	129.34	129.35
8940	90.14376	96.44377	95.64377	90.94376	9.275	11.219	122.92	122.72	126.45	126.65	129.14	129.18
9000	90.46976	96.76977	95.96977	91.26976	9.329	11.304	122.89	122.97	126.43	126.34	129.23	129.25
9060	90.62676	96.92677	96.12677	91.42676	9.278	11.277	122.66	122.99	126.2	125.87	129.55	129.78
9120	90.82176	97.12177	96.32177	91.62176	9.28	11.203	122.82	122.61	126.36	126.58	129.34	129.18
9180	90.41276	96.71277	95.91277	91.21276	9.311	11.297	122.69	122.56	126.23	126.36	129.21	129.34
9240	90.65776	96.95777	96.15777	91.45776	9.296	11.292	122.87	123.12	126.41	126.17	129.45	129.27
9300	90.94376	97.24377	96.44377	91.74376	9.364	11.364	121.6	121.41	126.41	126.6	129.45	129.49
9360	90.84576	97.14577	96.34577	91.64576	9.394	11.46	120.44	120.34	125.09	125.19	127.92	127.93
9420	90.65376	96.95377	96.15377	91.45376	9.418	11.541	119.42	119.49	123.91	123.84	126.56	126.55
9480	90.69053	97.1189	96.3189	91.49053	9.487	11.658	118.52	118.4	122.89	123	125.36	125.24
9540	91.49604	97.91713	97.11713	92.29604	9.519	11.73	117.75	117.89	122.01	121.87	124.34	124.43
9600	92.05957	98.40034	97.60034	92.85957	9.538	11.781	117.12	117.16	121.29	121.25	123.5	123.46
9660	92.19395	98.38199	97.58199	92.99395	9.512	11.78	116.63	116.44	120.72	120.91	122.85	123.02
9720	92.4339	98.39696	97.59696	93.2339	9.636	11.922	116.28	116.41	120.32	120.19	122.37	122.24

9780	92.58401	98.229	97.429	93.38401	9.599	11.895	116.07	115.89	120.08	120.25	122.09	122
9840	93.05078	98.682	97.882	93.85078	9.665	12.013	116.15	116.2	120.12	120.07	122.13	122.09
9900	93.03158	98.728	97.928	93.83158	9.725	11.987	116.19	116.2	120.07	120.06	122.14	122.19
9960	93.30868	98.768	97.968	94.10868	9.802	12.086	116.14	116.14	120.25	120.25	122.14	121.95
10020	93.46127	98.682	97.882	94.26127	9.737	12.077	116.33	116.21	120.07	120.19	122.02	122.2
10080	93.57481	98.205	97.405	94.37481	9.833	12.151	116.15	116.23	120.03	119.95	122.1	122.14
10140	94.00181	98.229	97.429	94.80181	9.966	12.297	116.11	116.07	120.22	120.26	122.06	121.88
10200	93.78381	98.682	97.882	94.58381	9.919	12.23	116.29	116.47	120.08	119.91	122.24	122.37
10260	93.84881	98.728	97.928	94.64881	9.109	11.412	116.16	116.02	120.26	120.4	122.1	121.92
10320	93.86681	98.768	97.968	94.66681	9.186	11.529	116.34	116.36	120.22	120.2	122.12	122.17
10380	93.97681	98.682	97.882	94.77681	9.188	11.438	116.29	116.87	120.21	119.63	122.7	122.71
10440	94.23481	98.205	97.405	95.03481	9.211	11.505	116.29	115.89	120.21	120.61	122.31	122.3
10500	94.07581	98.229	97.429	94.87581	9.201	11.526	116.29	116.38	120.2	120.1	122.4	122.42
10560	93.94981	98.682	97.882	94.74981	9.184	11.533	116.27	116.14	120.16	120.29	122.27	122.31
10620	94.06081	98.728	97.928	94.86081	9.192	11.465	116.23	116.4	120.13	119.96	122.44	122.47
10680	94.00481	98.768	97.968	94.80481	9.234	11.57	116.2	115.93	119.9	120.17	122.17	122.39
10740	94.20981	98.682	97.882	95.00981	9.201	11.547	115.98	115.99	120.07	120.06	122.18	122.01
10800	94.12181	98.205	97.405	94.92181	9.128	11.428	115.98	116.05	120.07	119.99	122.18	122.16
10860	94.24781	98.229	97.429	95.04781	9.1	11.446	111.61	111.78	118.24	118.08	119.73	119.84
10920	94.46981	98.682	97.882	95.26981	9.13	11.514	107.91	107.92	116.73	116.72	117.7	117.6
10980	94.32381	98.728	97.928	95.12381	9.178	11.591	104.94	105.06	115.54	115.43	116.09	116.11
11040	94.15309	98.768	97.968	94.95309	9.204	11.637	102.77	102.77	114.69	114.68	114.93	114.72
11100	94.40542	98.229	97.429	95.20542	9.174	11.619	101.44	101.49	114.17	114.12	114.23	114.33
11160	94.4717	98.104	97.304	95.2717	9.143	11.446	101.4	101.31	114.12	114.21	114.14	114.19
11220	94.3041	98.314	97.514	95.1041	9.145	11.488	101.4	101.36	114.13	114.17	114.1	114.1
11280	94.45174	98.205	97.405	95.25174	9.083	11.333	101.43	101.49	114.16	114.11	114.15	114.12
11340	95.02386	98.663	97.863	95.82386	9.154	11.448	101.32	101.14	114.05	114.23	113.97	114.08
11400	95.32386	98.768	97.968	96.12386	9.17	11.495	101.37	101.56	114.1	113.92	114.15	114.1

11460	95.17186	98.229	97.429	95.97186	9.204	11.553	101.41	101.2	114.14	114.34	113.94	113.91
11520	95.12986	98.104	97.304	95.92986	9.111	11.384	101.41	101.37	114.13	114.17	113.91	113.91
11580	95.30486	98.314	97.514	96.10486	9.097	11.433	101.38	101.49	114.11	113.99	114.02	114.05
11640	95.46086	98.205	97.405	96.26086	9.132	11.478	101.15	101.1	113.88	113.93	113.97	114.19
11700	95.43586	98.663	97.863	96.23586	9.091	11.391	101.32	101.42	114.04	113.94	114.07	113.91
11760	95.39786	98.768	97.968	96.19786	9.17	11.516	101.33	101.38	114.06	114.02	114.11	114.1
11820	95.19886	98.229	97.429	95.99886	9.159	11.543	101.23	101.23	113.96	113.96	114.11	114.21
11880	95.58586	98.104	97.304	96.38586	9.154	11.567	101.33	101.23	114.06	114.16	114.01	113.91
11940	95.58186	98.314	97.514	96.38186	9.07	11.503	101.31	101.33	114.04	114.02	114.03	114.05
12000	95.77486	98.205	97.405	96.57486	9.05	11.495	101.52	101.31	114.25	114.46	113.82	113.61
12060	95.61786	98.663	97.863	96.41786	9.087	11.52	101.42	101.52	114.15	114.04	113.92	114.03